DISCOVERY AND EVALUATION OF ANTIMALARIAL, ANTHELMINTIC, AND ANTIMICROBIAL MARINE NATURAL PRODUCTS

A Dissertation
Presented to
The Academic Faculty

by

Anne Marie Sweeney-Jones

In Partial Fulfillment
Of the Requirements for the Degree
Doctor of Philosophy in the
School of Chemistry and Biochemistry

Georgia Institute of Technology

August 2020

DISCOVERY AND EVALUATION OF ANTIMALARIAL, ANTHELMINTIC, AND ANTIMICROBIAL MARINE NATURAL PRODUCTS

Approved by:

Dr. Julia Kubanek, Advisor
School of Biological Sciences
School of Chemistry and Biochemistry
Georgia Institute of Technology

Dr. Neha Garg
School of Chemistry and Biochemistry
Georgia Institute of Technology

Dr. Facundo Fernández
School of Chemistry and Biochemistry
Georgia Institute of Technology

Dr. Anant Paravastu
School of Chemical and Biomolecular Engineering
Georgia Institute of Technology

Dr. Stefan France
School of Chemistry and Biochemistry
Georgia Institute of Technology

Date Approved: July 20th, 2020

ACKNOWLEDGEMENTS

During my time in graduate school, I have faced some of my greatest challenges and most rewarding successes. This journey would not have been possible without the boundless support I have been given along the way. I am incredibly appreciative for the mentoring I have received from my advisor, Dr. Julia Kubanek, during the last five years. She has been instrumental in my development as a scientist and I am thankful for her constructive feedback, insightful scientific discussions, and support towards my goals. I am also forever grateful for the opportunity I had to join her, members of Dr. Mark Hay's lab, and scientists at the University of the South Pacific on a unique field expedition in Fiji.

I would like to thank my committee members, Drs. Facundo Fernández, Neha Garg, Stefan France, Anant Paravastu, and for a short time, Christine Payne, for providing guidance that has enhanced the quality of my research. Much of my research has also greatly benefited from collaborations with other scientists including Dr. Case McNamara, Dr. Jenya Antonova-Koch, and Kerstin Gagaring at the California Institute for Biomedical Research; Drs. Raffi Aroian and Mostafa Elfawal at the University of Massachusetts Medical School; and Drs. Jeffrey Skolnick and Hongyi Zhou in the School of Biological Sciences at Georgia Tech.

I must also acknowledge the members of the Kubanek Lab and the neighboring Hay Lab, past and present, who have enriched my experience through collaborations, commiserations, and friendships: Dr. Serge Lavoie, Dr. Nazia Mojib, Dr. Samantha Mascuch, Dr. Remington Poulin, Dr. Hem Thapa, Dr. Nicole Johnston, Dr. Andrew Burns,

Dr. Jinu Mathew, Dr. Deanna Beatty, Emily Brown, Bhuwan Chhetri, Marisa Cepeda, Yifan Liang, Madison Greene, and Nolan Barrett. I am especially grateful for the opportunities I had to collaborate with Dr. Serge Lavoie and Bhuwan Chhetri towards publication of a review article in 2018 and co-chairing a conference session at the 2019 meeting of the International Society for Chemical Ecology, which were both highlights during my time at Georgia Tech.

Lastly, I would like to thank my family who are truly the ones that made this whole endeavor possible. My mother, Maura Sweeney, has always encouraged my interest in science and has been a constant source of inspiration and support throughout my life. She was also the catalyst that prompted me to pursue a doctoral degree after escaping to industry for several years. I am grateful for my grandparents, Dr. Thomas Sweeney and Jeanne Sweeney, who have been some of my most enthusiastic cheerleaders. Finally, I would like to recognize my husband, Sean Delano, who has been incredible during this journey with his continuous encouragement, emotional support, and tasty home-cooked meals.

TABLE OF CONTENTS

ACKNOWLEDGEMENTS **iii**

LIST OF TABLES **vii**

LIST OF FIGURES **ix**

LIST OF ABBREVIATIONS **xiv**

SUMMARY **xv**

CHAPTER 1. Antimalarial Peptide and Polyketide Natural Products from the Fijian Marine Cyanobacterium *Moorea producens*

1.1 Abstract **1**

1.2 Introduction **2**

1.3 Results and Discussion **3**

1.3.1 Molecular Structures of Natural Products from *Moorea producens* 3

1.3.2 Biological Activities of Cyanobacterial Natural Products 10

1.3.3 Putative Molecular Targets of Cyanobacterial Natural Products 11

1.4 Materials and Methods **15**

1.4.1 General Experimental Procedures 15

1.4.2 Biological Material and Species Identification 16

1.4.3 Extraction and Isolation 18

1.4.4 Antimalarial and Cytotoxicity Assays 19

1.4.5 Computational Binding Predictions 21

1.4.6 Actin Polymerization Assay 22

CHAPTER 2. Ecological Role of the Red Algal Natural Product Peyssonnoside A

2.1 Abstract **23**

2.2 Introduction **24**

2.3 Results and Discussion **25**

2.3.1 Evaluation of Antifeedant Properties 25

2.3.2 Surface Localization of Peyssonnoside A (**7**) 27

2.3.3 Assessment of Peyssonnoside A (**7**) as an Antifouling Agent 29

2.3.4 Antifungal Properties of Peyssonnoside A (**7**) 31

2.4 Materials and Methods **33**

2.4.1 Specimen Collection 33

2.4.2 Surface Extraction 33

2.4.3 Ash-free Dry Mass Measurement 34

2.4.4 Antifeedant Assay 34

2.4.5 Antifouling Assay 36

2.4.6 Antifungal Assay 37

CHAPTER 3. Discovery of Anthelmintic Cyanobacterial Natural Products from a Mixed Cyanobacterial Collection
3.1 Abstract 39
3.2 Introduction 39
3.3 Results 42
3.3.1 Screen for Anthelmintic Activity 42
3.3.2 Taxonomic Characterization of G-0978 45
3.3.3 Isolation and Dereplication of Natural Products in Anthelmintic Extract Fractions 48
3.4 Discussion 54
3.5 Next Steps and Future Directions 56
3.6 Materials and Methods 56
3.6.1 General Experimental Procedures 56
3.6.2 Biological Material and Species Identification 57
3.6.3 Extraction and Isolation 58
3.6.4 Anthelmintic Assays 59

CHAPTER 4. Metabolomics Analysis of the Impact of Cladophorol D from the Green Alga *Cladophora socialis* on Methicillin-Resistant *Staphylococcus aureus*
4.1 Abstract 61
4.2 Introduction 61
4.3 Experimental Design 67
4.3.1 Development of Intracellular Metabolite Extraction Procedure 67
4.3.2 Selection of Antibiotics 69
4.4 Results 72
4.4.1 Evaluation of Cladophorol D (**17**) against *S. aureus* Strains 72
4.4.2 Evaluation of Antibiotics with Known MOAs 73
4.4.3 Preliminary Evaluation of Metabolomics Workflow with Four of the Nine Antibiotics 78
4.5 Discussion 84
4.6 Materials and Methods 88
4.6.1 Determination of Antibiotic Dosage for Metabolomics 88
4.6.2 Sample Preparation, Intracellular Metabolite Extraction, and NMR Spectral Acquisition for Pilot Experiment 89
4.6.3 Metabolomic Data Analysis 90

CHAPTER 5. Conclusions and Future Directions 92

APPENDIX A. NMR Data Tables and Spectra 96

APPENDIX B. Permission for Reuse of Copyrighted Material 124

REFERENCES 125

LIST OF TABLES

Table 1. ^{1}H (700 MHz) and ^{13}C (175 MHz) NMR spectroscopic data of kakeromamide B (**1**) in CD_3CN. 7

Table 2. Antimalarial activities and cytotoxicities of natural products from *Moorea producens.* 9

Table 3. Proteins predicted to bind to kakeromamide B (1) using the protein-ligand prediction algorithm FINDSITE$^{comb2.0}$ [46]. Higher values for mTC (a Tanimoto Coefficient based fingerprint for similarity measure) and precision correspond to higher probability of the protein being a true target. 12

Table 4. Collections identified as hits (68 total from 324 extracts screened) in preliminary E2L *Ancylostoma ceylanicum* hookworm screening of the Georgia Tech marine organism extract library. Extracts were considered hits if they produced full or near-full inhibition of egg hatch or larval development at 5 µg/mL. Bolded collections were selected for further evaluation based on availability of field-collected samples for natural product isolation as well as taxonomic interest..... 43

Table 5. Activity of extracts from cyanobacterial collection G-0978 against the E2L and adult stages of the hookworm *Ancylostoma ceylanicum*. The dichloromethane-soluble extract fraction from G-0978 exhibited the most promising activity against *A. ceylanicum.* For E2L screening, black shading indicates full or near-full inhibition of egg hatch or larval development at the indicated concentration while gray means only partial inhibition. The average motility index for adult hookworm screening is based on qualitative observations made for six individual worms with the following assignments: 0 – dead worm; 1 – motile after stimulation by touch; 2 – motile; and 3 – highly motile. . 45

Table 6. Mass spectral features present in the low-resolution electrospray LC/MS data acquired for the hookworm-active HPLC fractions from cyanobacterial collection G-0978..... 53

Table 7. Antibiotics selected for inclusion in the metabolomics study to determine the MOA of cladophorol D (**17**), by comparison with antibiotics of known MOA. 70

Table 8. IC_{50} and MIC_{90} values measured for the nine antibiotics chosen for the MRSA metabolomics study for evaluating the MOA of cladophorol D (**17**). 74

Table A 1. Comparison of ^{1}H NMR chemical shifts of ulongamide A (**2**) reported in literature [47] (500 MHz, $CDCl_3$) to experimental values of **2** (700 MHz, $CDCl_3$)..... 104

Table A 2. Comparison of ^{1}H NMR chemical shifts of lyngbyabellin A (**3**) reported in literature [48] (500 MHz, $CDCl_3$) to experimental values of **3** (700 MHz, $CDCl_3$)..... 109

Table A 3. Comparison of ^{1}H NMR chemical shifts of *18E*-lyngbyaloside C (**4**) reported in literature [49,190] (600 MHz, $CDCl_3$) to experimental values of **4** (700 MHz, $CDCl_3$). 113

Table A 4. Comparison of ^{1}H NMR chemical shifts of lyngbyaloside (**5**) reported in literature [50] (600 MHz, $CDCl_3$) to experimental values of **5** (700 MHz, $CDCl_3$)..... 118

LIST OF FIGURES

Figure 1. Evolutionary relationship of *Moorea producens* G-0362 with closely related cyanobacterial species from the Family Oscillatoriaceae inferred by the 16S rRNA sequences using the Maximum Likelihood method based on the Kimura 2-parameter model in MEGA X. The percentage of replicate trees in which the associated species clustered together in the bootstrap test (1000 iterations) is shown next to the branches. The accession numbers of the 16S rRNA of respective cyanobacteria are mentioned in parentheses. The outgroup taxon is *Gloeobacter violaceus*. The 16S rRNA sequence from *Moorea producens* used in this study is underlined. The tree is drawn to scale, with branch lengths measured in the number of substitutions per site. 4

Figure 2. Natural products from the Fijian marine cyanobacterium *Moorea producens*, including the novel cyclic peptide kakeromamide B (**1**) [47-50]. 5

Figure 3. (A) Comparison of the known cyclic peptide kakeromamide A (**6**) [51] to the newly identified analog, kakeromamide B (**1**), with distinguishing moieties highlighted green. (B) Observed COSY (blue bonds) and HMBC (red arrows) correlations for kakeromamide B (**1**). 7

Figure 4. Effect of positive control latrunculin A (A) and kakeromamide B (**1**) (B) on mammalian actin polymerization. Latrunculin A stopped actin polymerization at concentrations of 1.2 µM and above whereas **1** promoted actin polymerization at the highest concentration tested but moderately suppressed polymerization at the lowest concentration tested. 14

Figure 5. Diterpene glycoside peyssonnoside A (**7**) isolated from the marine red alga *Peyssonnelia* sp.[90] 25

Figure 6. Response of hermit crabs *Clibanarius striolatus* to food laced with 1.1 mg/mL peyssonnoside A (**7**). These data indicate that **7** does not deter hermit crab feeding (mean ± standard error).[90] 27

Figure 7. Extracted LC/MS chromatogram of *m/z* 531 corresponding to **7** and calculated peak area from surface extracts of *Peyssonnelia* sp. individuals ranging from heavily calcified (tan) to fleshy (red and maroon). The inset of each chromatogram reports the relative amount of each individual algal specimen extracted for LC/MS analysis expressed as a percentage of the total mass of algae analyzed in this experiment. Larger amounts of **7** were extracted from the surfaces of algal specimens with less observed calcification. 29

Figure 8. Relative biofouling on phytagel surfaces treated with peyssonnoside A (**7**) and a paired solvent control, as indicated by the average color intensity with higher intensity

values corresponding to higher microbial content (mean ± 1 standard deviation). Gels were hung in ocean water for 4 days before being removed, stained, and imaged. 31

Figure 9. Top: Growth inhibition of the fungus *Dendryphiella salina* by peyssonnoside A (**7**) compared to the known antifungal drug nystatin (n = 3, mean ± standard error). Bottom: Comparison of fungal growth in the presence of nystatin, DMSO, and **7** showing the morphological change in the fungal colonies exposed to **7**.[90]..... 32

Figure 10. Feeding assay design using the hermit crab *C. striolatus*, consuming artificial food incorporated into a square of window screen (left). The resulting output of the feeding assay was window screen squares with varying degrees of artificial food consumed by the crab (right; "treatment" condition refers to artificial food with the addition of **7**)..... 35

Figure 11. Experimental set-up to evaluate if peyssonnoside A (**7**) prevented fouling on the surface of phytagel submerged in ocean water for four days. Gels were adhered to window screen (for quantification purposes) that was attached to petri dishes (left image) with paired controls prepared in a similar fashion and attached to the back of the plate containing gel infused with **7**. Plates were deployed under a floating dock off Ono Island, Fiji, for 4 days (right image). 37

Figure 12. Molecular structures of currently available drugs for the treatment of infectious hookworms.[115-117]..... 41

Figure 13. Photograph of a tuft from the cyanobacterial collection G-0978 soon after the specimen was collected from the field. 47

Figure 14. Agarose gel (1% w/v) displaying the PCR product (~1.4 kb) amplified from genomic DNA of the specimen G-0978 using bacterial 16S rRNA primers, 27f and 1492r. The first lane shows the DNA molecular weight marker (Fast DNA ladder, NEB). This work was performed by Bhuwan Chhetri. 47

Figure 15. Phylogenetic relationship of marine cyanobacteria from collection G-0978 with top cyanobacterial species matched from blastn search by 16S rRNA sequences using the Maximum Likelihood method based on the Kimura 2-parameter model in MEGA X. The percentage of replicate trees in which the associated species clustered together in the bootstrap test (1000 iterations) is shown next to the branches. The accession numbers of the 16S rRNA of respective cyanobacteria are mentioned in parentheses. The tree is drawn to scale, with branch lengths measured in the number of substitutions per site. This analysis was performed by Dr. Nazia Mojib. 48

Figure 16. Separation scheme for bioassay-guided fractionation of the worm active cyanobacterial collection (G-0978) identified in screening against the hookworm *A. ceylanicum*. Green circles describe the chemical separation step, red boxes indicate which fractions were submitted for testing against hookworms, and yellow boxes are fractions identified as worm-active. Due to bioassay testing constraints, not every fraction was

tested and in some cases, fractions were combined (e.g. HPLC fractions 1-6, 7-19, and 20-26 were combined). 50

Figure 17. ^{1}H NMR spectral data for hookworm-active HPLC fractions 20-26 from cyanobacterial collection G-0978 ($CDCl_3$, 700 MHz NMR)..... 51

Figure 18. Low-resolution mass spectrometry data for hookworm-active HPLC fractions 20-26 from cyanobacterial collection G-0978. 52

Figure 19. Cyanobacterial natural products that disrupt microtubule networks, one possible mechanism for anthelmintic activity. [124,127]..... 55

Figure 20. Molecular structures of phenolic natural products isolated from the green alga *Cladophora socialis*.[153] 66

Figure 21. Experimental design for extraction and analysis of intracellular metabolites from MRSA for the metabolomics mechanism of action study. 68

Figure 22. Nine antibiotics[163-165,167-172] included in MRSA metabolomics study to evaluate the MOA of cladophorol D (**17**). 71

Figure 23. Evaluation of cladophorol D (**17**) against multiple strains of *Staphylococcus aureus* (UAMS1: osteomyelitis methicillin-sensitive *S. aureus* (ATCC 49230); AH1263: MRSA strain regularly used by the Quave lab; CDC470: a multidrug-resistant (MDR) *S. aureus* strain resistant to tetracycline and susceptible to oxacillin; CDC474: an MDR *S. aureus* strain susceptible to tetracycline and resistant to oxacillin; CDC480: an MDR *S. aureus* strain resistant to both tetracycline and oxacillin). Data generated by Dr. Cassandra Quave's lab at Emory University. 73

Figure 24. Growth inhibition of MRSA treated with nine antibiotics in a 96-well microplate. Growth of this strain of *S. aureus* (ATCC 33591) was not inhibited by exposure to clindamycin (**24**), isoniazid (**25**), or sulfacetamide (**30**) treated with a maximum concentration of 650, 650, and 320 µg/mL, respectively. 74

Figure 25. MRSA growth curves exposed to each of nine antibiotics (selected for the metabolomics experiment). Optical density (OD) readings at 600 nm were recorded regularly over the course of 6.5 hours to track growth of MRSA, with higher OD values indicating greater cell density. The goal was to achieve a final OD reading for the antibiotic treatment conditions that was between 50-80% of the maximum signal obtained for MRSA treated with a solvent control. 77

Figure 26. Follow-up evaluation of MRSA growth exposed to adjusted concentrations of the antibiotics clindamycin (**24**), kanamycin (**26**), linezolid (**27**), rifampicin (**29**), and sulfacetamide (**30**) as well as cladophorol D (**17**). 78

Figure 27. ^{1}H NMR spectra (phosphate buffered D_2O, 800 MHz NMR) of intracellular metabolite extracts from MRSA treated with ciprofloxacin (red), monensin (green), sulfacetamide (purple), vancomycin (orange), or a solvent control (black). 80

Figure 28. Principal component analysis (PCA) scores plots of metabolomics data from ^{1}H NMR spectra of polar, intracellular metabolites from MRSA (ATCC 33591) treated with either ciprofloxacin (n=4), monensin (n=5), sulfacetamide (n=4), vancomycin (n=5), or a solvent control (n=5). Colored circles correspond to the 95% confidence interval for each treatment. 82

Figure 29. A. PCA loadings for ^{1}H NMR metabolomics of polar, intracellular extracts of MRSA (ATCC 33591). Spectroscopic features with positive loadings are associated with metabolites exhibiting increased concentrations in treatments that fall in the positive region of the scores plot (e.g. ciprofloxacin and monensin treatments for PC 2) while spectroscopic features with negative loadings indicate metabolites with increased concentrations correspond to treatments that fall in the negative region of the scores plot (e.g. sulfacetamide, vancomycin, and solvent control treatments for PC 2). B. Overlay of loadings plots from PC 2 (red), PC 3 (orange), and PC 4 (black) in NMR spectral region with the greatest amount of variability. 83

Figure 30. Overlay of loadings plot for PC 3 with NMR spectral data acquired for intracellular metabolite extracts from MRSA treated with ciprofloxacin, the treatment condition differentiated by PC 3. Positive loadings values correspond to NMR spectral signals that are upregulated in the ciprofloxacin treatment condition. 84

Figure A 1. HRESIMS of kakeromamide B (**1**), *m/z* $[M+H]^+$ calculated for $C_{42}H_{59}N_6O_7S$ 791.4166, found 791.4150 (Δ = 2.0 ppm); $[M+Na]^+$ calculated for $C_{42}H_{58}N_6O_7SNa$ 813.3985, found 813.3958 (Δ = 3.3 ppm). 96

Figure A 2. ^{1}H NMR spectrum of kakeromamide B (**1**) in CD_3CN (700 MHz). 97

Figure A 3. COSY spectrum of kakeromamide B (**1**) in CD_3CN (700 MHz). 98

Figure A 4. HSQC NMR spectrum of kakeromamide B (**1**) in CD_3CN (700 MHz). 99

Figure A 5. HMBC NMR spectrum of kakeromamide B (**1**) in CD_3CN (700 MHz). 100

Figure A 6. HRESIMS of ulongamide A (**2**), *m/z* $[M + Na]^+$ calculated for $C_{32}H_{45}N_5O_6Sna$ 650.2983, found 650.2971 (Δ = 1.8 ppm). 101

Figure A 7. ^{1}H NMR spectrum of ulongamide A (**2**) in $CDCl_3$ (700 MHz). 102

Figure A 8. COSY spectrum of ulongamide A (**2**) in $CDCl_3$ (800 MHz). 103

Figure A 9. HRESIMS of lyngbyabellin A (**3**), *m/z* $[M + H]^+$ calculated for $C_{29}H_{41}Cl_2N_4O_7S_2$ 691.1788, found 691.1771 (Δ = 2.5 ppm); *m/z* $[M + Na]^+$ calculated for $C_{29}H_{40}Cl_2N_4O_7S_2Na$ 713.1608, found 713.1590 (Δ = 2.5 ppm). 106

Figure A 10. ^1H NMR spectrum of lyngbyabellin A (**3**) in $CDCl_3$ (700 MHz)..... 107

Figure A 11. COSY NMR spectrum of lyngbyabellin A (**3**) in $CDCl_3$ (700 MHz). 108

Figure A 12. HRESIMS of 18*E*-lyngbyaloside C (**4**), *m/z* $[M + Na]^+$ calculated for $C_{30}H_{49}BrO_{10}Na$ 671.2401, found 671.2383 (Δ = 2.7 ppm)..... 110

Figure A 13. ^1H NMR spectrum for 18*E*-lyngbyaloside C (**4**) in $CDCl_3$ (700 MHz). ... 111

Figure A 14. COSY NMR spectrum for 18*E*-lyngbyaloside C (**4**) in $CDCl_3$ (700 MHz). 112

Figure A 15. HRESIMS of lyngbyaloside (**5**) *m/z* $[M + Na]^+$ calculated for $C_{31}H_{49}BrO_{10}Na$ 683.2401, found 683.2385 (Δ = 2.3 ppm)..... 115

Figure A 16. ^1H NMR spectrum for lyngbyaloside (**5**) in $CDCl_3$ (700 MHz)..... 116

Figure A 17. COSY NMR spectrum for lyngbyaloside (**5**) in $CDCl_3$ (700 MHz). 117

Figure A 18. HRESIMS of lyngbyabellin-like 1 (**LYN1**). 120

Figure A 19. ^1H NMR spectrum of lyngbyabellin-like 1 (**LYN1**) in $CDCl_3$ (700 MHz). 121

Figure A 20. HRESIMS of lyngbyabellin-like 2 (**LYN2**). 122

Figure A 21. ^1H NMR spectrum of lyngbyabellin-like 2 (**LYN2**) in $CDCl_3$ (700 MHz). 123

LIST OF ABBREVIATIONS

^{13}C	carbon-13
^{1}H	proton
COSY	correlation spectroscopy
EC_{50}	half-maximal effective concentration
HMBC	heteronuclear multiple bond coherence
HSQC	heteronuclear single quantum correlation
IC_{50}	half-maximal inhibitory concentration
LC/MS	liquid chromatography-mass spectrometry
nM	nanomolar
NMR	nuclear magnetic resonance
sp.	species
μg/ml	micrograms per milliliter
μM	micromolar

SUMMARY

Historically, natural products have served as valuable sources of drugs to treat many human diseases.[1] Examples include the antimalarial drugs quinine from the cinchona tree[2] and artemisinin from the sweet wormwood,[3] the antiparasitic drug ivermectin, a derivative of the natural product avermectin from the bacterium *Streptomyces avermitilis*,[4] and the antibiotic vancomycin from the soil bacterium *Amycolatopsis orientalis*.[5] Although many natural products are derived from terrestrial sources, the marine environment has the potential to provide a vast array of novel drug molecules.[6]

Approximately 35,000 natural products from marine sources have been chemically characterized, including seven FDA-approved marine-derived drugs for cancer, viral diseases, chronic pain, and reducing triglyceride levels in blood.[7,8] These discoveries represent only a fraction of the natural products present in the marine environment since more than 70% of Earth's surface is covered by relatively unexplored ocean habitats.[9] Additionally, advances in technology and improvements in culturing and isolation techniques have fueled studies of underexplored marine natural products produced by marine microbes.[10,11] Marine organisms are exposed to a wide variety of pathogenic microbes and are subject to selection pressures as a result of predation, disease, herbivory, and competition for limited resources in their native environments, resulting in the evolution of a vast array of unique secondary metabolites.[12,13] In addition, due to the high abundance of halides in the marine environment, many marine organisms incorporate chlorine, bromine, and iodine into secondary metabolites, which are not as common in terrestrial natural products and confer additional functionality.[12]

One area of marine natural products research that has shown great promise is the application of these compounds as treatments for infectious diseases such as malaria and hookworm infection.[14] In fact, there is a dire need to identify new treatment options for infection by the malarial parasite *Plasmodium* which has evolved resistance to currently available antimalarial drugs.[15-17] Additionally, two species of *Plasmodium*, *P. vivax* and *P. ovale*, can develop into hypnozoites, a dormant form of the parasite's life cycle located in the host's liver that do not cause symptoms and can trigger a new occurrence of malaria months to years after initial infection.[18,19] Chapter 1 details the characterization of five natural products isolated from a cyanobacterium *Moorea producens* that exhibit promising activity against both blood and liver-stages of malaria. Soil-transmitted helminths, such as hookworms, can negatively impact human physical and cognitive development, impair productivity, and be generally debilitating.[20,21] According to a survey of neglected tropical disease experts, there is consensus that current drugs, vaccines, and vector controls are not adequate for the elimination of soil-transmitted helminth infections.[22] Efforts to eradicate infectious worms are hindered by the evolution of resistance to currently available drugs, limited treatment options, and a high frequency of reinfection. Chapter 3 presents separation and structural characterization of natural products from a mixed cyanobacterial collection that exhibited activity against infectious hookworms.

Since marine organisms do not encounter the same pathogens as humans in their own habitats, a relevant question to ask is what roles newly discovered marine natural products play in natural environments. Previous studies have shown that bioactive molecules can act as defense molecules against ecologically relevant pathogens,[23] as allelopathic agents against competitors,[24] as antifouling chemicals that prevent

attachment of biofoulers on organismal surfaces,[25] or as feeding deterrents against predators, among many other roles.[26] In chapter 2, the natural product peyssonnoside A, isolated from a red alga *Peyssonnelia* sp., was found to suppress growth of a marine fungus, indicating that peyssonnoside A exhibits an antifungal ecological role.

An important aspect of the drug discovery process is evaluation of the mechanism of action (MOA) of bioactive molecules.[27] Numerous methods exist for probing small molecule MOA including microscopy, biochemical techniques (e.g., affinity-based purification, gene expression-based profiling), molecular modeling and docking, and omics-based approaches (e.g., metabolomics, proteomics, transcriptomics, genomics).[28,29] Chapter 1 includes computational predictions used to generate hypotheses about protein-ligand binding as a means of evaluating possible MOAs for antimalarial cyanobacterial natural products isolated in minute quantities. Applying computational modeling as a step in evaluating possible MOAs is valuable since it allows for prioritization of laboratory experiments for confirming predictions while minimizing the consumption of precious natural products. A metabolomics approach is presented in chapter 4 for evaluating the MOA of a natural product isolated from the green alga *Cladophora socialis* against methicillin-resistant *Staphylococcus aureus*. Metabolomics allows for the systematic comparison of complex mixtures of small molecules present in different biological systems, for example, comparing the metabolomes of a pathogen under different treatment conditions enables detection of metabolic pathways altered upon exposure to a candidate drug.[30] Of the omics-based techniques, metabolomics provides the closest representation of cellular phenotype as it probes differences in metabolites that reflect the underlying biochemical pathways.[31,32]

In summary, this dissertation provides a comprehensive view of the many milestones involved in the natural product drug discovery process, from collection of marine organisms in the field to isolation and structural elucidation of bioactive natural products, and exploration of their biological functions. Important insights were gained by probing the ecological role of a natural product in its natural environment and evaluating possible MOAs of isolated natural products against human pathogens.

CHAPTER 1. ANTIMALARIAL PEPTIDE AND POLYKETIDE NATURAL PRODUCTS FROM THE FIJIAN MARINE CYANOBACTERIUM *MOOREA PRODUCENS*

This section is adapted from the paper A.M. Sweeney-Jones, K. Gagaring, J. Antonova-Koch, H. Zhou, N. Mojib, K. Soapi, J. Skolnick, C.W. McNamara, and J. Kubanek, *Marine Drugs*, 2020, 18(3), 167; https://doi.org/10.3390/md18030167.

1.1 Abstract

A new cyclic peptide, kakeromamide B (**1**), and previously described cytotoxic cyanobacterial natural products ulongamide A (**2**), lyngbyabellin A (**3**), 18*E*-lyngbyaloside C (**4**), and lyngbyaloside (**5**) were identified from an antimalarial extract of the Fijian marine cyanobacterium *Moorea producens*. Compounds **1** and **2** exhibited promising activity against *Plasmodium falciparum* blood-stages with EC_{50} values of 0.89 and 0.99 μM, respectively, whereas **3** was very potent with an EC_{50} value of 0.15 nM. Compounds **1**, **4**, and **5** displayed liver-stage antimalarial activity against *P. berghei* liver schizonts with EC_{50} values of 1.1, 0.71, and 0.45 μM, respectively. The threading-based computational method FINDSITE$^{comb2.0}$ predicted the binding of **1** and **2** to potentially druggable proteins of *Plasmodium falciparum,* prompting formulation of hypotheses about possible mechanisms of action. Kakeromamide B (**1**) was predicted to bind to several *Plasmodium* actin-like proteins and a sortilin protein suggesting possible interference with parasite invasion of host cells. When **1** was tested in a mammalian actin polymerization assay, it stimulated actin polymerization in a dose-dependent manner, suggesting that **1** does, in fact, interact with actin.

1.2 Introduction

Current malaria drugs are inadequate for future control of the disease due to the evolution of resistance by the malaria parasite, necessitating the discovery of medicines with novel mechanisms of action (MOA).[33,34] Additionally, pharmaceutical options remain limited for the liver-stage of malaria infection. Natural products such as artemisinin discovered by Nobel-prize winner Tu Youyou have served as valuable sources of drugs to treat malaria. [3,9] Promising nanomolar antimalarial activity has been reported for a wide range of marine-derived natural products including the polycyclic aromatic polyketide trioxacarcin A from a marine *Streptomyces* sp.,[35] the polyketide-derived cyanobacterial polyhydroxy macrolide bastimolide A,[36] and the β-carboline alkaloid manzamine A produced by a bacterial sponge symbiont.[37] Two sponge-derived antimalarial terpene isonitriles, diisocyanoadociane and axisonitrile-3, were predicted based on molecular dynamics simulations to interfere with heme detoxification, the same MOA as chloroquine.[38] Evolution of an efflux pump that prevents drug accumulation in the parasite's food vacuole has resulted in resistance of *Plasmodium* to chloroquine,[39] illustrating the need for discovery of natural products with unique molecular targets to support future disease management.

Marine cyanobacteria produce a wide variety of secondary metabolites, including peptides, polyketides, alkaloids, lipids, glycosidic macrolides, and terpenes,[40] with diverse bioactivities such as antibacterial, antifungal, anticancer, immunosuppressive, and anti-inflammatory.[41] Although the chemical space of this phylum has been extensively studied with over 800 natural products reported in the MarinLit™ database, treatments for parasitic infections have been relatively understudied, leading to opportunities to leverage

the diverse chemistry of marine cyanobacteria for pharmacological exploration. The pursuit of antiparasitic natural products has led to promising discoveries, such as the antimalarial cyanobacterial peptides carmabin A,[42] gallinamide A,[43] and venturamide A.[44] Exploration of new chemical entities and novel bioactivities of known compounds constitute promising routes for inspiring the development of new drug molecules.

An extract of the marine cyanobacterium *Moorea producens* collected off the Northern Lau Islands of Fiji exhibited strong potency against the human malarial parasite *Plasmodium falciparum* and low toxicity to human liver cells. The goal of the present study was to characterize the natural products responsible for the observed antimalarial effects and to explore the intersection of blood-stage and liver-stage activities. These molecules were evaluated for possible protein binding targets using computational predictions generated by the program FINDSITE$^{comb2.0}$,[45,46] a threading-based, virtual ligand-screening method that takes advantage of binding site conservation for evolutionarily distant proteins, and one of the putative molecular targets was confirmed via in vitro testing.

1.3 Results and Discussion

1.3.1 Molecular Structures of Natural Products from Moorea producens

A Fijian collection of cyanobacteria identified by 16S rRNA sequencing as *Moorea producens* (Figure 1) was freeze-dried, extracted, and the resulting extract was subjected to vacuum liquid chromatography. Bioassay-guided fractionation using both blood-stage *Plasmodium falciparum* and liver-stage *Plasmodium berghei* pointed to four adjacent fractions that demonstrated potent blood and liver-stage antimalarial activity. Subsequent

purification of compounds from these fractions using solid-phase extraction (SPE) and high-performance liquid chromatography (HPLC) led to the isolation of **1**–**5** (Figure 2).

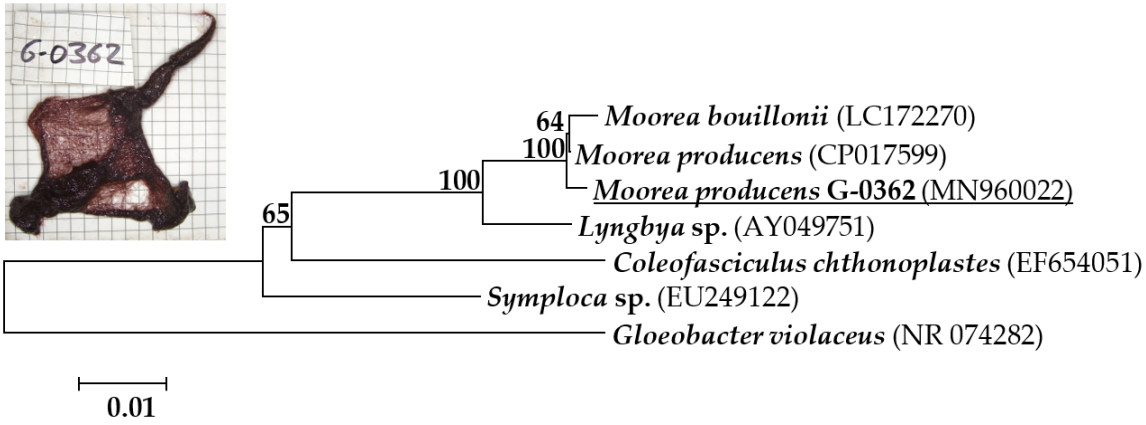

Figure 1. Evolutionary relationship of *Moorea producens* G-0362 with closely related cyanobacterial species from the Family Oscillatoriaceae inferred by the 16S rRNA sequences using the Maximum Likelihood method based on the Kimura 2-parameter model in MEGA X. The percentage of replicate trees in which the associated species clustered together in the bootstrap test (1000 iterations) is shown next to the branches. The accession numbers of the 16S rRNA of respective cyanobacteria are mentioned in parentheses. The outgroup taxon is *Gloeobacter violaceus*. The 16S rRNA sequence from *Moorea producens* used in this study is underlined. The tree is drawn to scale, with branch lengths measured in the number of substitutions per site.

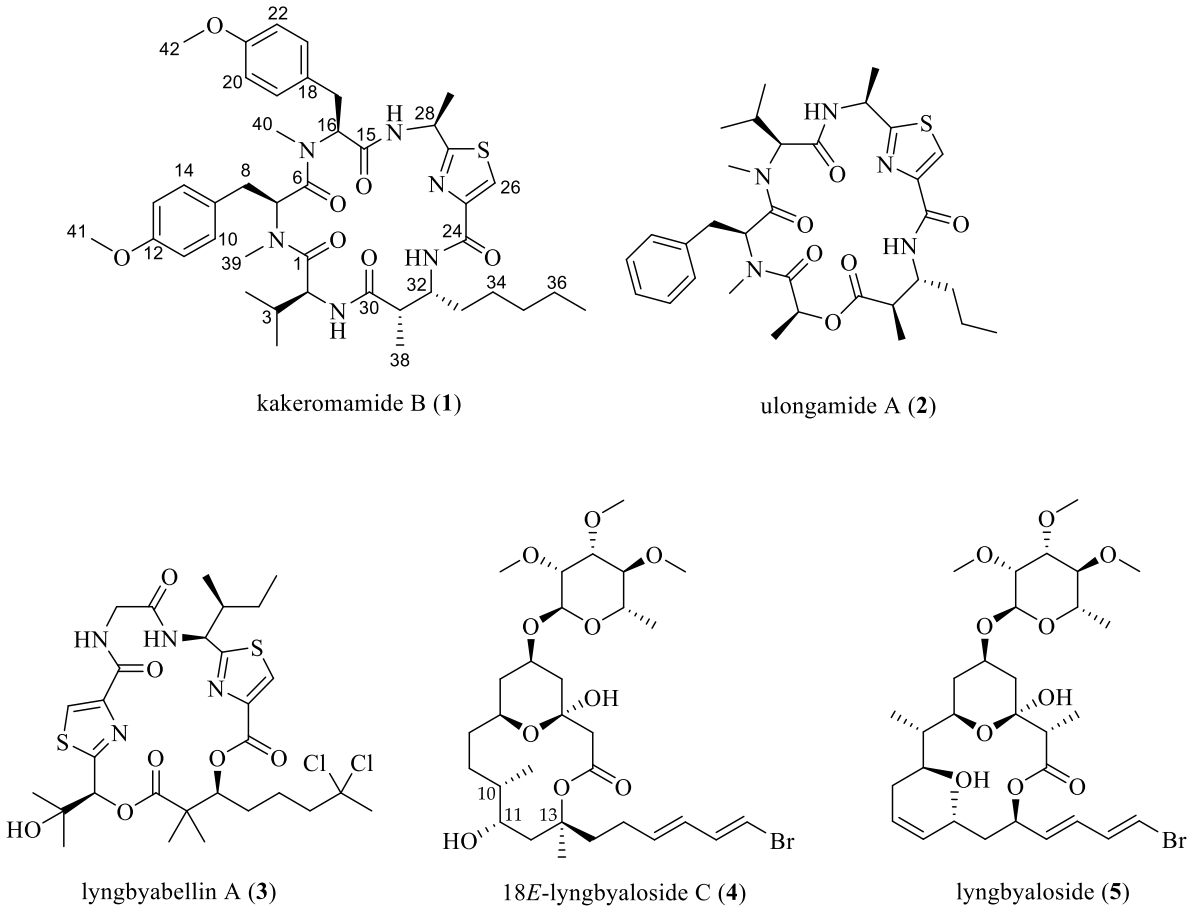

Figure 2. Natural products from the Fijian marine cyanobacterium *Moorea producens*, including the novel cyclic peptide kakeromamide B (**1**) [47-50].

High-resolution electrospray ionization mass spectrometry (HRESIMS) was used to assign the molecular formula of **1** as $C_{42}H_{58}N_6O_7S$ with 17 degrees of unsaturation from the pseudomolecular ions $[M + H]^+$ at *m/z* 791.4150 and $[M + Na]^+$ at *m/z* 813.3958. This matched the molecular formula of the known natural product kakeromamide A (**6**) (Figure 2A),[51] but differences in nuclear magnetic resonance (NMR) chemical shifts indicated unique bond connectivities. The ^{1}H NMR spectral data (Table 1) suggested a peptide based on the presence of three amide protons (δ_H 6.32, 8.61, and 8.71), two *N*-methyl singlets (δ_H

2.87 and 3.02), and four *α*-protons (δ_H 4.30, 5.23, 5.45, and 5.63), nearly identical to **6**. In **6,** two methyl doublets at δ_H 0.78 and 0.94 corresponded to valine, missing in **1**, while the ^{1}H NMR spectrum of **1** had a methyl doublet at δ_H 1.40 absent in **6**. 2D NMR spectroscopic analysis using COSY, HSQC, and HMBC experiments identified these differing subunits as an alanine-derived thiazole carboxylic acid and a 3-amino-2-methyloctanoic acid (Amoa), distinct from the valine-derived thiazole carboxylic acid and 3-amino-2-methylhexanoic acid (Amha) in **6**. 2D NMR spectroscopy also confirmed the presence of valine and two *N*,*O*-dimethyl-tyrosines. The linear peptide sequence was established based on HMBC correlations between α-protons, *N*-methyls, or NHs and carbonyl carbons (Figure 3B; Table 1: H-2/C-1, H-39/C-1 and C-7, H-40/C-6 and C-16, NH-28/C-15, H-28/C-27, H-26/C-25 and C-27, NH-32/C-24, and NH-2/C-30). The relative and absolute configurational assignments in **1** are proposed based on the similarity of chemical shifts and *J* couplings to **6**, which was subjected to a modified Marfey's method to establish absolute configuration.[51] In the current work, acid hydrolysis towards Marfey's analysis was attempted, but yields were inadequate for confirming absolute configuration, given that most isolated **1** was needed for pharmacological assessment.

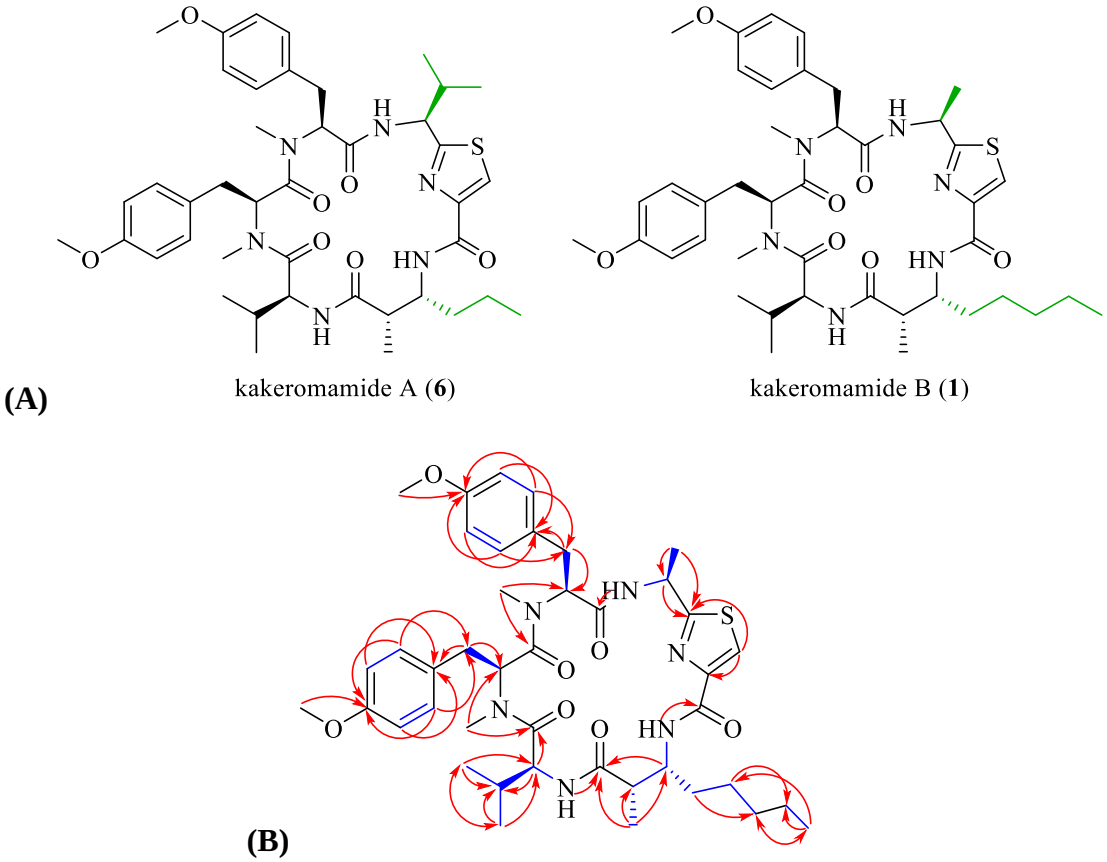

Figure 3. (A) Comparison of the known cyclic peptide kakeromamide A (**6**) [51] to the newly identified analog, kakeromamide B (**1**), with distinguishing moieties highlighted green. (B) Observed COSY (blue bonds) and HMBC (red arrows) correlations for kakeromamide B (**1**).

Table 1. ^{1}H (700 MHz) and ^{13}C (175 MHz) NMR spectroscopic data of kakeromamide B (**1**) in CD_3CN.

no.	δ_C (mult., *J* in Hz)	δ_H (mult., *J* in Hz)	COSY	HMBC
1	176.3			
2	56.9	4.30 t (7.1)	H-3,2-NH	C-1^{w},C-3,C-4^{w}
2-NH		6.32 d (6.6)	H-2	C-30^{w}
3	30.8	1.80 m	H-2,H-4,H-5	
4	18.6	0.78 d (6.9)	H-3	C-2,C-3,C-5
5	19.0	0.80 d (6.8)	H-3	C-2,C-3,C-4
6	172.1			
7	50.3	5.63 dd (4.9, 10.9)	H-8a,H-8b	
8a	33.2	1.37 m	H-7,H-8b	C-9^{w}

Table 1 (continued)

8b		2.74 dd (11.0, 16.1)	H-7,H-8a	C-7,C-9
9	129.8			
10/14	130.0	6.89 d (8.5)	H-11/13	C-8[w],C-12
11/13	114.7	6.78 d (8.7)	H-10/14	C-9
12	159.1			
15	168.9			
16	62.9	5.23 dd (5.0, 10.0)	H-17a,H-17b	
17a	34.8	2.67 dd (10.1, 14.4)	H-16,H-17b	C-16
17b		2.92 dd (4.9, 14.4)	H-16,H-17a	C-18
18	130.7			
19/23	131.4	7.00 d (8.6)	H-20/22	C-17,C-21
20/22	114.9	6.60 d (8.7)	H-19/23	C-18
21	159.4			
24	169.5			
25	150.2			
26	123.2	8.02 s		C-25[w],C-27
27	171.6			
28	48.1	5.45 p (7.4)	28-NH,H-29	C-27[w]
28-NH		8.61 d (7.8)	H-28	C-15[w]
29	24.0	1.40 d (6.9)	H-28	C-27,C-28
30	173.6			
31	44.5	2.63 qd (3.7, 6.8)	H-32,H-38	
32	53.1	4.02 m	H-31,32-NH,H-33a,b	C-30[w]
32-NH		8.71 d (10.2)	H-32	C-24[w]
33a	41.8	1.13 m	H-32,H-33b,H-34a,b	C-35[w]
33b		1.72 m	H-32,H-33a,H-34a,b	
34a	30.4	1.29 m	H-33a,b	C-36[w]
34b		1.45 m	H-33a,b	
35	33.7	1.35 m		C-37[w]
36	24.5	1.35 m	H-37	
37	14.9	0.88 t (6.6)	H-36	C-34,C-35,C-36
38	19.6	1.09 d (6.9)	H-31	C-30,C-31,C-32
39	31.4	3.02 s		C-1,C-7
40	28.7	2.87 s		C-6,C-16
41	56.0	3.74 s		C-12
42	55.7	3.49 s		C-21

[w]Indicates weak correlation.

Compounds **2**–**5** were identified by comparison of HRESIMS, ^{1}H NMR, and COSY spectral data to the literature [47-50] (data provided in Appendix A). Total syntheses have been reported for **2**–**4**, confirming the structures of **2** [52] and **3** [53] while leading to the structural revision of three stereogenic centers (C-10, 11, and 13) of **4.**[54] Two natural products that appeared to belong to the lyngbyabellin class of natural products, referred to as lyngbyabellin-like 1 (**LYN1**) and 2 (**LYN2**), were isolated in very low yields (2.2 and 2.8 µg, respectively) which hindered full structure elucidation. Similarities to known lyngbyabellins included the presence of two chlorines as determined from MS isotopic patterns, two downfield proton singlets (**LYN1**: δ_H 8.12, 8.16; **LYN2:** δ_H 8.11, 8.27) suggestive of thiazole moieties, and methyl singlets with chemical shifts matching the methyl adjacent to the dichloromethylene in **3** (**LYN1**: δ_H 2.04; **LYN2:** δ_H 2.07). Since these natural products exhibited promising blood-stage antimalarial activity (Table 2), HRESIMS and ^{1}H NMR spectral data are included in the appendix section even though complete structures were not determined.

Table 2. Antimalarial activities and cytotoxicities of natural products from *Moorea producens*.

	Blood-stage *P. falciparum*[a]	**Liver-stage *P. berghei*[a]**	**HEK293T Cytotoxicity[b]**	**HepG2 Cytotoxicity[b]**
1	0.89	1.1[d], > 1.2[e]	>2.3	>2.3
2	0.99	>4.0[c]	>4.8	not tested
3	0.00015	>1.0[d,e]	1.9	0.33
4	> 1.9	0.71[d], > 1.6[e]	>3.1	1.7
5	> 0.79	0.45[d], > 0.63[e]	>1.3	>1.3
lyngbyabellin-like 1 **(LYN1)**	0.0073	>0.32[e,d]	>0.65	0.45
lyngbyabellin-like 2 **(LYN2)**	0.11	>0.26[e,d]	>0.52	>0.52
Atovaquone (+ control)	0.0061	< 0.00028[c], 0.0017[d], 0.0037[e]	>2.0	not tested

Table 2 (continued)

[a]Half-maximal effective concentration (EC_{50}) (μM). [b]Half-maximal cytotoxicity concentration (μM). [c]Natural product tested against *P. berghei* sporozoites sourced from New York University (NYU) School of Medicine. Later liver-stage *P. berghei* testing used sporozoites from the University of Georgia (UGA)[d] and University of California San Diego (UCSD)[e].

1.3.2 Biological Activities of Cyanobacterial Natural Products

The antimalarial activities of **1**–**5** were evaluated against asexual blood-stage *Plasmodium falciparum* and liver-stage *P. berghei* assays while cytotoxicity was measured with HEK293T and HepG2 human cell lines (Table 2). Lyngbyabellin A (**3**) exhibited remarkable activity against blood-stage *P. falciparum* with a half-maximal effective concentration (EC_{50}) value of 0.15 nM. Additionally, **3** exhibited a high selectivity index of 13,000 and 2,200 for *Plasmodium* versus normal kidney epithelial cells (HEK293T) and human liver carcinoma cells (HepG2), respectively. Lynbyabellin A (**3**) was more potent than atovaquone (Table 2), indicating that it could be a promising antimalarial drug candidate, especially since a route to production via total synthesis exists.[53] Lyngbyabellins **LYN1** and **LYN2** also exhibited promising activity against blood-stage *P. falciparum* with EC_{50} values of 0.0073 and 0.11 μM, respectively. To date, 18 lyngbyabellins have been reported, all structurally related to dolabellin [55] with two disubstituted thiazole rings and a dichloro substituted aliphatic chain.[48,49,56-61] Lyngbyabellins possess varying degrees of cytotoxicity against cancer cell lines but had not previously been evaluated for antimalarial properties. Due to the promising antimalarial activities reported in the current study (Table 2), future experiments could evaluate antimalarial mechanisms of action and structure-activity relationships of lyngbyabellins.

Although less potent, cyclic depsipeptide **2** and cyclic peptide **1** still exhibited promising blood-stage antimalarial activity with a EC_{50} values of 0.99 and 0.89 μM, respectively, whereas **4** and **5** were inactive (Table 2). Evaluation of liver-stage antimalarial activity indicated that **1**, **4**, and **5** are inhibitory against *P. berghei* liver schizont development (sourced from UGA) with EC_{50} values of 1.1, 0.71, and 0.45 μM, respectively. These same natural products were less active against *P. berghei* sourced from UCSD. None of these natural products exhibited cytotoxicity against HEK293T or HepG2 human cell lines. Characteristics of the ideal drug candidate for treating malaria include safety, especially for vulnerable populations such as children under the age of five, and targeting more than one *Plasmodium* life stage.[62] Although **1** did not exhibit the most potent antimalarial activity of the cyanobacterial natural products evaluated, its ability to inhibit both the blood and liver life stages of *Plasmodium* coupled with its low cytotoxicity towards human cell lines make it a promising lead for drug discovery.

1.3.3 Putative Molecular Targets of Cyanobacterial Natural Products

Modeling of protein-ligand interactions with the FINDSITE$^{comb2.0}$ [46] prediction algorithm suggested that numerous *Plasmodium* proteins are likely to interact directly with these cyanobacterial natural products. Several malarial protein classes were predicted to bind to kakeromamide B (**1**) including actin-like proteins, sortilin, and glutamyl-tRNA(Gln) amidotransferase subunit A. Ranking of protein-ligand interactions by mTC, a composite Tanimoto Coefficient based on fingerprint for ligand similarity measurement, and precision values indicated that actins had the highest probability of binding **1** (Table 3). One of the *Plasmodium* actins predicted to bind with **1**, actin-1, has been found to be involved with host cell invasion.[63] Since the malarial parasite life cycle requires entry

into human erythrocytes, inhibiting the ability of *Plasmodium* to invade host cells could be a viable mechanism of action. The malarial protein with the next highest mTC and precision values for binding **1**, sortilin, is important for the formation of apical complex components and creation of merozoites.[64] In parasite strains where the expression of sortilin is suppressed, new merozoites, which are the invasive form of the parasite, cannot be formed. Thus, like actin, inhibition of sortilin could impact *Plasmodium's* ability to infect host cells suggesting that this protein could also be a feasible target for future exploration. Glutamyl-tRNA(Gln) amidotransferase subunit A is essential for the parasite's blood-stage.[65] This protein is required for the synthesis of glutamyl-tRNA-gln, a protein synthesis building block needed for parasite propagation.[66] Since the precision value for glutamyl-tRNA(Gln) amidotransferase subunit A was relatively low, this target is less promising.

Table 3. Proteins predicted to bind to kakeromamide B (1) using the protein-ligand prediction algorithm FINDSITE$^{comb2.0}$.[46] Higher values for mTC (a Tanimoto Coefficient based fingerprint for similarity measure) and precision correspond to higher probability of the protein being a true target.

Accession Number	Protein Description	mTC	Precision
Q8ILW9	Actin-2	0.50	0.77
Q8ILM5	Actin-related protein homolog, arp4	0.50	0.77
Q8IIW6	Actin-like protein, putative	0.50	0.77
Q8IIQ4	Actin-like protein homolog, ALP1	0.50	0.77
Q8IBH5	Actin-like protein, putative	0.50	0.77
Q8I4X0	Actin-1	0.50	0.77
Q8I450	Actin-like protein, putative	0.50	0.77
Q8I345	Actin-like protein, putative	0.50	0.77
Q8I2A2	Actin-related protein, ARP1	0.50	0.77
Q8I1V9	Actin-like protein, putative	0.50	0.77
Q8IKV8	Sortilin, putative	0.48	0.45
Q8I1S6	Glutamyl-tRNA(Gln) amidotransferase subunit A, putative	0.46	0.26

Of the proteins predicted to bind to kakeromamide (**1**), actin and sortilin were deemed worthy of further evaluation given their higher predicted binding values. However, no *in vitro* sortilin assay is available. In contrast, actin polymerization assays are frequently employed to assess agents that affect actin dynamics, albeit using mammalian homologs of actin. Since **1** was predicted to bind to both *Plasmodium* and mammalian actin proteins but only mammalian actin assays are commercially available, an actin polymerization assay that uses pyrene-labeled rabbit muscle actin was employed. Several natural products are known to disrupt actin's function by either inhibiting or stabilizing polymerization, which could arise from ligand binding.[67-70] Since apicomplexan actins (including those of *Plasmodium*) and mammalian actins are relatively divergent,[71] *Plasmodium* actin might be a useful molecular target. Additionally, since **1** did not exhibit toxicity towards human cell lines (Table 2), the predicted interactions with human actin apparently did not translate to a negative outcome for host cells, at least *in vitro*. The effect of **1** on rabbit actin polymerization was compared to the known actin polymerization inhibitor, latrunculin A. While latrunculin A suppressed polymerization at concentrations above 1.2 µM (Figure 4A), **1** exhibited unique behavior with the highest tested concentration, 2.5 µM, enhancing actin polymerization whereas the lowest tested concentration, 0.0025 µM, moderately suppressed polymerization relative to controls (Figure 4B). This suggests that **1** causes a concentration-dependent modulation in mammalian actin function. Cyclic peptides such as phalloidin [67] from the death cap mushroom and jasplakinolide [70] from a marine sponge have been found to induce polymerization and stabilize actin filaments in a dose-dependent manner. Similar activity by **1** could be one possible explanation for the observed increase in actin polymerization with increasing concentrations of **1.** Although **1**

appears to impact mammalian actin polymerization, future tests evaluating the impact of **1** on *Plasmodium* actin function would be worthwhile in order to further elucidate whether interactions with actin are relevant to this natural product's mechanism of action on the malaria parasite.

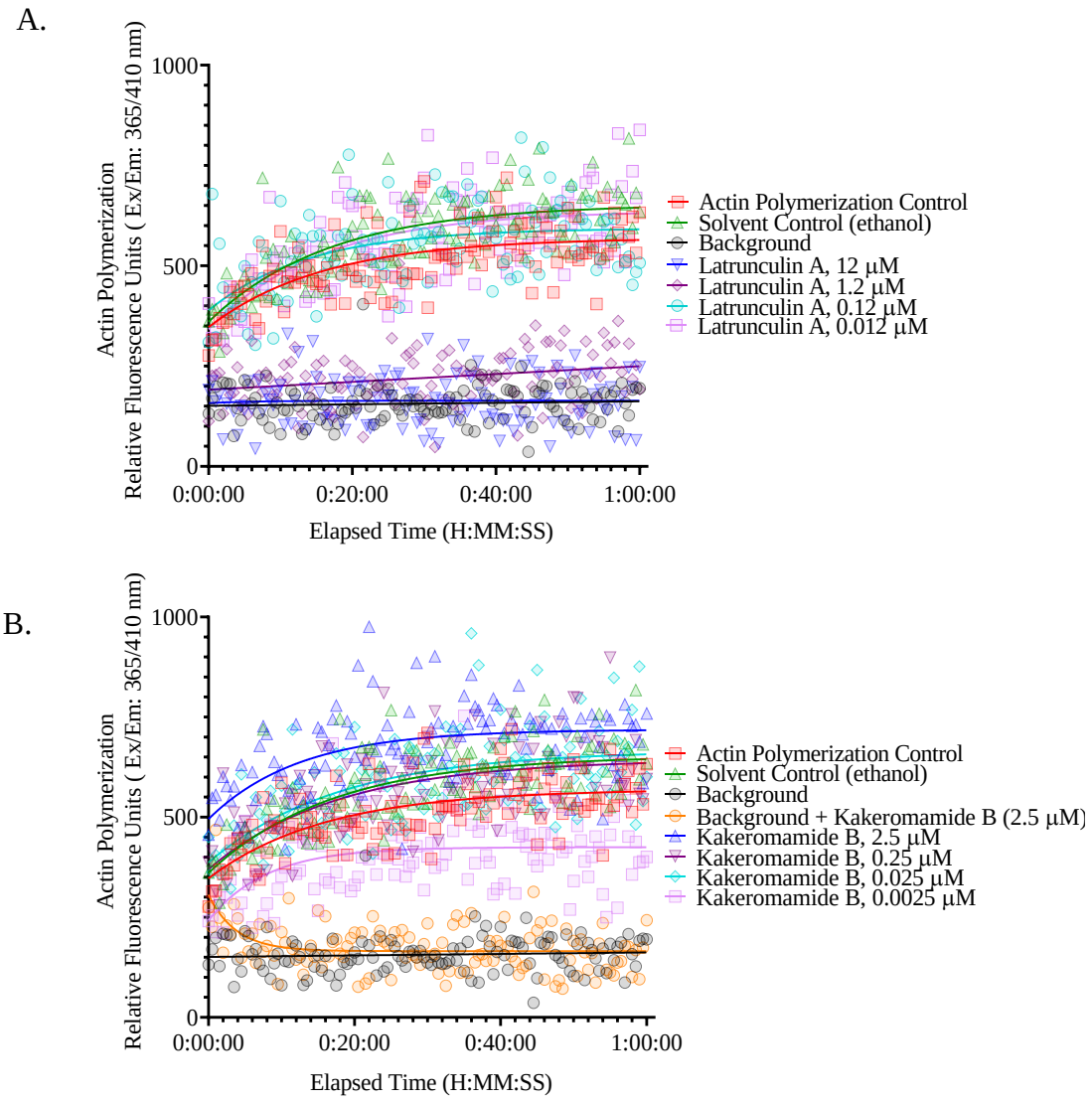

Figure 4. Effect of positive control latrunculin A (A) and kakeromamide B (**1**) (B) on mammalian actin polymerization. Latrunculin A stopped actin polymerization at concentrations of 1.2 µM and above whereas **1** promoted actin polymerization at the highest concentration tested but moderately suppressed polymerization at the lowest concentration tested.

Ulongamide A (**2**) was predicted to bind to one protein, an aspartyl protease, with mTC and precision values of 0.47 and 0.35, respectively. Aspartyl protease is involved with remodeling the erythrocyte by trafficking parasite proteins into erythrocytes, which ultimately aids the parasite in evading host recognition and response.[72] In fact, targeting aspartyl proteases in HIV has led to the development of clinically available antiretrovirals, which have also shown inhibition towards *Plasmodium* growth.[73] Taken together, aspartyl protease seems like a potentially promising target for **2**.

Lyngbyabellin A (**3**), the most potent antimalarial natural product isolated from *Moorea producens* in the current study, did not deliver any putative molecular targets via FINDSITE$^{comb2.0}$ protein-ligand binding calculations. Even a linear analog of **3**, lyngbyabellin I,[57] was not predicted to bind to *Plasmodium* proteins. It is possible that the structural motifs of **3** are inadequately represented among ligands known to bind malarial proteins as sampled from the literature; however, **3** was predicted to bind to several human proteins. Thus, there exist compounds structurally similar enough to **3** in ligand databases to enable prediction of some protein binding events, but apparently not with *Plasmodium* proteins. We are, therefore, unable to propose hypotheses of possible molecular targets of **3**. The promising selectivity of **3** towards *Plasmodium*, the availability of a total synthesis route, and the substantial collection of known lyngbyabellins warrants further study as a possible treatment option for malaria.

1.4 Materials and Methods

1.4.1 General Experimental Procedures

^{1}H, COSY, HSQC, and HMBC NMR spectra were acquired on either a 16.4 T (700 MHz for ^{1}H and 175 MHz for ^{13}C) Bruker Advance III HD instrument with a 5mm indirect broadband cryoprobe or an 18.8 T (800 MHz for ^{1}H and 200 MHz for ^{13}C) Bruker Avance III HD instrument equipped with a 3 mm triple resonance broadband cryoprobe. Spectra were recorded in CD_3CN or $CDCl_3$ and referenced to solvent residual peaks (δ_H 1.94 and δ_C 118.26 or δ_H 7.26 and δ_C 77.16, respectively). Spectra were processed and analyzed using MestReNova 12.0.0. Vacuum liquid chromatography (VLC) was performed using SiliCycle's SiliaFlash F60, 40−63 μm silica gel. Supelco Supelclean ENVI-18 was used for solid-phase extraction (SPE). High-performance liquid chromatography (HPLC) separations were done with a Waters 1525 binary pump and either a Waters 2487 dual wavelength absorbance detector set at 254 nm or a Waters 2996 photodiode array detector, using two different columns: a 4.6 × 250 mm, C18-silica reversed-phase (Grace Alltima, 5 μm particle size) and a 4.6 × 250 mm phenyl-hexyl phase (Phenomenex Luna, 5 μm particle size). High-resolution mass spectrometry (HRMS) data were collected with a ThermoFisher Scientific LTQ Orbitrap XL ETD spectrometer in positive ion mode. The masses of isolated natural products were estimated by quantitative NMR (qNMR) using a capillary filled with benzene-d6 as an internal standard that was placed inside an NMR tube containing a known amount of caffeine and tubes containing the identified compounds dissolved in the same amount of solvent.[74]

1.4.2 Biological Material and Species Identification

The dark purple marine cyanobacteria were found carefully organized into curtains covering snapping shrimp holes located on reef slopes offshore of Tuvuca Island in Fiji. The cyanobacteria were collected on September 25, 2007 from two separate locations (S

17°44.43′, W 178°39.155′ and S 17°30.546′, W 178°42.443′) and combined based on similarity in sample appearance and habitat. Voucher specimens identified as collection G-0362 were stored at the University of the South Pacific and Georgia Institute of Technology in aqueous ethanol and formaldehyde. Bulk cyanobacterial sample was stored at the Georgia Institute of Technology in a −80 °C freezer.

The cyanobacterium was identified as *Moorea producens* through morphological and 16S rRNA phylogenetic analyses. Briefly, the ethanol-preserved genomic DNA of cyanobacterial specimen G-0362 was extracted with the DNeasy Blood and Tissue kit (Qiagen) using the manufacturer's protocol. Polymerase chain reaction (PCR) was utilized to amplify the single 16S rRNA gene fragment from genomic DNA using bacterial 16S rRNA primers, 27f, and 1492r.[75] A 25 μl reaction volume was used for PCR amplification with the following components: 200 μM of each dNTP, 50 ng of purified genomic DNA, 1 μM of each oligonucleotide primer, 1.0 U Taq DNA Polymerase, and 1× Standard PCR reaction buffer (NEB, Ipswich, MA). A GeneAmp PCR system 2700 thermocycler (Applied Biosystems, Foster City, CA) was used to perform the PCR amplification with the following parameters for temperature cycling: 94 °C for 4 min for initial denaturation followed by 40 cycles of amplification (each cycle = denaturation for 50 s at 94 °C, primer annealing for 50 s at 55 °C, and primer extension for 2 min at 72 °C). The incompletely synthesized DNA underwent final extension at 72 °C for 7 min. Agarose gel electrophoresis (1% wt/vol) was used to analyze the PCR product, and an ethidium bromide stain was applied before the gel was visualized with a UV transilluminator. Forward and reverse primers were utilized to sequence the PCR product and the CAP3 Sequence Assembly Program was used to manually edit and assemble sequences.[76] The assembled

16S rRNA sequence (1338 bp) was submitted to GenBank (accession no. MN960022). The blastn program was used to assess the sequence similarity of the assembled contig of cyanobacterial 16S rRNA to other known cyanobacteria from Family Oscillatoriaceae by comparing it with the non-redundant nucleotide database (NCBI).[77] To determine the closest phylogenetically related species of *Moorea producens*, the 16S rRNA sequence of collection G-0362 was compared with those of known representatives from Family Oscillatoriaceae (Order Oscillatoriales) and *Gloeobacter violaceous* was included as a distant evolutionary taxon. MEGA X [78] was used for phylogenetic analysis using the Maximum Likelihood method based on the Kimura 2-parameter model [79] with 1000 bootstrap iterations.

1.4.3 Extraction and Isolation

The cyanobacterial biomass (43 g) was freeze-dried (to 8.0 g) and exhaustively extracted (four times) using a 2:1 mixture of dichloromethane and methanol. The resulting crude extract (0.80 g) was purified by VLC with 80 mL of silica gel in a glass vacuum funnel (8 cm diameter by 9 cm high) with a glass frit. The fractions were collected using a stepped gradient of hexanes, EtOAc, and MeOH (nine fractions, 100% hexanes, 10% EtOAc/90% hexanes, 20% EtOAc/80% hexanes, 40% EtOAc/60% hexanes, 60% EtOAc/40% hexanes, 80% EtOAc/20% hexanes, 100% EtOAc, 25% MeOH/75% EtOAc, and 100% MeOH). The fractions eluting from 40% EtOAc/60% hexanes (14.1 mg), 60% EtOAc/40% hexanes (7.4 mg), 80% EtOAc/20% hexanes (5.8 mg), and 100% EtOAc (3.7 mg) were further separated using reversed phase SPE (stepwise gradient of decreasing polarity starting with 15% MeOH in H_2O to 100% MeOH, resulting in five fractions). Fractions 3, (50% MeOH in H_2O, 2.4 mg), 4 (75% MeOH in H_2O, 2.0 mg) and 5 (100%

MeOH, 4.2 mg) were subjected to C_{18}-silica HPLC (50% MeCN/50% H_2O held for 5 min, gradient from 50% MeCN/50% H_2O to 100% MeCN from 5 to 40 min, and 100% MeCN from 40 to 60 min at 1 mL/min) to obtain nearly pure **1**–**5**. Fractions containing **1** and **3** underwent one more round of purification with C18-silica HPLC (60% MeCN/40% H_2O + 0.05% trifluoroacetic acid (TFA) held for 5 min, gradient from 60% to 70% MeCN from 5 to 20 min, and 70% MeCN held from 20 to 25 min at 1 mL/min) to give **1** (t_R = 17.5 min, 18 µg) and **3** (t_R = 12.2 min, 6.9 µg). The same C_{18}-silica HPLC column was also used to purify **2** (isocratic method of 50% MeCN/50% H_2O + 0.05% TFA held for 25 min at 1 mL/min), resulting in pure **2** (t_R = 18.5 min, 340 µg). A mixture containing **4** and **5** was purified using phenyl-hexyl silica HPLC (gradient from 80% MeOH/H_2O to 90% MeOH/H_2O over 20 min at 0.8 mL/min) to give **4** (t_R = 14.5 min, 20 µg) and **5** (t_R = 15.7 min, 8.3 µg). The reported isolated yields do not include losses during separation or material subjected to bioassays and thus underestimate natural concentrations.

Kakeromamide B (**1**): ^{1}H and ^{13}C NMR data, see Table 1; HRMS (ESI) *m/z* $[M + H]^+$ calcd for $C_{42}H_{59}N_6O_7S$ 791.4166, found 791.4150; $[M + Na]^+$ calcd for $C_{42}H_{58}N_6O_7SNa$ 813.3985, found 813.3958.

1.4.4 Antimalarial and Cytotoxicity Assays

A standard method for evaluating antimalarial activity with asexual blood-stage *P. falciparum* and SYBR Green detection was used to assess the potency of extracts, fractions, and compounds.[80] Screening media was prepared from complete media supplemented with 0.05% Albumax II (but without human serum). Dr. David Fidock of Columbia University provided *P. falciparum* strain Dd2L, which was cultured with fresh O+

erythrocytes (TSRI Normal Blood Donation). Compounds were transferred to assay plates using a Labcyte ECHO acoustic liquid handler. Fresh and parasitized erythrocytes were prepared in screening media before inoculating plates (Multi-Flo; BioTek, VT) with a final hematocrit of 2.5% and a final parasitemia of 0.3%. The assay plates were incubated for 72 h in a chamber at 37 °C with a low oxygen gas formulation with daily gas exchanges. After incubation, a Multi-Flo liquid dispenser transferred SYBR Green lysis buffer to the wells, and the plates were incubated for another 24 h at room temperature to achieve optimal development of fluorescence signal, which was read by an Envision Multimode Reader (PerkinElmer, MA). Atovaquone, ganaplacide, and mefloquine were used as positive controls (EC_{50} = 0.00040, 0.0059, and 0.0029 μM, respectively).

Activity against liver-stage *P. berghei* was quantified for extracts, fractions, and pure compounds using a slightly modified 48 h luminescence-based assay.[81] The salivary gland of infected *Anopheles stephensi* was dissected to harvest *P. berghei*-ANKA-GFP-LucSMCON (Pb-Luc) sporozoites (originally received from Dr. Ana Rodriguez of NYU School of Medicine; last round of testing to evaluate pure **1**, **3**–**5** used infected mosquitoes from Elizabeth Winzeler at UCSD and Dennis Kyle at UGA) which were filtered through a 20 μm nylon net filter twice (Steriflip, Millipore, MA), counted with a hemocytometer, and adjusted to achieve a final concentration of 200 sporozoites/1 μL in the assay media (DMEM without Phenol Red (Life Technologies, CA), 5% FBS, and 5 × Pen−Strep and glutamine (Life Technologies, CA)). A Multi-Flo (BioTek, VT) with a 1 μL cassette was used to transfer purified sporozoites, 1×10^3 sporozoites per well (5 μL), to assay plates containing HepG2 cells. After incubation at 37 °C for 48 h, a bioluminescence measurement was taken to assess the liver-stage growth. More specifically, media was

removed by inverting the plates, and spinning them at 150 × g for 30 s, and 2 μL per well of BrightGlo (Promega, WI) was added for quantification of Pb-Luc viability. The luminescence was measured immediately after addition of the luminescence reagent using an Envision Multilabel Reader (PerkinElmer, MA).

A previously described method was utilized to evaluate cytotoxicity against HepG2 and HEK293T cells as a measure of general human toxicity.[82] Assay data generated for *Plasmodium* was analyzed with a Genedata Screener (v13.0-Standard). Inhibitors (puromycin for cytotoxicity and atovaquone for liver-stage parasites) were subtracted from neutral controls to normalize data. The Smart Fit function of the Genedata Analyzer generated dose-response curves that were used to calculate the half-maximal effective concentrations (EC_{50}).

1.4.5 Computational Binding Predictions

FINDSITE$^{comb2.0}$ [46] was applied to screen cyanobacterial natural products against the whole genome of *P. falciparum* (isolate 3D7) (PF). FINDSITE$^{comb2.0}$ builds structural models using a threading approach by taking the protein amino acid sequence as input and applying TASSER refinement.[83] Models were built for 4,962 (92.5%) protein sequences out of a total of 5,364 PF sequences downloaded from UniProt (www.uniprot.org). For each target protein, the pockets were identified in their respective models and compared to the ligand-binding pockets located in PDB [84] structures as well as ChEMBL [85] and DrugBank [86] libraries. Pockets that best matched target pockets were selected, and their corresponding binding ligands were employed as template ligands. These template ligands were used for virtual screening as seed ligands for a given molecule with a fingerprint

comparison method to evaluate the binding probability of the molecule to the protein targets. The mTC virtual screening score, a measure of the similarity of the given molecule to the template ligands of a protein target in FINDSITE$^{comb2.0}$, was used to rank the targets. The mTC correlates with the likelihood of the protein target being a true target of the molecule, and its value ranges between 0 and 1 with 1 indicating the best fit. An mTC of 0.5 corresponds to the expected precision of ~0.76 based on large scale benchmark statistics.[46]

1.4.6 Actin Polymerization Assay

The computationally predicted binding of **1** to actin was experimentally evaluated using a rabbit muscle actin polymerization assay kit from Abcam (kit ab239724) using the manufacturer's protocol. Mean signal for n = 3 (actin polymerization control, solvent control, and background) or n = 2 (four different concentrations of latrunculin A and kakeromamide B (**1**)) replicates was acquired for time points taken every 30 s for 1 h on a Synergy H4 plate reader. The results were plotted in GraphPad Prism 8 with an exponential plateau curve.

CHAPTER 2. ECOLOGICAL ROLE OF THE RED ALGAL NATURAL PRODUCT PEYSSONNOSIDE A

This chapter is an expanded report of findings included in B.K. Chhetri, S. Lavoie, A.M. Sweeney-Jones, N. Mojib, V. Raghavan, K. Gagaring, B. Dale, C.W. McNamara, K. Soapi, C.L. Quave, P.L. Polavarapu, and J. Kubanek, *Journal of Organic Chemistry*, 2019, 84(13), 8531-8541; https://pubs.acs.org/doi/10.1021/acs.joc.9b00884. Permission for reuse of portions of this publication was obtained from ACS and the letter granting reuse is included in Appendix B.

2.1 Abstract

In the underwater environment, many organisms make use of secondary metabolites for defense against consumers, competitors, and pathogens. For sessile organisms, chemical defenses are especially important: numerous examples exist of secondary metabolites from marine sponges and algae acting as feeding deterrents towards consumers, antimicrobials targeting the many pathogenic microbes that exist in seawater, allelopathic chemicals for competing with neighboring organisms for space in crowded reef environments, and antifouling agents that prevent biofouling on organismal surfaces. The red alga *Peyssonnalia* sp. produces a unique diterpene glycoside, peyssonnoside A (**7**), in relatively high abundance (0.42% of dry weight). Field and shore-based experiments exploring various ecological roles for this secondary metabolite led to a conclusion that **7** functions as an antimicrobial defense, based on significant growth inhibition of the saprophytic marine fungus *Dendryphiella salina* when exposed to realistic concentrations of **7**. Additionally, based on the lack of deterrence observed in antifeedant assays with a

generalist crustacean grazer and observed biofouling in field antifouling assays, there is no evidence that **7** functions as a chemical defense against herbivores or microbial fouling.

2.2 Introduction

The field of marine chemical ecology began several decades ago with the goal of understanding the biological roles of marine natural products by combining the expertise of natural product chemists and ecologists.[87] Natural products are genetically encoded for biosynthesis by specific organisms and exhibit specialized functions related to defense against consumers, competitors, pathogens, and biofoulers; settlement cues for larvae; and pheromones for mate finding.[88] Experimental methods to probe the roles of secondary metabolites have greatly benefited from the interdisciplinary nature of this field. For example, expertise of field ecologists informed the importance of applying ecologically relevant doses that represent realistic exposure of organisms to natural products while chemists provided valuable insight into which molecules are responsible for the observed interactions.[89]

Natural products found in high abundance in organismal tissues are good candidates for testing hypotheses about possible ecological roles. An example of such a natural product is the novel diterpene glycoside peyssonnoside A (**7**) (Figure 5) isolated from a red alga *Peyssonnelia* sp.[90] Chemical ecology experiments sought to answer if **7** acts as an antifeedant agent against an omnivorous generalist consumer, if **7** prevents the surface attachment of biofouling microbes, and/or if **7** inhibits growth of a marine fungus. For each experiment, realistic "enemies" were chosen to model the natural environment of

Peyssonnelia sp. and attempts were made to design experiments using near-natural concentrations of **7**.

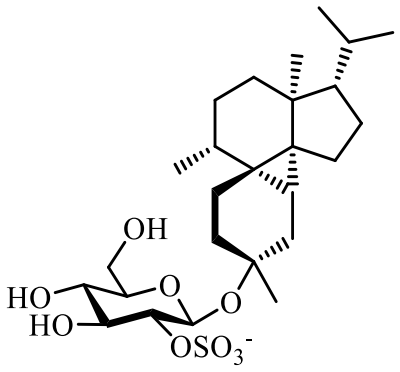

Figure 5. Diterpene glycoside peyssonnoside A (**7**) isolated from the marine red alga *Peyssonnelia* sp.[90]

2.3 Results and Discussion

2.3.1 Evaluation of Antifeedant Properties

Using a standard feeding assay,[26] peyssonnoside A (**7**) was evaluated for feeding deterrence against one generalist marine omnivore, the hermit crab *Clibanarius striolatus*. When incorporated into artificial diets at a concentration of 1.1 mg/ml, which is 20% the natural abundance of **7** in the alga, **7** was ineffective at deterring feeding by *C. striolatus* collected from an intertidal zone off Ono Island in Fiji: both control foods and food impregnated with **7** were consumed equally (Figure 6).

Generalist consumers eat a wide variety of foods and are a good model to use when determining the presence of antifeedant properties since a molecule that deters a generalist

consumer will likely deter other consumers as well.[91] A specialist, on the other hand, has a much more limited diet and in some cases has evolved an ability to consume a food source that is deleterious to other consumers, such as the mollusc *Stylocheilus striatus* that feeds on cyanobacteria *Lyngbya* spp. that is toxic to generalist consumers.[92] Since **7** did not deter consumption by a generalist consumer, at least at the concentration tested, it likely does not have antifeedant properties against generalist consumers. The experiment could have been improved if a larger quantity of **7** had been available, enabling testing at full natural concentration. The nutritional content of the artificial food is also an important component of the experimental design as it should ideally match the nutritional content of the organism being modeled, in this case *Peyssonnelia*. For this experiment, the artificial food was assembled using a similar formulation to one devised for another type of calcified alga, *Halimeda*.[26] To determine the nutritional content of *Peyssonnelia*, the ash-free dry mass was calculated by combusting dried algal material in a furnace (114 mg/mL). This artificial food created for the feeding assay used an equivalent amount of the freeze-dried green alga *Ulva*, an alga that is palatable to a wide range of consumers.

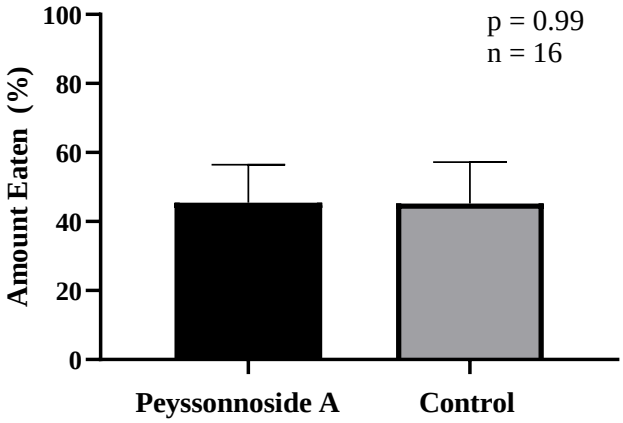

Figure 6. Response of hermit crabs *Clibanarius striolatus* to food laced with 1.1 mg/mL peyssonnoside A (**7**). These data indicate that **7** does not deter hermit crab feeding (mean ± standard error).[90]

*2.3.2 Surface Localization of Peyssonnoside A (**7**)*

Before evaluating whether **7** reduces surface fouling or exhibits antimicrobial properties against an ecologically relevant pathogen, an experiment was performed to determine if **7** is present on the surface of *Peyssonnelia* sp. A qualitative method similar to what was proposed by de Nys et al. that employed a hexane surface extraction indicated that **7** is in fact present on the surface of *Peyssonnelia* sp. (Figure 7), supporting its putative role in surface-mediated defense.[93] Hexane was chosen for the surface extraction because a short exposure (less than 60 seconds) minimizes damage to algal tissue, whereas other organic solvents typically lyse cells even during brief extraction. Since the collection of *Peyssonnelia* sp. contained individuals with various morphologies, surface extractions were performed on algal pieces ranging from highly calcified with a tan color to pieces that were very fleshy with a red to maroon color. This comparison revealed that fleshier algal

pieces with red coloration contained relatively more **7** than more highly calcified pieces (Figure 7), further supporting the surface defense hypothesis and additionally suggesting that more vulnerable tissues require greater amounts of **7** for protection, consistent with the optimal defense theory.[94,95] In addition to evaluating the presence of **7** on the surface of algal tissues, a preliminary experiment confirmed the partial extractability of **7** from a surface into hexanes, albeit only 0.11% of **7** was removed from a glass surface by hexanes while the remaining residue was removed with methanol. This suggests that the amount of **7** extracted from the surface of *Peyssonnelia* sp. by hexane is only a small portion of what is present on the algal surface, further supporting the high surface abundance of **7** and the role of **7** in surface-mediated ecological interactions.

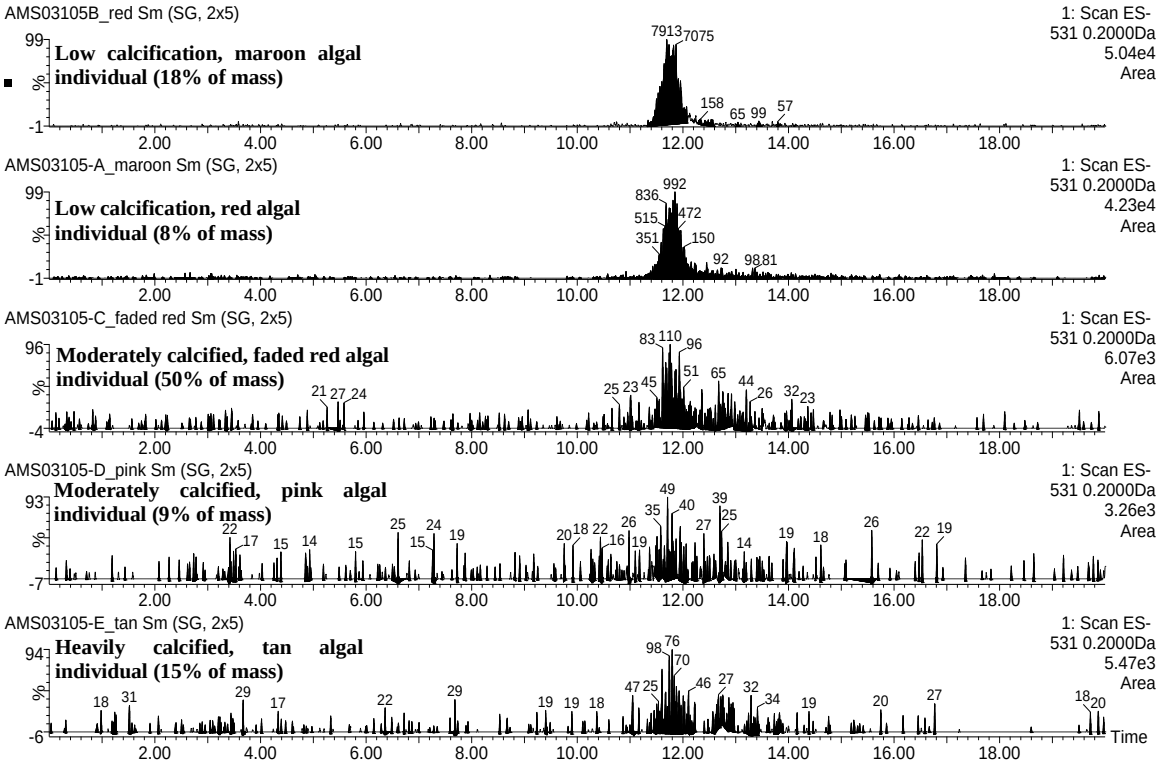

Figure 7. Extracted LC/MS chromatogram of *m/z* 531 corresponding to **7** and calculated peak area from surface extracts of *Peyssonnelia* sp. individuals ranging from heavily calcified (tan) to fleshy (red and maroon). The inset of each chromatogram reports the relative amount of each individual algal specimen extracted for LC/MS analysis expressed as a percentage of the total mass of algae analyzed in this experiment. Larger amounts of **7** were extracted from the surfaces of algal specimens with less observed calcification.

2.3.3 Assessment of Peyssonnoside A (7) as an Antifouling Agent

Evaluation of whether **7** deters biofouling was accomplished using a modified version of the method presented by Henrikson and Pawlik.[96] In short, **7** was incorporated into a phytagel substrate at the same concentration used for the antifeeding assay, 1.1 mg/mL, and paired with a solvent-only control which was then adhered to a petri dish. The petri dish was suspended in ocean water off the coast of Ono Island, Fiji, near a coral reef

where *Peyssonnelia* sp. naturally occurs, for a total of four days, exposing a natural community of fouling organisms to **7** in the field. The experiment was not of long enough duration to assess the settling of larval propagules and algae. Analysis of settled bacteria revealed that there was no significant difference in the amount of biofouling present on the surface of phytagel containing **7** versus a phytagel control without **7** (Figure 8).

Although staining indicated that there was some microbial biofouling occurring within the four day experiment, there were several issues noted during the experiment that suggested an antifouling role for **7** should not be ruled out. First, growth of fouling organisms was not visible to the naked eye on phytagel surfaces after exposure to ocean water for four days, appearing similar to before the gels were submerged. Second, the stain used for determining the presence of cellular respiration on the surface of the gels, 2,3,5-triphenyl tetrazolium chloride, is light-sensitive; the field setting of this experiment made it difficult to avoid light exposure during staining. Thus, it is possible that the observed color change on stained phytagel resulted from light exposure rather than an indication of the presence of microbial biofoulers. Finally, attempts to extract RNA from gel samples preserved in RNAlater did not yield any RNA suggesting that settlement of biofoulers on the gels was negligible. One possible reason for the lack of biofouling on phytagel surfaces could be that the time period the gels were deployed was too short. Overall, there is no experimental evidence for an antifouling role but based on the high surface abundance of **7**, we suspect that a longer exposure period could have resulted in statistically significant deterrence of biofouler settlement on the surface of gels containing **7**.

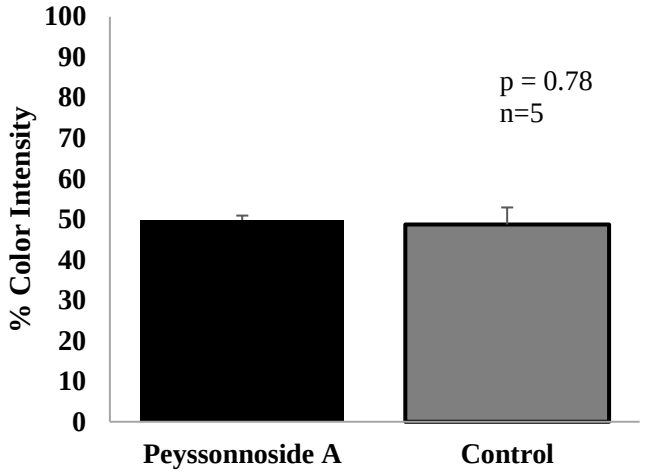

Figure 8. Relative biofouling on phytagel surfaces treated with peyssonnoside A (**7**) and a paired solvent control, as indicated by the average color intensity with higher intensity values corresponding to higher microbial content (mean ± 1 standard deviation). Gels were hung in ocean water for 4 days before being removed, stained, and imaged.

*2.3.4 Antifungal Properties of Peyssonnoside A (**7**)*

When peyssonnoside A (**7**) was tested for antifungal effects on the saprophytic filamentous fungus *Dendryphiella salina*,[97] a dose-dependent inhibition of *D. salina* growth was observed with an IC_{50} of 0.14 µM (Figure 9). Considering that the natural abundance of **7** is 5.4 mg per mL of wet alga, inhibition of *D. salina* at a concentration of 0.070 µg/mL indicates that **7** is both a potent and a highly abundant antifungal agent present in and on algal tissues. Microscopic imaging of media containing **7** indicated that this secondary metabolite promoted morphological changes consistent with an antifungal effect (Figure 9). Taken together with the high natural abundance of **7**, these data are suggestive that **7** is a novel antimicrobial chemical defense.

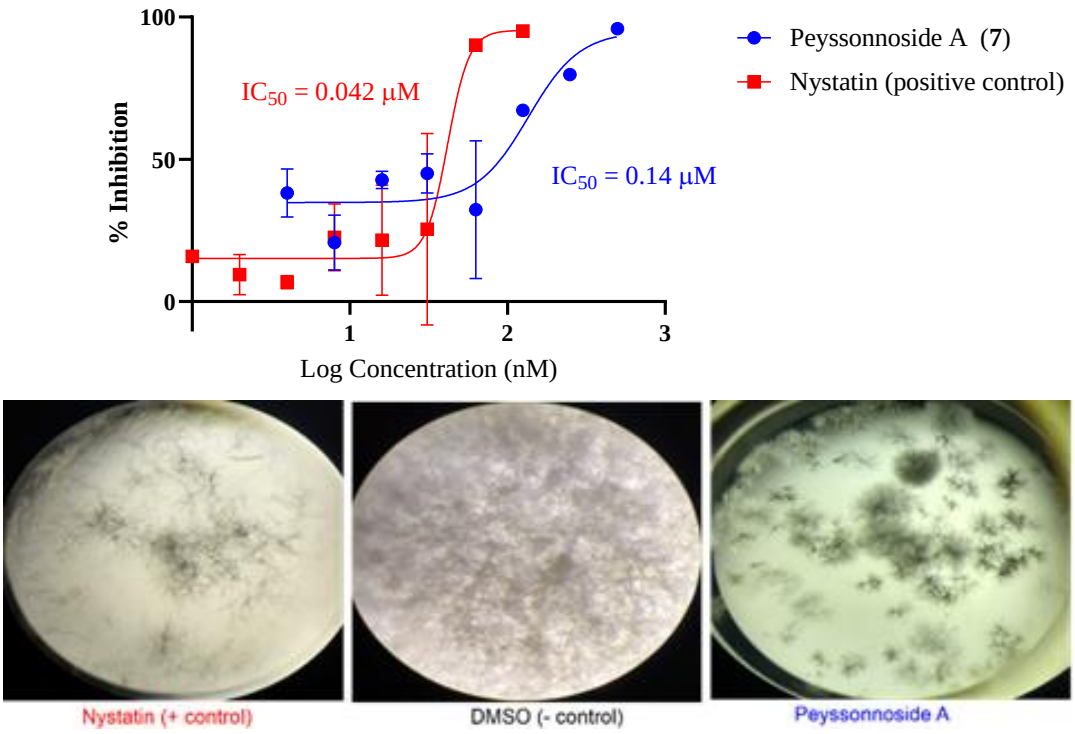

Figure 9. Top: Growth inhibition of the fungus *Dendryphiella salina* by peyssonnoside A (**7**) compared to the known antifungal drug nystatin (n = 3, mean ± standard error). Bottom: Comparison of fungal growth in the presence of nystatin, DMSO, and **7** showing the morphological change in the fungal colonies exposed to **7**.[90]

Previous studies surveying the antimicrobial defenses of seaweeds have found that extracts and pure natural products from these marine organisms typically exhibit activity against one or more pathogenic marine microorganisms suggesting that this type of defense is fairly ubiquitous.[23,98,99] For the present experiment, *D. salina* was chosen for its global distribution in the marine environment; however, since it is a saprophytic fungus that breaks down dead and decaying organic matter, its relevance as a threat to live algae is uncertain. We failed to successfully culture the pathogenic fungus *Lindra thalassiae*, which would have been more relevant for evaluating the defensive properties of **7** against disease-causing fungi. Limited studies suggest that antifungal marine natural products that inhibit

D. salina also inhibit *L. thalassiae* [23,100] meaning that even without data from additional fungi, **7** may function as a general antifungal agent.

2.4 Materials and Methods

2.4.1 Specimen Collection

Peyssonnoside A (**7**) was isolated from *Peyssonnelia* sp. (G-1163) collected on March 17, 2012 from Singi Locale, Tetepare Island, Solomon Islands (S 8°42.561', E 157º26.500') and *Peyssonnelia* sp. (G-1588) collected on June 17, 2017 off Uepi Island, Solomon Islands (S 8°26.549′, E 157º56.695′).[90] *Peyssonnelia* sp. co-occurs with the organisms used for the ecological experiments detailed in this chapter.

2.4.2 Surface Extraction

Before evaluating if **7** was present at the surface of *Peyssonnelia* sp., solubility of **7** in hexanes, the solvent chosen for surface extraction,[93] was assessed. A solution containing a small amount of **7** was added to a glass scintillation vial and dried. Two mL of hexanes was added to the scintillation vial, shaken for 30 seconds, and transferred to a clean vial. Both vials were dried then redissolved in methanol for LC/MS evaluation. Comparison of the chromatographic peak area for **7** removed by hexanes versus the residual **7** remaining in the original scintillation vial revealed that 0.11% of **7** was removed by hexanes, which was sufficient for detection by LC/MS.

A collection of *Peyssonnelia* sp. (G-1588) known to contain **7** was chosen for evaluation of the surface localization of **7**. Morphological variations related to the level of calcification were noted and as a result, five distinct algal individuals were selected, ranging from heavily calcified with minimal red pigment to red and maroon colored leaves

with little calcification. The individual samples were patted dry to remove excess moisture without damaging the surface of the tissue, weighed, and then added to a scintillation vial containing 2 mL of hexanes. The samples were agitated for 30 seconds and then removed. The remaining solution was dried, redissolved in methanol, and evaluated by LC/MS. The peak associated with **7** (*m/z* 531) was extracted from each chromatogram to determine if **7** was present and if the morphological characteristics impacted the relative amount extracted from the surface of the algal specimen.

2.4.3 Ash-free Dry Mass Measurement

After measuring the wet mass of *Peyssonnelia* sp. G-1588 (1.62 g), the alga was freeze-dried resulting in a dry mass of 1.30 g (80% of the wet mass). The dried algal pieces were ground with a mortar and pestle, weighed, and evenly distributed to five different porcelain crucibles. The crucibles were placed in a Fisher Scientific Isotemp Muffle Furnace set to 450 °C for 6 hours.[26] The remaining ash was measured and subtracted from the starting dry mass to obtain the ash-free dry weight (22.7 ± 0.3 mg, n=5, 9.0% of the starting dry mass). This value was divided by the volume of the alga (1.0 mL total, 0.20 mL per replicate) subjected to ash-free dry mass analysis to approximate nutritional content (114 mg/mL).

2.4.4 Antifeedant Assay

Artificial food was prepared using a mixture of molten agar (0.02 g/mL) and *Ulva* sp. (100 mg/mL), a green alga palatable to a wide range of marine herbivores, incorporated into window screen.[26] Peyssonnoside A (**7**) was dissolved in 0.48 mL methanol and added to 10 mL of the artificial food, resulting in a final concentration of 1.1 mg/mL which is

approximately 20% of the natural concentration of **7**, lower than its actual abundance in algal tissue but still a considerably high concentration for a natural product. The full natural concentration was not used due to constraints on the total amount of natural product available for ecological studies. Control foods were prepared by using an equivalent amount of solvent in the artificial food mix. One square containing artificial food with **7** and a second square with the control food were placed in deli dishes housing hermit crabs (2 food squares per deli dish) (Figure 10). After approximately 50% of the control or treated food available to any given hermit crab was consumed, the food-containing window screens were removed and analyzed for total amount consumed of each treatment by counting the number of empty squares versus total that started with food, analyzing with a two-tailed t-test. Replicates where crabs ate less than 10% or more than 90% of the total food available to them were excluded. Of the 36 crabs housed individually for the assay, 16 produced usable results.

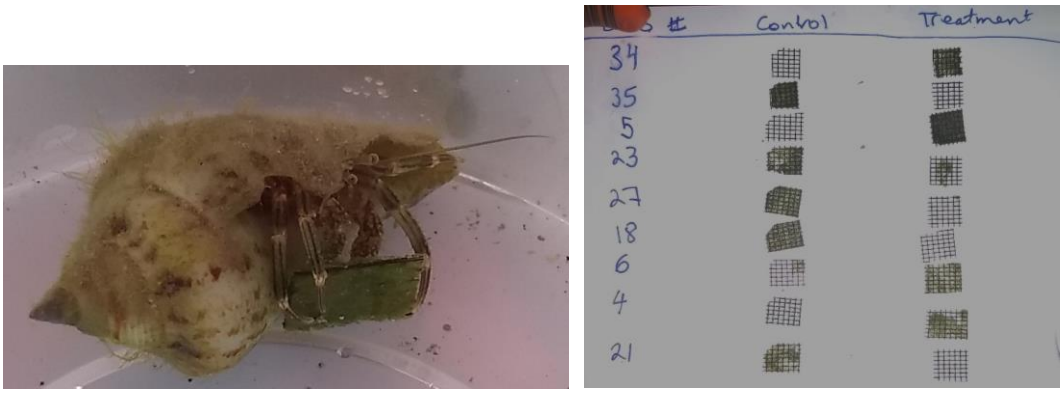

Figure 10. Feeding assay design using the hermit crab *C. striolatus*, consuming artificial food incorporated into a square of window screen (left). The resulting output of the feeding assay was window screen squares with varying degrees of artificial food consumed by the crab (right; "treatment" condition refers to artificial food with the addition of **7**).

2.4.5 Antifouling Assay

Peyssonnoside A (**7**) or methanol (solvent control) was incorporated into phytagel (n = 5 for each condition) and hung for four days off a floating dock in Oneta Bay off Ono Island, Fiji (18°53'07.3"S, 178°30'39.6"E) (Figure 11). Phytagel was prepared at the field site by adding 1.5 g of phytagel powder to 50 mL of boiling tap water (0.03 g/mL). Peyssonnoside A (**7**) was dissolved in 0.30 mL methanol and added to 6 mL of hot phytagel solution (final concentration 1.7 mg/mL; 30% of natural concentration). This mixture was split into five replicates applied to window screen squares adhered to the surfaces of petri dishes (Figure 11). Solvent controls were prepared using an equivalent ratio of methanol to phytagel and the resulting gels were applied to a second petri dish glued to the one containing **7**. The petri dishes were tied to a rope before being deployed under the floating dock for 4 days. After removal from the field, the plates were sprayed with a 1% (w/v) solution of 2,3,5-triphenyl tetrazolium chloride, which is a colorless water-soluble dye reduced to the red, insoluble compound formazan by respiration-dependent enzymatic processes in cells.[101,102] Images were taken of each gel from the same distance and evaluated using ImageJ software.

Figure 11. Experimental set-up to evaluate if peyssonnoside A (**7**) prevented fouling on the surface of phytagel submerged in ocean water for four days. Gels were adhered to window screen (for quantification purposes) that was attached to petri dishes (left image) with paired controls prepared in a similar fashion and attached to the back of the plate containing gel infused with **7**. Plates were deployed under a floating dock off Ono Island, Fiji, for 4 days (right image).

2.4.6 Antifungal Assay

Fungal culture was grown at 24 °C in 790 By+ medium (1.0 g/L yeast extract, 1.0 g/L peptone, 5.0 g/L D-(+)-glucose, in 1 L of seawater). A tissue grinder was used to homogenize fungal hyphae before distributing *D. salina* in 790 By+ media to a sterile 96-well plate. The antifungal assay was performed with a 1:1 serial dilution ranging from 0.0070 µM to 0.94 µM for **7**, much lower than the natural concentration of **7** in *Peyssonnelia* sp. which is 10mM.[90] Nystatin was used as positive control at concentrations of 0.14 µM to 0.0010 µM. After three days, relative cell concentrations were measured as turbidity using a BioTek ELx800 Absorbance Microplate Reader at 600 nm. Percent growth inhibition at each concentration was calculated relative to fungus exposed to solvent (DMSO). Images were recorded using a dissecting microscope to

confirm that elevated optical density readings corresponded to fungal growth. The growth inhibition data were fit to a sigmoidal dose-response curve using GraphPad and the IC_{50} of **7** was calculated after 3 days incubation with *D. salina*.

CHAPTER 3. DISCOVERY OF ANTHELMINTIC CYANOBACTERIAL NATURAL PRODUCTS FROM A MIXED CYANOBACTERIAL COLLECTION

3.1 Abstract

Although more than 500 million people suffer from hookworm infections per year worldwide with observed resistance to all available anthelmintic drugs, research into new therapeutic agents has been neglected. Collaboration with the Aroian lab at the University of Massachusetts Medical School resulted in identification of a mixture of cyanobacterial natural products from a cyanobacterial collection that exhibited potent and reproducible hookworm inhibition. Extracts, semi-purified chromatographic fractions, and near-pure natural products reproducibility decreased hookworm survival and motility, an indicator of deleterious effects on the worm's neuromuscular system which is a viable drug target. Efforts are currently ongoing to identify and characterize natural product(s) within the mixture responsible for the observed anthelmintic activity.

3.2 Introduction

According to a survey of neglected tropical disease experts, there is consensus that current drugs, vaccines, and vector controls are not adequate for the elimination of soil-transmitted helminth (STH) infections, including those caused by hookworms.[22] Infectious worms emerge from contaminated soil, invade a human host by penetrating the skin, establish themselves in the host's intestines, and cause illness and disability associated with diminished nutritional status such as growth retardation, anemia, and

cognitive impairment.[103] In the past decade, five prevalent neglected tropical diseases (NTDs) including those caused by STHs were prioritized by the World Health Organization (WHO) and the international community as targets for eventual eradication as a global health problem.[104,105] This decision provided opportunities to develop and deploy treatments for diseases that had otherwise been underfunded since they disproportionately impact impoverished regions and result in morbidity more often than death. Partnerships established between public and private entities have resulted in success in controlling some NTDs including lymphatic filariasis, trachoma, and onchocerciasis, especially through use of mass administration of drugs and infection surveillance of impacted areas, although the low efficacy of currently available anthelmintic compounds (Figure 12) and the evolution of resistance have presented challenges in control of STH infections.[106-111] Additionally, inadequate sanitation often leads to reinfection necessitating periodic de-worming, providing further opportunity for drug resistance.[112-114] In order to effectively control STH infections in vulnerable human populations long term, it is imperative that new anthelmintic therapeutics are added to the drug discovery pipeline to combat the rising incidence of resistance and improve efficacy of available treatment options.

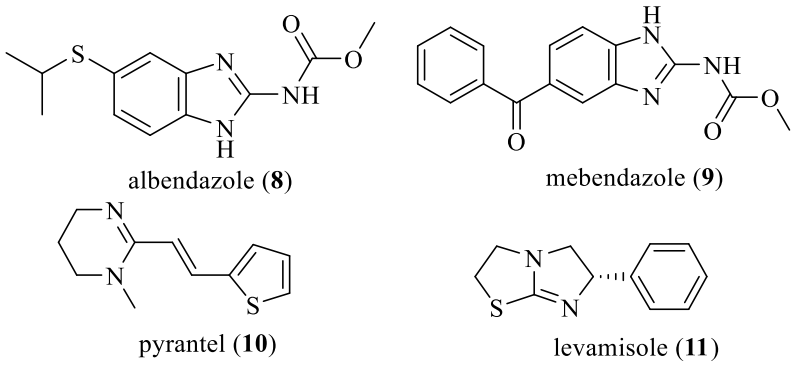

Figure 12. Molecular structures of currently available drugs for the treatment of infectious hookworms.[115-117]

Assessing pure compound or extract libraries for anthelmintic properties has been hindered by the low-throughput nature of STH assays and lack of validation to ensure proposed screening systems accurately predict activity against adult STHs responsible for the disease burden while minimizing false positives and false negatives.[118] Adult STHs are obligate parasites that require a host for survival, complicating assay design and resulting in low-throughput pipelines for screening of drug candidates. High-throughput screening assays using *C. elegans*, which are free-living nematodes that are easier to maintain, have been associated with a high false negative rate. This is attributed to *C. elegans* having a genome optimized for host-free survival for the duration of its lifespan which improves biotransformation and elimination of anthelmintic drugs bydetoxification enzymes.[119] From evaluation of multiple screening methodologies (including use of several life stages of *C. elegans* and the hookworm *Ancylostoma ceylanicum*),[118] an assay that used the free-living egg-to-larval (E2L) stage of *A. ceylanicum* for screening a library of 1280 approved drugs most accurately predicted efficacy against adult hookworms while minimizing the number of false negatives. Additionally, the E2L stage

provides an advantage for drug screening since it can be accessed from feces of infected (hamster) host rather than by host dissection. Hits identified in the E2L screen led to a higher false positive rate than other screening methods necessitating a secondary screen with adult infectious worms to confirm relevant anthelmintic compounds.

Anthelmintic hits from a marine organism extract library at Georgia Tech were identified via the aforementioned screening methodology. Use of this multi-step screening approach enabled exploration of an extract from a mixed collection of cyanobacteria with promising activity against both larval and adult stages of hookworm. Efforts are currently ongoing to characterize natural products present in the worm active fractions from this collection.

3.3 Results

3.3.1 Screen for Anthelmintic Activity

E2L screening of 324 extracts from a diverse array of marine organisms collected in Fiji and the Solomon Islands resulted in identification of 68 extracts that inhibited egg hatching or impaired larval development of the hookworm *A. ceylanicum* (Table 4). Of these, ten were prioritized based on availability of adequate field-collected sample for bioassay-guided fractionation of extracts and on a lack of prior literature reports of natural products associated with its taxonomic group. Of the ten prioritized organisms, a collection containing a mixture of cyanobacterial species (sample G-0978) exhibited promising activity against E2L and adult hookworms in subsequent follow-up screening while the other nine collections exhibited weak or no activity against E2L worms after scaled-up extraction of field-collected samples. Further separation of the extract using liquid/liquid

partitioning revealed that the dichloromethane-soluble extract fraction was the most potent with inhibition of E2L worms at 1.25 µg/mL and substantial reduction in motility of adult hookworms, as indicated by an average motility index of 1.2 after 24 hours and 0.80 after 48 hours (Table 5).

.

Table 4. Collections identified as hits (68 total from 324 extracts screened) in preliminary E2L *Ancylostoma ceylanicum* hookworm screening of the Georgia Tech marine organism extract library. Extracts were considered hits if they produced full or near-full inhibition of egg hatch or larval development at 5 µg/mL. Bolded collections were selected for further evaluation based on availability of field-collected samples for natural product isolation as well as taxonomic interest.

Collection Identifier	Taxonomy
G-0998	ascidian *Polyandrocarpa polypora*
G-0910	cyanobacterium *Lyngbya* sp.
G-0913	**red alga *Peyssonnelia* sp.**
G-0914	cnidarians *Eleutherobia* sp.
G-0920	green alga *Tydemania expeditionis*
G-0923	unknown cyanobacterium
G-0932	green alga *Tydemania expeditionis*
G-0950	**brown alga *Lobophora* sp.**
G-0951	sponge *Axinyssa* sp.
G-0956	sponge *Acanthella cavernosa*
G-0964	sponge *Hippospongia* sp.
G-0967	sponge *Halichondria sp.*
G-0976	sponge *Axinyssa* sp.
G-0978	**mixed cyanobacterial collection**
G-0979	unknown sponge
G-0980	sponge *Diacarnus spinipoculum*
G-0984	sponge *Dysidea* sp.
G-0990	**green alga *Valonia aegagropila***
G-0991	sponge *Dysidea* sp.
G-0995	unknown sponge
G-1000	sponge *Dysidea* sp.
G-1004	**red alga *Peyssonnelia* sp.**
G-1006	sponge *Haliclona* sp.
G-1009	unknown sponge
G-1018	unknown sponge

Table 4 (continued)

G-1025	**red alga *Laurencia* sp.**
G-1046	unknown sponge
G-1047	cnidarians *Rumphella suffruticosa*
G-1048	sponge *Phyllospongia* sp.
G-1049	sponge *Coscinoderma mathewsi*
G-1054	sponge *Acanthella cavernosa*
G-1056	**green alga *Caulerpa* sp.**
G-1058	sponge *Jaspis* sp.
G-1085	sponge *Diacarnus spinipoculum*
G-1093	**green alga *Tydemania expeditionis***
G-1098	sponge *Axinyssa* sp.
G-1103	sponge *Haliclona* sp.
G-1106	unknown sponge
G-1116	unknown sponge
G-1120	sponge *Thorecta* sp.
G-1122	sponge *Dysidea* sp.
G-1131	sponge *Dictyodendrilla* sp.
G-1146	cnidarians *Junceella* sp.
G-1147	sponge *Axinyssa* sp.
G-1149	cnidarian *Briareum* sp.
G-1150	**red alga *Amphiroa* sp.**
G-1152	sponge *Dysidea* sp.
G-1153	sponge *Lamellodysidea* sp.
G-1154	sponge *Dysidea* sp.
G-1156	unknown sponge
G-1159	unknown sponge
G-1163	red alga *Peyssonnelia* sp.
G-1173	unknown sponge
G-1174	sponge *Spongosorites* sp.
G-1177	sponge *Ianthella basta*
G-1178	unknown sponge
G-1184	sponge *Dysidea* sp.
G-1186	sponge *Aka* sp.
G-1188	**sponge *Agelas* sp.**
G-1190	sponge *Callyspongia* sp.
G-1192	sponge *Callyspongia* sp.
G-1193	unknown foraminifera
G-1196	sponge Callyspongia sp.
G-1197	sponge Axinyssa sp.
G-1198	sponge *Axinella* sp.
G-1202	sponge *Cladocroce* sp.

Table 4 (continued)

G-1226	unknown sponge
G-1229	sponge *Thorecta* sp.

Table 5. Activity of extracts from cyanobacterial collection G-0978 against the E2L and adult stages of the hookworm *Ancylostoma ceylanicum*. The dichloromethane-soluble extract fraction from G-0978 exhibited the most promising activity against *A. ceylanicum.* For E2L screening, black shading indicates full or near-full inhibition of egg hatch or larval development at the indicated concentration while gray means only partial inhibition. The average motility index for adult hookworm screening is based on qualitative observations made for six individual worms with the following assignments: 0 – dead worm; 1 – motile after stimulation by touch; 2 – motile; and 3 – highly motile.

		***A. ceylanicum* E2L Screening Concentration (µg/mL)**				***A. ceylanicum* Adult Screening Average Motility Index (10 µg/ml, n=6 worms)**	
Collection ID	**Type of fraction**	**10**	**5**	**2.5**	**1.25**	**24 hours**	**48 hours**
G-0978 (mixed cyanobacterial collection)	crude extract					2.2	1.0
	hexane-soluble extract fraction					2.3	1.8
	dichloromethane-soluble extract fraction					1.2	0.8
	recombined liquid/liquid partition fractions					2.0	2.7

3.3.2 Taxonomic Characterization of G-0978

The cyanobacterial collection was tentatively identified as *Symploca* sp. based on morphological examination (Figure 13). However, analysis of the DNA voucher specimen by Bhuwan Chhetri and Dr. Nazia Mojib of the Kubanek lab using 16S rRNA phylogenetic analysis revealed that collection G-0978 is in fact a mixture of different cyanobacterial species. Although 16S rRNA was successfully amplified from the genomic DNA extracted

from the specimen G-0978 (Figure 14), initial sequencing reactions were unsuccessful. Upon analysis of the chromatograms, there were multiple peaks suggesting presence of more than one genotype, reflecting the existence of more than one cyanobacterial species in the collection. With multiple attempts and separate sequencing reactions, use of reverse primer 1492r produced four different 16S rRNA sequences of ~250 bp. The resulting phylogenetic tree indicates that sequences 1-3 are more closely related to each other than the other known cyanobacterial species (Figure 15). Additionally, sequence 4 is a unique species that does not cluster with any of the other species in the phylogenetic tree. The cyanobacteria of this phylogenetic tree fall into different cyanobacterial subsections, which are classifications based on morphological differences.[120] *Halothece* sp. and *Chroococcidiopsis* sp. are unicellular cyanobacteria that belong to subsections I and II, respectively. *Leptolyngbya* sp., *Oscillatoria salina*, and *Prochlorothrix* sp. all belong to subsection III which consists of filamentous cyanobacteria of varying morphological complexity. The clustering of filamentous cyanobacteria with unicellular species in the phylogenetic trees is attributed to the polyphyletic origins within filamentous cyanobacteria.[121] Comparison of known morphologies with taxonomic information in the hierarchical cluster resulted in identification of *Symploca* as the most morphologically similar to the tuft-like structure observed in collection G-0978 (Figure 13). However, since the species identified from collection G-0978 are in distinct clusters in the phylogenetic tree, they are most likely not *Symploca* and might instead belong to either a genus of cyanobacteria that has not yet been classified by 16S rRNA or a novel cyanobacterial genus.

Figure 13. Photograph of a tuft from the cyanobacterial collection G-0978 soon after the specimen was collected from the field.

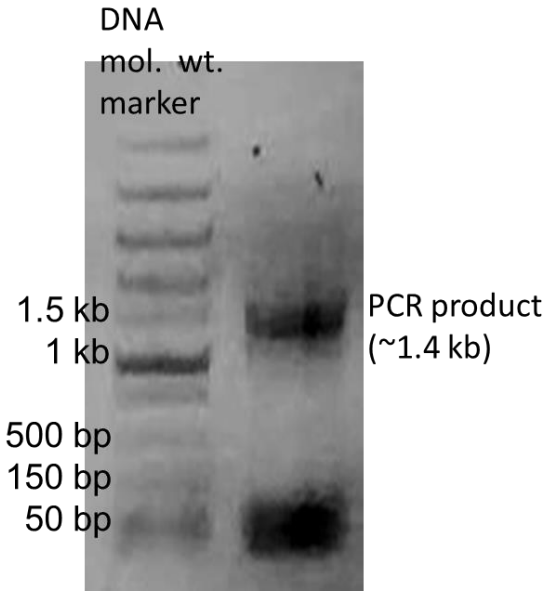

Figure 14. Agarose gel (1% w/v) displaying the PCR product (~1.4 kb) amplified from genomic DNA of the specimen G-0978 using bacterial 16S rRNA primers, 27f and 1492r. The first lane shows the DNA molecular weight marker (Fast DNA ladder, NEB). This work was performed by Bhuwan Chhetri.

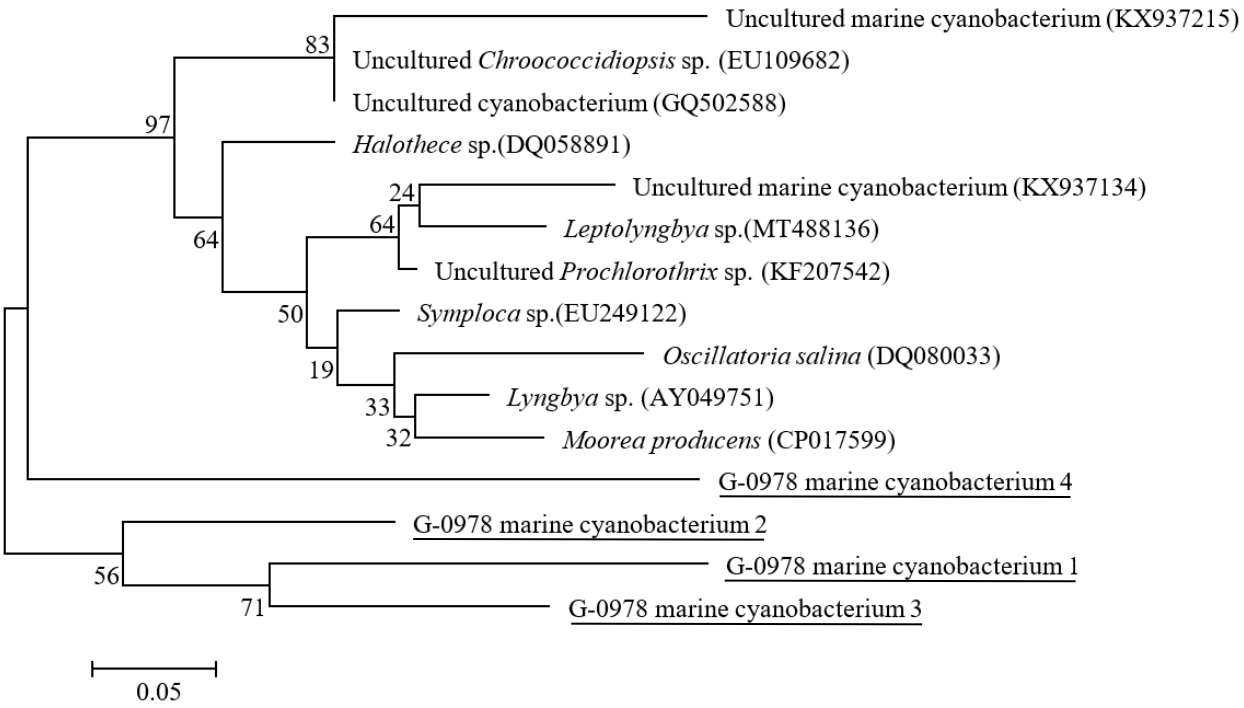

Figure 15. Phylogenetic relationship of marine cyanobacteria from collection G-0978 with top cyanobacterial species matched from blastn search by 16S rRNA sequences using the Maximum Likelihood method based on the Kimura 2-parameter model in MEGA X. The percentage of replicate trees in which the associated species clustered together in the bootstrap test (1000 iterations) is shown next to the branches. The accession numbers of the 16S rRNA of respective cyanobacteria are mentioned in parentheses. The branch lengths are calculated by the number of substitutions per site and the tree is portrayed to scale. This analysis was performed by Dr. Nazia Mojib.

3.3.3 Isolation and Dereplication of Natural Products in Anthelmintic Extract Fractions

To determine if any previously characterized natural products were present in the worm-active dichloromethane(DCM)-soluble extract fraction (as a form of dereplication), it was evaluated by proton nuclear magnetic resonance (NMR) spectroscopy as well as low-resolution mass spectrometry (MS). The NMR spectral data contained signals indicative of peptides while the MS data suggested the presence of several known natural products including the anticancer cyclic hexadepsipeptide veraguamide G,[122] the

neurotoxic cyclic depsipeptide hoiamide B,[123] and the antimitotic tetrapeptide belamide A.[124] Since none of these natural products have previously been evaluated for anthelmintic activity, the DCM-soluble extract fraction underwent bioassay-guided fractionation to isolate the molecule(s) responsible for the observed bioactivity (Figure 16). Separation with normal phase silica column chromatography resulted in 25 fractions. Due to limits on the number of adult hookworms available for screening, only a subset of fractions, including some combined fractions, were tested. The fraction AMS04001-2, comprised of materials that eluted at 98% DCM/2% methanol (MeOH) and 96% DCM/4% MeOH, exhibited promising activity against adult *A. ceylanicum* with a 48 hour average worm motility index of 0.17. Fraction AMS04001-2 was further separated using normal phase high-performance liquid chromatography (HPLC), resulting in 28 fractions. NMR and LC/MS spectral data were acquired for each of these fractions before recombining fractions (again, due to bioassay testing limitations) and evaluating against adult *A. ceylanicum*. Fractions eluting between 23 and 36 minutes (fractions 20-26) had a 24 hour average worm motility index of 0.8 and a 48 hour average worm motility index of 0.2 when tested with adult *A. ceylanicum* hookworms. NMR and LC/MS spectral data acquired for fractions 20-26 (Figure 17, Figure 18, and Table 6) indicated that each fraction either was nearly pure or contained a mixture of six or fewer natural products with NMR spectral features suggestive of peptide natural products. Also, searching the LC/MS data for masses corresponding to veraguamide G, hoiamide B, and belamide A revealed that these natural products were not present in the worm-active HPLC fractions, raising the possibility that these fractions contain previously undiscovered natural products. The Aroian lab is currently evaluating the individual HPLC fractions 20-26 for worm activity.

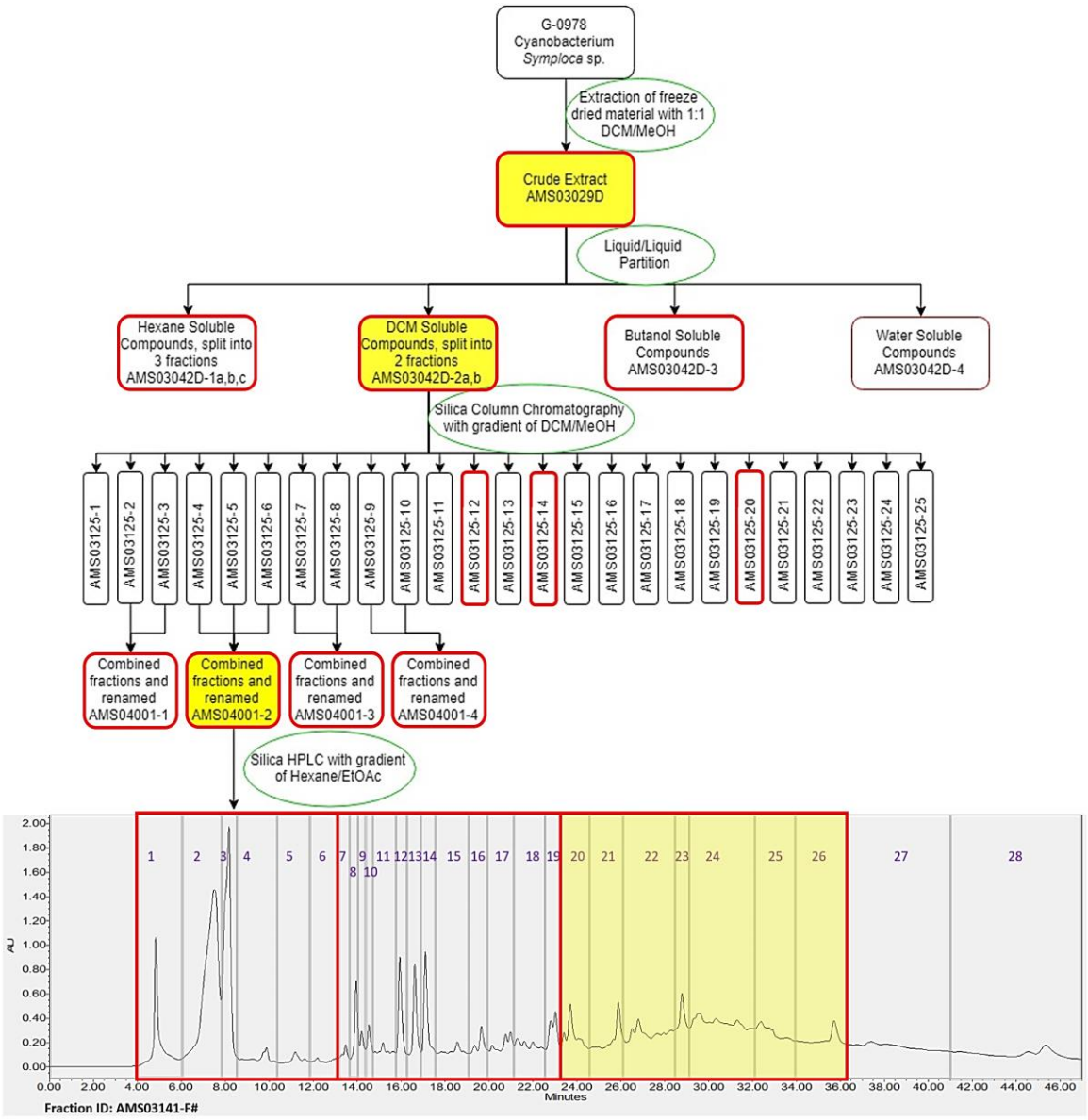

Figure 16. Separation scheme for bioassay-guided fractionation of the worm active cyanobacterial collection (G-0978) identified in screening against the hookworm *A. ceylanicum*. Green circles describe the chemical separation step, red boxes indicate which fractions were submitted for testing against hookworms, and yellow boxes are fractions identified as worm-active. Due to bioassay testing constraints, not every fraction was tested and in some cases, fractions were combined (e.g. HPLC fractions 1-6, 7-19, and 20-26 were combined).

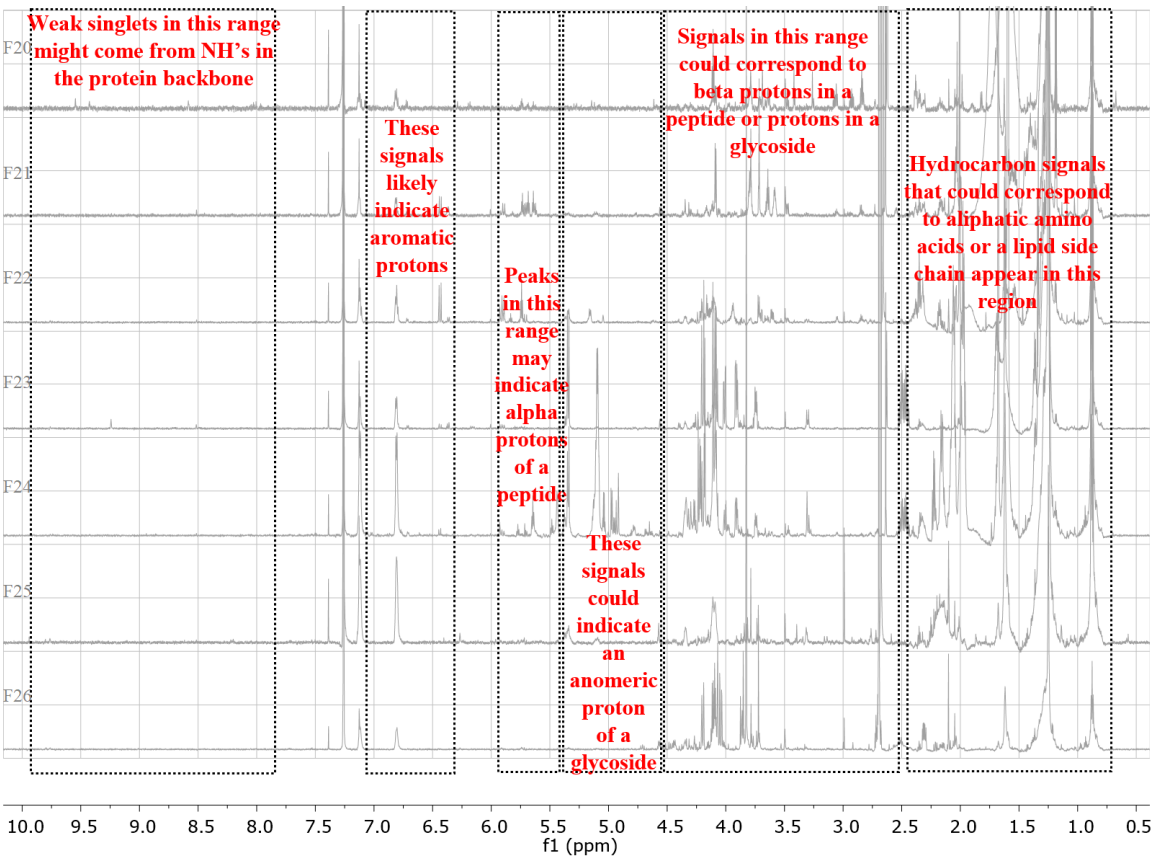

Figure 17. ^{1}H NMR spectral data for hookworm-active HPLC fractions 20-26 from cyanobacterial collection G-0978 ($CDCl_3$, 700 MHz NMR).

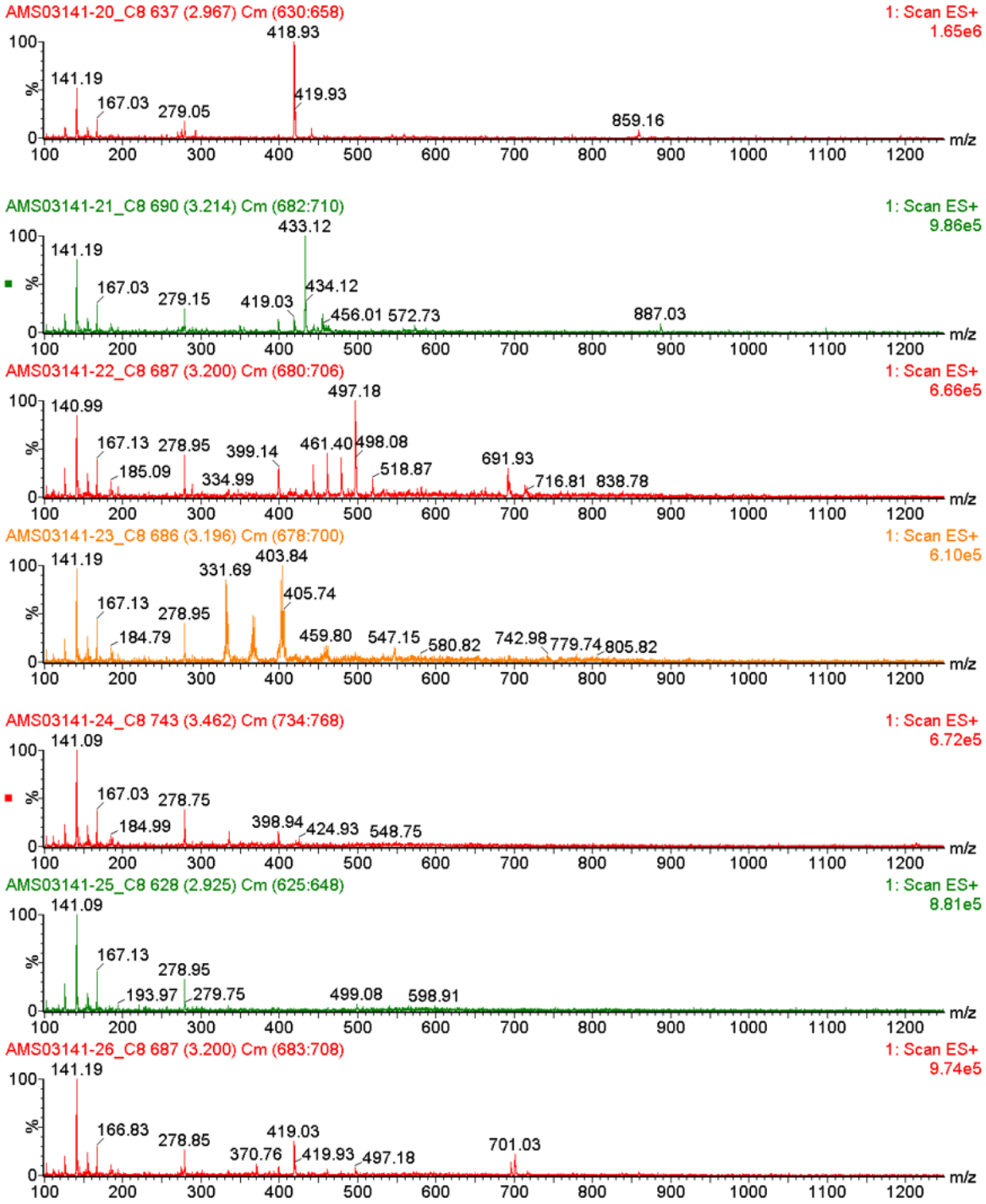

Figure 18. Low-resolution mass spectrometry data for hookworm-active HPLC fractions 20-26 from cyanobacterial collection G-0978.

Table 6. Mass spectral features present in the low-resolution electrospray LC/MS data acquired for the hookworm-active HPLC fractions from cyanobacterial collection G-0978.

HPLC Fraction ID	Mass Spectral Features
AMS03141-20	$[M+H]^+$ = *m/z* 418.93 $[M+Na]^+$ = *m/z* 440.92 $[2M+Na]^+$ = *m/z* 859.16
	$[M+H]^+$ = *m/z* 543.95
	$[M+H]^+$ = *m/z* 558.94
AMS03141-21	$[M+H]^+$ = *m/z* 349.88
	$[M+H]^+$ = *m/z* 354.78
	$[M+H]^+$ = *m/z* 398.94
	$[M+H]^+$ = *m/z* 419.03
	$[M+H]^+$ = *m/z* 433.12 $[M+Na]^+$ = *m/z* 455.01 $[2M+Na]^+$ = *m/z* 887.03
AMS03141-22	$[M+H]^+$ = *m/z* 334.89
	$[M+H]^+$ signals that are *m/z* 18 apart = *m/z* 443.11, *m/z* 461.20, *m/z* 479.19, *m/z* 497.18 $[M+Na]^+$ = *m/z* 518.87
	$[M+H]^+$ = *m/z* 691.83 $[M+Na]^+$ = *m/z* 713.81
AMS03141-23	$[M+H]^+$ = *m/z* 331.89
	$[M+H]^+$ = *m/z* 363.77
	$[M+H]^+$ = *m/z* 399.84
	$[M+H]^+$ = *m/z* 545.75
AMS03141-24	$[M+H]^+$ = *m/z* 334.59
	$[M+H]^+$ = *m/z* 398.94
	$[M+H]^+$ = *m/z* 420.93
	$[M+H]^+$ = *m/z* 424.93
AMS03141-25	$[M+H]^+$ = *m/z* 334.89
	$[M+H]^+$ = *m/z* 499.08
AMS03141-26	$[M+H]^+$ = *m/z* 334.89
	$[M+H]^+$ = *m/z* 370.96
	$[M+H]^+$ = *m/z* 398.94
	$[M+H]^+$ = *m/z* 419.03
	$[M+H]^+$ = *m/z* 696.03
	$[M+H]^+$ = *m/z* 701.03

3.4 Discussion

Although there are no cyanobacterial natural products previously reported to be active against infectious worms, earlier mechanistic studies provide insight for how these compounds might inhibit parasitic worms, especially when compared to known mechanisms of action of other anthelmintic compounds. The benzimidazole anthelmintics albendazole (**8**) and mebendazole (**9**) have been found to selectively inhibit microtubule synthesis by selectively binding to nematode β-tubulin at the colchicine site which blocks tubulin polymerization.[125,126] This adversely effects worms by interrupting formation of spindle fibers needed for cell division and by disrupting cytoplasmic microtubules involved in nutrient uptake. Also, poor host tissue absorption of these compounds from the digestive tract minimizes toxic side effects while still effectively targeting parasites. Antimitotic cyanobacterial peptides such as dolastatin 10 (**12**) [127] and belamide A (**13**) [124] (Figure 19) have been reported to disrupt microtubule networks through interactions with β-tubulin. Thus, it is possible that these cyanobacterial natural products might also act as anthelmintics. Although the natural products present in the worm-active fraction from the cyanobacterial collection G-0978 appear to have peptide-like features, mass spectral signatures expected for **12** ($[M+H]^+$ *m/z* 785.5029) and **13** ($[M+H]^+$ *m/z* 605.3643) are not present in the low-resolution LC/MS data. The ^{1}H NMR spectral data, however, includes signals suggestive of methyls, *N*-methyls, aromatic protons, NHs, and α-protons, structural moieties that are also present in **12** and **13** which suggests that the anthelmintic natural products could be structural analogs.

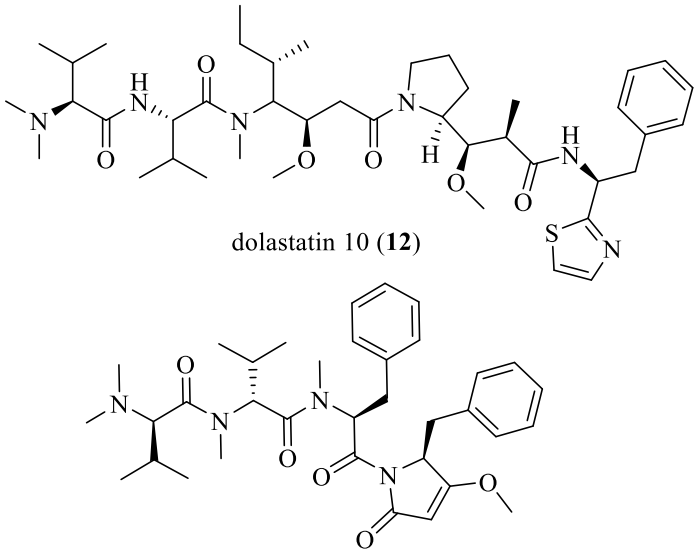

Figure 19. Cyanobacterial natural products that disrupt microtubule networks, one possible mechanism for anthelmintic activity.[124,127]

Other known targets of anthelmintic compounds are ion channels. For example, the anthelmintic drugs levamisole and pyrantel act as a nicotinic acetylcholine agonists that cause paralysis in worms by prolonged excitation at neuromuscular junctions.[128] The freshwater cyanobacterium *Anabaena flos-aquae* produces alkaloid neurotoxins anatoxin-a and homoanatoxin-a that act as nicotinic acetylcholine agonists;[129] however, examples of natural products from marine cyanobacteria with this type of activity are not represented in the literature. The natural product hoimamide A, a cyclic depsipeptide from the marine cyanobacterium *Lyngbya majuscula*, interacts with voltage-gated sodium channels and activates sodium influx in mouse neocortical neurons.[130] Identifying natural products that target sodium channels has been of interest for identifying possible analgesic therapeutics and treatments for neurodegenerative disorders. Given that nematodes, including hookworms, possess potassium and calcium channels instead of sodium channels,[131]

studies to identify natural products that target sodium channels will most likely not translate to anthelmintic activity.

3.5 Next Steps and Future Directions

The current work exhibits the successful application of a multi-step screen for hookworm activity and the use of bioassay-guided fractionation to obtain nearly pure natural products present in an anthelmintic fraction. Once hookworm bioassay results are received from the Aroian lab, final purification steps will be performed to obtain pure natural product(s) that will undergo full structural characterization techniques such as 2D NMR spectroscopy and high-resolution mass spectrometry. Pure, quantified natural product will be quantitatively evaluated against adult hookworms to determine anthelmintic potency and their mechanisms of action will be explored.

3.6 Materials and Methods

3.6.1 General Experimental Procedures

^{1}H NMR spectra were acquired on a 16.4 T (700 MHz for ^{1}H and 175 MHz for ^{13}C) Bruker Avance III HD instrument with a 5 mm indirect cryoprobe. Spectra were recorded in $CDCl_3$ and referenced to the solvent residual peak (δ_H 7.26) and spectra were processed and analyzed using MestReNova 12.0.0. Column chromatography was performed using SiliCycle's SiliaFlash F60, 40−63 μm silica gel. High-performance liquid chromatography (HPLC) separations were achieved with a Waters 1525 binary pump and a Waters 2996 photodiode array detector using either a 4.6 × 250 mm silica column (Phenomenex Luna, 5 μm particle size) or a 10 x 250 mm silica column (Waters Spherisorb Silica OBD Prep

Column, 5 μm particle size). Low-resolution mass spectrometry (HRMS) data were collected in positive ion mode using a Waters QDa spectrometer.

3.6.2 Biological Material and Species Identification

Tough bunches of a purple marine cyanobacteria with a white interior were collected from reef rubble in a lagoon off Ono-i-Lau, Fiji on August 7, 2011 (S 20°37.12′, W 178°44.24′). Voucher specimens identified as collection G-0978 were stored at the University of the South Pacific and Georgia Institute of Technology in aqueous ethanol and formaldehyde. Bulk cyanobacterial material was stored at the Georgia Institute of Technology in a −80 °C freezer.

Genomic DNA from both ethanol-preserved and bulk frozen cyanobacterial specimen (G-0978) was extracted using the DNeasy Blood and Tissue kit (Qiagen) according to the manufacturer's protocol. The single 16 rRNA gene fragment from genomic DNA was amplified via the polymerase chain reaction (PCR), using bacterial 16S rRNA primers, 27f and 1492r.[75] The PCR amplification was performed in a 25 μl reaction volume consisting of 50 ng of purified genomic DNA; 200 μM of each of the dNTPs; 1 μM of each of the oligonucleotide primers and 1.0 U Taq DNA Polymerase, and 1× Standard PCR reaction buffer (NEB, Ipswich, MA). The PCR amplification was performed in a GeneAmp PCR system 2700 (Applied Biosystems, Foster City, CA) thermocycler using the following temperature cycling parameters: initial denaturation at 94°C for 4 min followed by a total of 40 cycles of amplification in which each cycle consisted of denaturation at 94°C for 50 s, primer annealing at 55°C for 50 s and primer extension at 72°C for 2 min. After amplification, final extension of the incompletely synthesized DNA

was carried out at 72°C for 7 min. The PCR product was analyzed by agarose gel electrophoresis (1% wt/vol). The gel was stained with ethidium bromide and visualized under a UV transilluminator. The PCR product was sequenced with forward or reverse primers, and sequences were manually edited. The sequence similarity of the cyanobacterial 16S rRNA to other known cyanobacteria was determined by comparing it with the non-redundant nucleotide database (NCBI) using the blastn program.[77] MEGA X[78] was employed to conduct phylogenetic analysis using the Maximum Likelihood method based on the Kimura 2-parameter model[79] with 1000 bootstrap iterations.

3.6.3 Extraction and Isolation

Cyanobacterial biomass (2339 g) was freeze-dried (849 g) and exhaustively extracted (four times) using a 1:1 mixture of dichloromethane and methanol. The resulting crude extract (79.3 g) was separated by liquid/liquid partition resulting in hexane (18.5 g), dichloromethane (4.7 g), and butanol/water (45.4 g) soluble fractions. The DCM-soluble fraction was subjected to silica column chromatography with 279 g of silica gel in a (40 cm diameter by 550 cm high) column with a glass frit. The fractions were collected using a stepped gradient of DCM and MeOH (13 fractions, 100% DCM, 99% DCM/1% MeOH, 98% DCM/2% MeOH, 97% DCM/3% MeOH, 96% DCM/4% MeOH, 95% DCM/5% MeOH, 94% DCM/6% MeOH, 93% DCM/7% MeOH, 92% DCM/8% MeOH, 91% DCM/9% MeOH, 90% DCM/10% MeOH, 50% DCM/50% MeOH, 100% MeOH). The fractions eluting from 96% DCM/4% MeOH (2.18 g) and 95% DCM/5% MeOH (46.4 mg) were further separated using semi-prep silica HPLC (90% hexanes/10% ethyl acetate held for 5 minutes, gradient from 90% hexanes/10% ethyl acetate to 100% ethyl acetate from 5 to 55 minutes, held 100% ethyl acetate for 5 minutes at 4 mL/min).

3.6.4 Anthelmintic Assays

3.6.4.1 Hookworm Developmental Screening (E2L)

Initial screening for anthelmintic activity was performed using an egg-to-larva (E2L) hookworm development screen.[118] Briefly, infectious *Ancylostoma ceylanicum* larvae (L3i) were orally administered to immunosuppressed male Syrian hamsters and after 18 days, worm eggs were isolated from feces. Eggs were transferred to a 96-well plate pre-coated with an E. coli food source, test conditions were added, and plates were incubated for 7 days at 28 °C. Inhibition of egg hatch or larval development were used to assess the inhibitory effect of test conditions.

3.6.4.2 Adult Hookworm *In Vitro* Screening

Hamsters infected with *A. ceylanicum* were dissected 11 days post-infection to retrieve young adult worms from the hamster's small intestine.[118] Worms were washed with prewarmed medium three times (RPMI1640, 100 µg/ml streptomycin, 100U penicillin, 10 µg/ml amphotericin) before being transferred to a 96-well screening plate with 97 µl of medium (3 worms per well). Marine organism extracts and fractions were dissolved in DMSO and added to screening plates at a final concentration of 5 µg/mL. After incubation at 37 °C and 5% CO_2 for 24 hours, inhibition of worms was assessed using the standard motility index.[132] The index ranked worm motility from 0 to 3 with 0 indicating dead worms, 1 corresponding to worms that exhibit movement after stimulation, 2 for moving worms, and 3 for highly active worms. Treatment conditions that resulted in a motility index of 1 or less for at least two worms were considered inhibitory. For each

treatment condition, six worms were tested and subjectively assigned a motility index value based on researcher observations, which was then averaged.

CHAPTER 4. METABOLOMICS ANALYSIS OF THE IMPACT OF CLADOPHOROL D FROM THE GREEN ALGA *CLADOPHORA SOCIALIS* ON METHICILLIN-RESISTANT *STAPHYLOCOCCUS AUREUS*

4.1 Abstract

An increasing incidence of infections by antibiotic-resistant bacteria and a dearth of new treatment options in the development pipeline necessitates the discovery of new antibiotics. An important component in this development is understanding the mechanism of action (MOA) of novel drug leads as this information allows for intelligent deployment of antibiotics. The objective of the present study was to identify putative MOAs of a novel antibiotic oligomeric polyphenol, cladophorol D, isolated from a green alga *Cladophora socialis*, using LC/MS and NMR-based metabolomics to chemically profile methicillin-resistant *Staphylococcus aureus* (MRSA) treated with this new natural product compared with nine antibiotic pharmaceuticals with different known MOAs. Currently, the experimental design for this project has been completed and pilot experiments confirming the design have been conducted but cladophorol D (**17**) exposure experiments and metabolomics analyses have yet to be finished.

4.2 Introduction

In the United States, more than 35,000 people die annually from more than 2.8 million infections caused by antibiotic-resistant bacteria and fungi.[133] One Gram-positive antibiotic-resistant bacterium, methicillin-resistant *Staphylococcus aureus* (MRSA), has been classified as a serious threat by the CDC due to its resistance to many first-line

antibiotics. Unfortunately, since major pharmaceutical companies have shrunk or abandoned their antibiotic discovery programs, there are few antibiotics in the development pipeline, causing concern that the rise of evolved resistance among bacterial pathogens is outpacing the advancement of new treatment options.[134] In early 2020 the World Health Organization warned of the threat of antibiotic resistance as a result of the drying drug pipeline as well as the concern that the majority of drugs currently in development are variations on existing antibiotics with only a handful addressing the most serious drug-resistant infections.[135] Pursuing analogs of current antibiotics is limited by the number of modifications that can be made to a single chemical core.[136] Additionally, analogs are more likely to target the same pathways as the parent compound making them more susceptible to encountering bacterial resistance due to cross-resistance with existing antibiotics. Currently, only 10 of the 41 antibiotics in development represent either a new drug class or target a new mechanism of action.[137] Understanding the mechanism by which newly discovered antibiotics target bacteria is a necessary step for mitigating the possible evolution of resistance and for expanding the approaches by which we control these pathogens, such as by use of combination therapies.[138] Identifying combinations of drugs through such approaches as checkerboard assays helps prioritize promising treatment options by exploring synergistic interactions of compounds against bacteria and by discovering antibiotic mixtures that thwart bacterial resistance pathways.[139,140]

Metabolomics has recently expanded with technological advancements in detection methods, data processing capabilities, and database availability.[141] Simultaneous analysis of many metabolites (small molecule intermediates or end products of metabolism) enables evaluation of phenotypic differences among cells, tissues, organs, or organisms exposed to

different conditions.[32] Due to its ability to provide selective, rapid, and sensitive analysis of metabolites, mass spectrometry (MS) has been the technique of choice for the vast majority of recent metabolomics studies.[142] MS detects readily ionized metabolites present in the submicromolar range and below, and it has both better resolution and a larger dynamic range compared to other available techniques. The disadvantages of MS include poor uniformity and repeatability of results arising from inconsistent sample preparation, ionization, and chromatography. Failure of some molecules to ionize, suppression of ionization by other components present in complex biological matrices, and a lack of quantitativeness are further weaknesses. Another widely used option for metabolomics, nuclear magnetic resonance (NMR) spectroscopy, requires minimal, non-destructive sample handling to quantitatively detect the most abundant metabolites but NMR is not particularly sensitive, failing to detect metabolites in the submicromolar range.[143] Signal overlap due to limited spectral dispersion is another weakness of NMR spectroscopy, particularly with ^{1}H NMR, however other NMR approaches with greater ability to resolve overlapping resonances (e.g., *J*-resolved spectroscopy; HSQC; TOCSY; and those detecting nuclei other than ^{1}H) suffer from even weaker sensitivity. ^{1}H-based NMR techniques only detect molecules with non-exchangeable protons so metabolites that contain few protons or primarily exchangeable protons are poorly sampled by NMR-based metabolomics. Vibrational spectroscopy techniques (e.g., Fourier transform infrared spectroscopy and surface-enhanced Raman spectroscopy) are additional options for metabolomics studies which are less expensive and have a higher throughput than MS and NMR but are limited by their relatively poor specificity and sensitivity.[144] Despite the variety of available options for chemically profiling metabolomes, no single approach

detects all metabolites in a sample. Several recent publications have suggested that combining multiple methods, for example NMR spectroscopy and MS, can help overcome limitations of a single analysis type while improving detection and structural characterization of metabolites and expanding the coverage of the metabolome.[142,145] NMR and MS are complementary techniques that expand the measurable metabolome by detecting different metabolites in addition to some metabolites in common, allowing for both confirmation of compound identities by multiple methods as well as detection of a greater number of metabolites.[146,147] Additionally, NMR and MS have undergone substantial technological advancements in instrumentation and are widely accessible to research groups, making them preferred analytical tools for the metabolomics community. Thus, combining multiple analytical techniques and connecting the resulting datasets is the optimal approach for improving confidence in metabolite assignments and increasing the total number of features detected in the metabolome.

Metabolomics shows special promise for the evaluation of drug mechanism of action (MOA).[30] Metabolomics provides a wealth of information about the effects of drugs on a pathogen by surveying thousands of metabolites that are the result of complex biochemical pathways.[148] This information provides a global snapshot of how an antibiotic affects pathogen phenotype. The pathogen of interest for the present study, *Staphylococcus aureus*, has been the focus of numerous investigations on how strains respond metabolically to various antibiotic classes, providing useful information about changes in biochemical pathways that occur upon exposure to different drugs.[149-151] Metabolomics has also been employed to evaluate the MOA of novel antibiotics by comparison to drugs with fully characterized MOAs or by annotating all metabolite

perturbations to identify impacted pathways in cases where the compound acts via a new mechanism.[148,152]

The antibiotic oligomeric polyphenols, cladophorols A – I (**14**–**22**) (Figure 20), were isolated from a Fijian green alga, *Cladophora socialis*, and identified using a combination of NMR spectroscopy, mass spectrometric analysis, and computational modeling with DFT calculations.[153] Polyphenols are not commonly found in green algae; only a few examples exist of related green algal natural products including the brominated polyphenolic feeding deterrent avrainvilleol and its condensation product, rawsonol [154-156] as well as two vanillic acid analogs from Australian *Cladophora socialis* that disrupt insulin cell signaling.[157] When evaluated against a panel of Gram-positive and Gram-negative bacteria and two pathogenic fungi, cladophorols B (**15**), C (**16**), D (**17**), E (**18**), F (**19**), and G (**20**) showed selectivity towards MRSA with MIC_{90} values of 13 ± 2, 1.4 ± 0.3, 9 ± 2, 25 ± 3, 14 ± 3, and 31 ±3 μg/ml, respectively.[153] Cladophorol B (**15**) was also active against blood-stage *P. falciparum* with an EC_{50} of 1.9 μg/ml. These natural products exhibited weak cytotoxicity against immortalized human keratinocytes at concentrations well above those at which MRSA was susceptible, indicating that the antibiotic cladophorols could be viable antibiotics for further pharmaceutical development due to their selectivity towards MRSA and low toxicity.

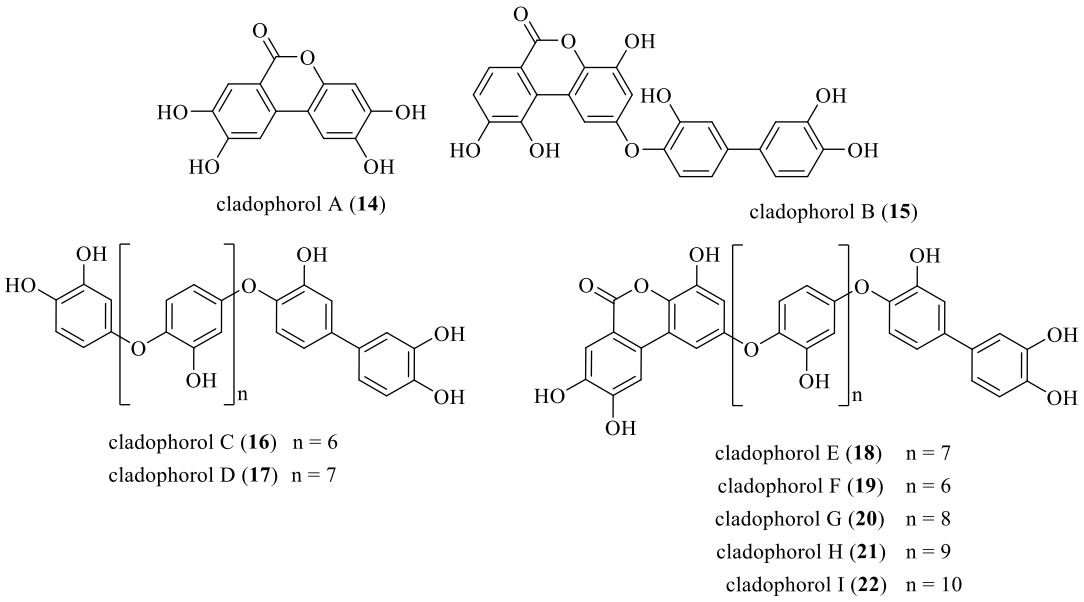

Figure 20. Molecular structures of phenolic natural products isolated from the green alga *Cladophora socialis*.[153]

Although broad spectrum antibiotics are often preferred, their use poses increased risk for evolution of drug resistance and can also have negative consequences for human microbiomes, which provide essential physiological functions to their human hosts and which are sensitive to antibiotic exposure.[158] Disruptions to the microbiome can result in disrupted nutrient absorption, vitamin production, and immune response and can also lead to lowered bacterial diversity, increasing susceptibility to opportunistic pathogens such as *Clostridium difficile*. In cases where the identity of the infection-causing bacterium is known, application of a narrow spectrum antibiotic, such as the MRSA-selective cladophorol natural products, can avoid some of these issues. Selectivity towards a few strains of one species of bacterial pathogen suggests that the cladophorols have a specific MOA. For the present study, cladophorol D (**17**) was chosen for evaluating the MOA of this class of natural products against MRSA using a metabolomics-based approach due to

compound availability and the relatively high potency of **17** against MRSA. Additionally, a strain of *S. aureus* resistant to **17** was identified (unpublished results from C. Quave's lab) which allows for future studies comparing the sensitive MRSA strain in order to identify possible mechanisms of resistance.

4.3 Experimental Design

4.3.1 Development of Intracellular Metabolite Extraction Procedure

Since there is no universal method in microbial metabolomics for growing or processing bacterial samples, different procedures reported in literature were evaluated to identify techniques that maximize metabolite yield while minimizing media components, metabolite losses, and chemical changes among metabolites caused by sample processing. The first consideration was the type of media that would be used for growing MRSA. Relative to typically used complex growth media, a previous study found that growth of MRSA on minimal media resulted in a metabolite profile indicative of survival mode.[159] To avoid putting cells in such a state which would confound experimental exposure to antibiotics, the complex media Nutrient Broth was selected. Two practices commonly used for separating bacterial cells from media, fast-filtration and centrifugation, have been found to differently impact cellular stress, with centrifugation resulting in greater stress.[151,160] To minimize the production of stress metabolites, fast filtration was selected for the current experiment. Another important factor for metabolite extraction is the quenching step which should be reproducible, fast, and prevent leakage of intracellular metabolites prior to addition of extraction solvent. A number of methods have been used to quench metabolism of bacterial cells including immersion in cold methanol, cold ethanol, perchloric acid, or

glycerol-saline solutions, and dipping cells in liquid nitrogen.[161] Cold ethanol was chosen for the current experiment. For cell disruption, required to access the intracellular metabolites, a mechanical method is preferred since organic solvents are often not sufficient for breaking open the cell wall of *S. aureus*.[160] Bead beating with zirconia/silica beads was used to access intracellular metabolites. An overview of the experimental design is provided in Figure 21.

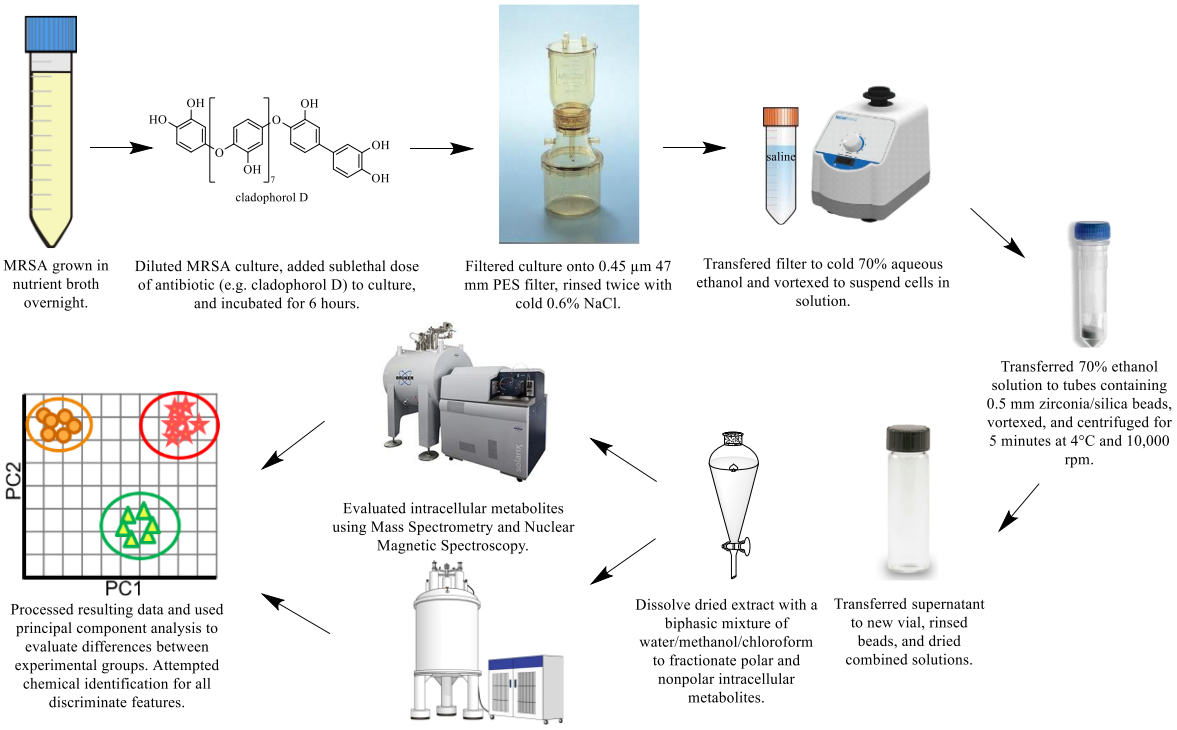

Figure 21. Experimental design for extraction and analysis of intracellular metabolites from MRSA for the metabolomics mechanism of action study.

4.3.2 Selection of Antibiotics

A total of nine clinically relevant antibiotics with a variety of mechanisms of action (MOAs) were selected for inclusion in the metabolomics experiment to determine putative MOAs by which cladophorol D (**17**) acts as an antibiotic (Table 7, Figure 22). Antibiotic concentrations were selected so that MRSA growth would be suppressed by 20-50% relative to MRSA treated with a solvent control. Inhibiting MRSA growth by greater than 50% might result in the production of metabolites associated with cellular death while inhibition less than 25% might not cause detectable metabolite perturbations or could possibly promote production of metabolites associated with cell signaling.[148,162] The optimal antibiotic concentration was determined by comparing the growth of MRSA treated with a solvent control to MRSA growth when exposed to each antibiotic in Table 7.

Table 7. Antibiotics selected for inclusion in the metabolomics study to determine the MOA of cladophorol D (**17**), by comparison with antibiotics of known MOA.

Drug	Solubility	Drug Class	Mechanism of Action
ciprofloxacin (23)	dilute aqueous acetic acid	fluoroquinolone	Inhibits cell division by interfering with DNA gyrase and a type II topoisomerase, topoisomerase IV, required for separating bacterial DNA.[163]
clindamycin (24)	water	lincosamide	Binds to the 23S RNA of the 50S subunit of the bacterial ribosome resulting in inhibition of bacterial protein synthesis.[164]
isoniazid (25)	water	pyridine carboxylic acid	Disrupts bacterial cell wall by inhibiting synthesis of mycolic acids.[165,166]
kanamycin (26)	water	aminoglycoside	Binds to the 30S subunit of the bacterial ribosome resulting in inhibition of protein synthesis.[167]
linezolid (27)	water	oxazolidinone	Inhibits initiation process of protein synthesis. [168]
monensin (28)	ethanol	ionophore	Acts as an ionophore by interfering with cell membrane permeability.[169]
rifampicin (29)	dimethyl sulfoxide	ansamycin	Inhibits DNA-dependent RNA polymerase, leading to a suppression of RNA synthesis and cell death.[170]
sulfacetamide (30)	methanol	sulfonamide	Interferes with biosynthesis of folic acid by competitively binding to bacterial para-aminobenzoic acid (PABA) required for bacterial growth.[171]
vancomycin (31)	water	glycopeptide	Complexes with D-Ala-D-Ala terminal of peptide chain resulting in inhibition of cell wall synthesis.[172]

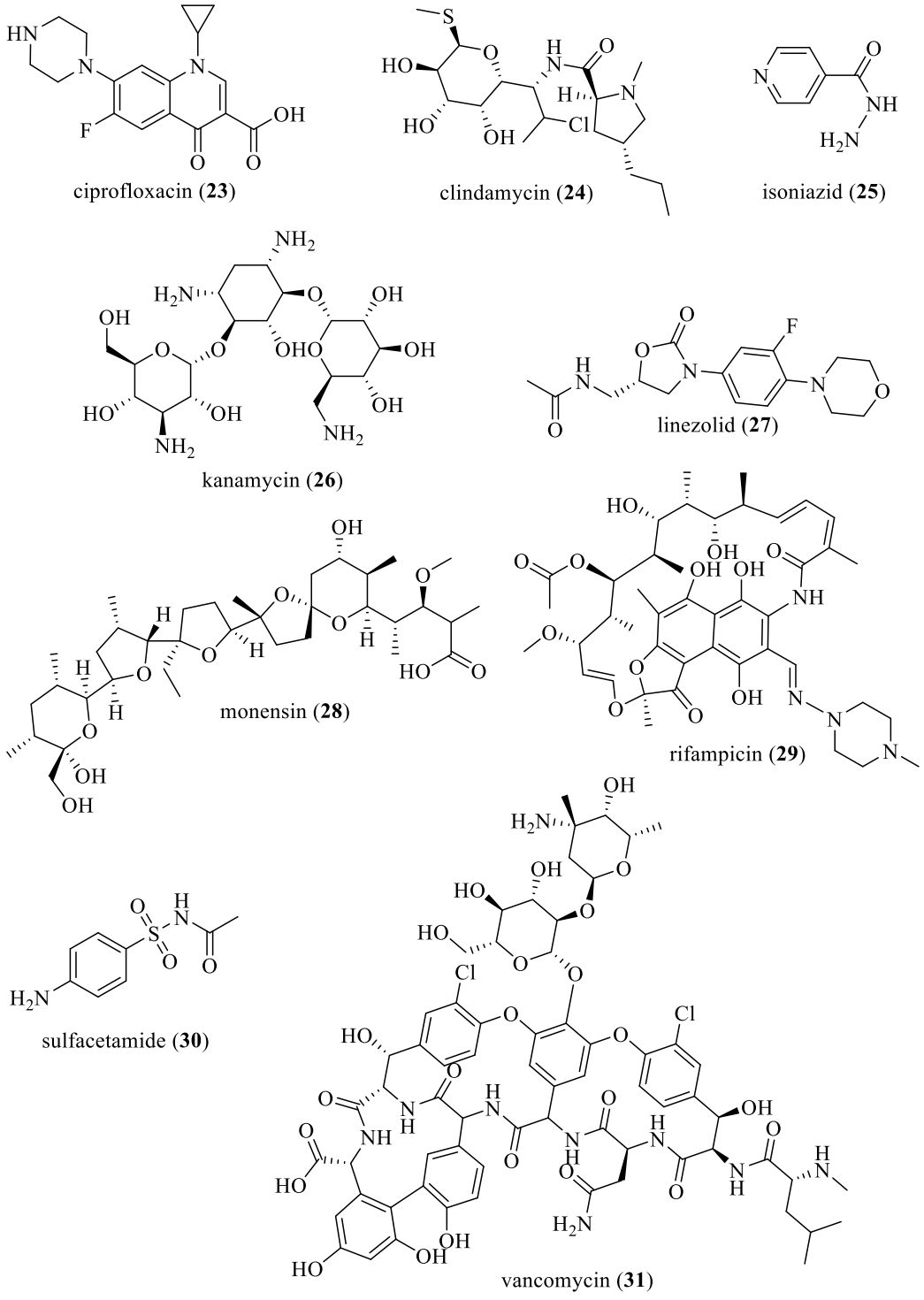

Figure 22. Nine antibiotics [163-165,167-172] included in MRSA metabolomics study to evaluate the MOA of cladophorol D (**17**).

4.4 Results

*4.4.1 Evaluation of Cladophorol D (**17**) against S. aureus Strains*

To probe the selectivity of cladophorol D (**17**) and to identify resistant strains of *S. aureus*, experiments were performed by Dr. Cassandra Quave's lab at Emory University to evaluate activity of **17** against multiple *S. aureus* strains. This testing indicated that **17** inhibits three of five strains of *S. aureus* tested, including a methicillin-resistant strain of *S. aureus* (AH1263) and two multi-drug resistant (MDR) strains provided by the CDC (CDC474 and CDC480) (Figure 23). Two strains, a methicillin-sensitive *S. aureus* (UAMS1) and an MDR strain resistant to tetracycline and susceptible to oxacillin (CDC470), were resistant to **17**, making them viable options for pursuing a metabolomics study comparing the metabolome of sensitive versus resistant *S. aureus* in the presence of **17** for possible elucidation of mechanisms of resistance.

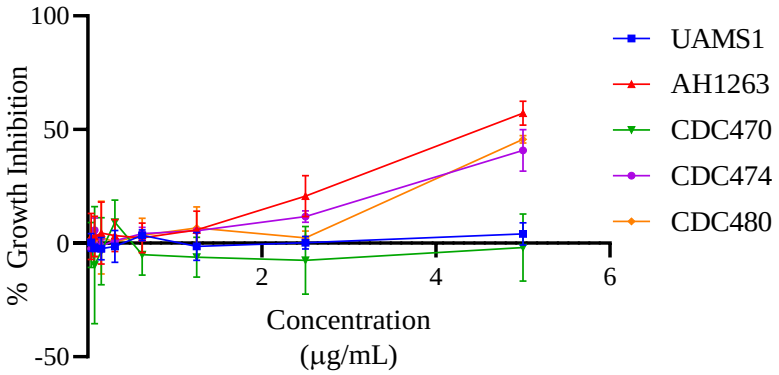

Figure 23. Evaluation of cladophorol D (**17**) against multiple strains of *Staphylococcus aureus* (UAMS1: osteomyelitis methicillin-sensitive *S. aureus* (ATCC 49230); AH1263: MRSA strain regularly used by the Quave lab; CDC470: a multidrug-resistant (MDR) *S. aureus* strain resistant to tetracycline and susceptible to oxacillin; CDC474: an MDR *S. aureus* strain susceptible to tetracycline and resistant to oxacillin; CDC480: an MDR *S. aureus* strain resistant to both tetracycline and oxacillin). Data generated by Dr. Cassandra Quave's lab at Emory University.

4.4.2 Evaluation of Antibiotics with Known MOAs

Before starting the metabolomics experiment, each selected antibiotic was evaluated against an in-house strain of MRSA (ATCC 33591) to determine their IC_{50} and MIC_{90} values (Table 8, Figure 24). Since IC_{50} and MIC_{90} values are impacted by experimental conditions, it was important to experimentally obtain these measurements while using reported literature values as a starting point. Of the antibiotics tested, MRSA strain ATCC 33591 was relatively insensitive to clindamycin (**24**), isoniazid (**25**), and sulfacetamide (**30**). Since these antibiotics act via unique MOAs, they were included in the experiment despite their relative lack of inhibition against MRSA, which could be anticipated to result in modest, if any, disruption to the MRSA metabolome.

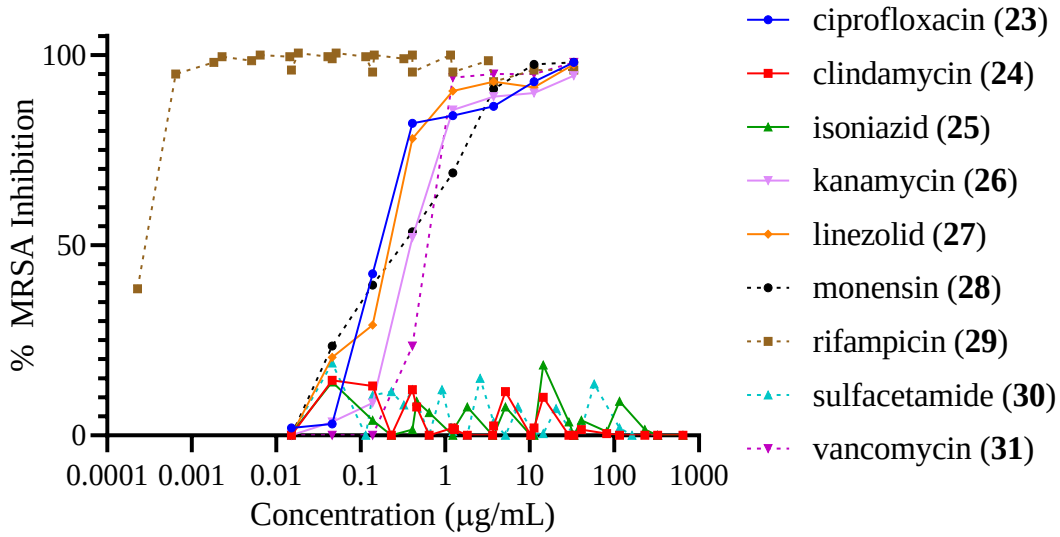

Figure 24. Growth inhibition of MRSA treated with nine antibiotics in a 96-well microplate. Growth of this strain of *S. aureus* (ATCC 33591) was not inhibited by exposure to clindamycin (**24**), isoniazid (**25**), or sulfacetamide (**30**) treated with a maximum concentration of 650, 650, and 320 µg/mL, respectively.

Table 8. IC_{50} and MIC_{90} values measured for the nine antibiotics chosen for the MRSA metabolomics study for evaluating the MOA of cladophorol D (**17**).

	IC_{50} (µg/mL)	**MIC_{90} (µg/mL)**
ciprofloxacin (23)	0.12	0.39
clindamycin (24)	> 650	> 650
isoniazid (25)	> 650	> 650
kanamycin (26)	0.34	0.93
linezolid (27)	0.160	0.64
monensin (28)	0.33	0.57
rifampicin (29)	< 0.00023	< 0.00064
sulfacetamide (30)	> 320	> 320
vancomycin (31)	0.55	0.84

The results of the antibiotic dose response experiment were subsequently used to choose concentrations to evaluate at the culture volume planned for the metabolomics experiment. More specifically, the goal was to identify concentrations that inhibited MRSA

growth relative to a solvent control by between 20 and 50%. This range was chosen so that the effect of a given antibiotic on the MRSA metabolome could be observed while minimizing the amount of dead cells, which could skew results by focusing on metabolites associated with catabolism and cell death. Since the culture environment varied drastically from the initial evaluation performed in 96-well plates, the concentrations selected did not result in ideal MRSA growth suppression for all of the antibiotics tested in scaled-up preliminary experiments (Figure 25). Additionally, the dose response curve for some of the antibiotics exhibited very steep slopes, indicating great sensitivity to minute differences in antibiotic concentration. Ciprofloxacin (**23**), monensin (**28**), and vancomycin (**31**) produced optimal MRSA growth inhibition between 20 and 50% at 0.050, 0.35, and 0.25 µg/mL, respectively. Isoniazid (**25**) and rifampicin (**29**) did not suppress MRSA growth sufficiently at any tested concentrations with the highest concentrations tested being 1.5 mg/mL and 0.23 ng/mL, respectively. Since **25** did not suppress MRSA growth at any concentration tested in the 96-well plate format (maximum concentration of 650 µg/mL), there will likely not be an observable reduction of MRSA growth with this antibiotic. Therefore, the concentration of 1.5 mg/mL for **25** will be used for the metabolomics experiment. Clindamycin (**24**), kanamycin (**26**), linezolid (**27**), and sulfacetamide (**30**) suppressed MRSA growth too much at the concentrations tested. For the antibiotics that did not achieve ideal growth curves at any of the tested concentrations, a follow-up experiment was performed to identify optimal antibiotic concentrations (Figure 26). Additionally, cladophorol D (**17**) was included in this evaluation. Results from the follow-up growth curve experiment identified the following optimal concentrations: 0.45 mg/mL

for clindamycin (**24**), 0.10 µg/mL for kanamycin (**26**), 0.15 µg/mL for linezolid (**27**), 0.50 mg/mL for sulfacetamide (**30**), and 0.20 µg/mL for cladophorol D (**17**).

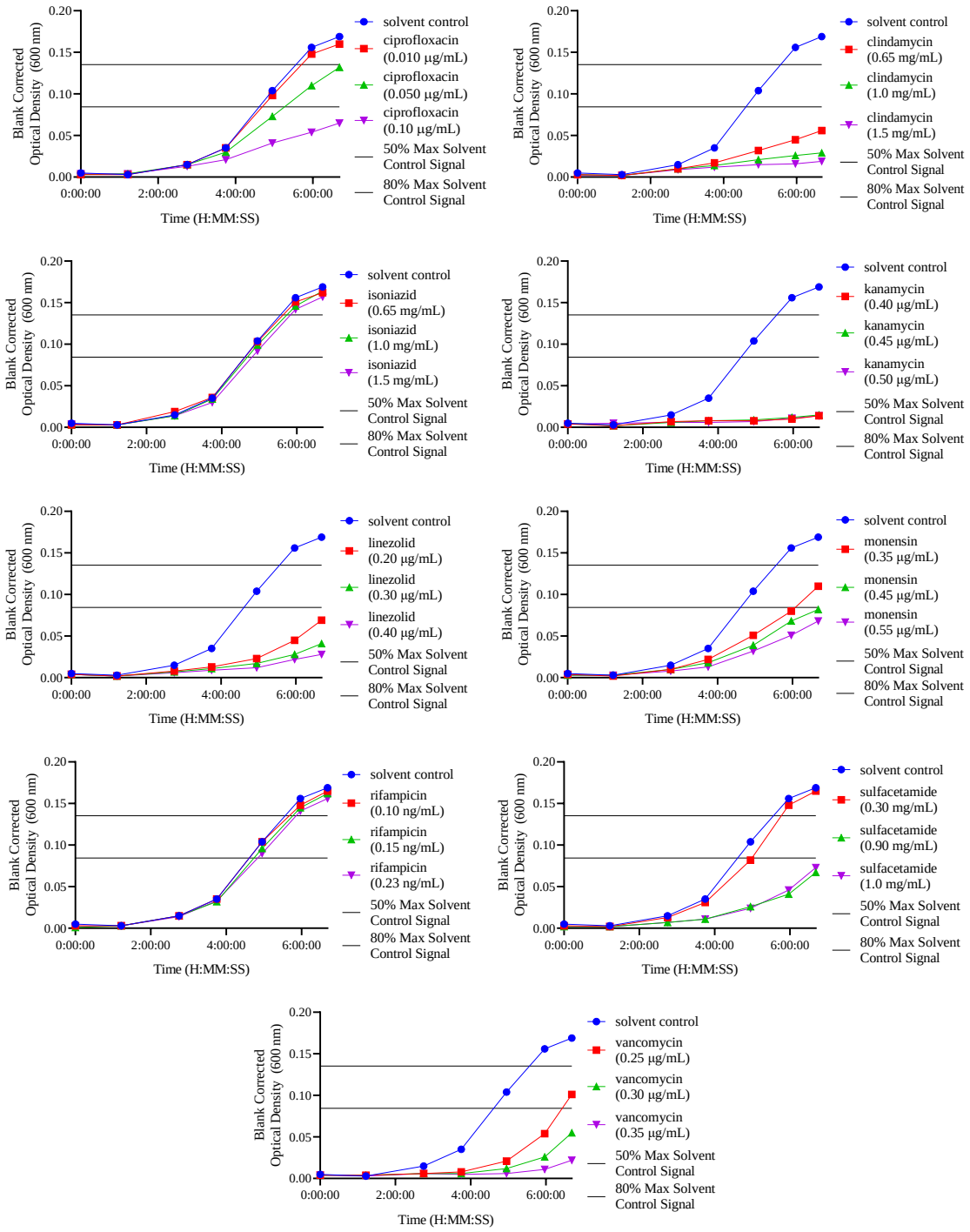

Figure 25. MRSA growth curves exposed to each of nine antibiotics (selected for the metabolomics experiment). Optical density (OD) readings at 600 nm were recorded regularly over the course of 6.5 hours to track growth of MRSA, with higher OD values indicating greater cell density. The goal was to achieve a final OD reading for the antibiotic treatment conditions that was between 50-80% of the maximum signal obtained for MRSA treated with a solvent control.

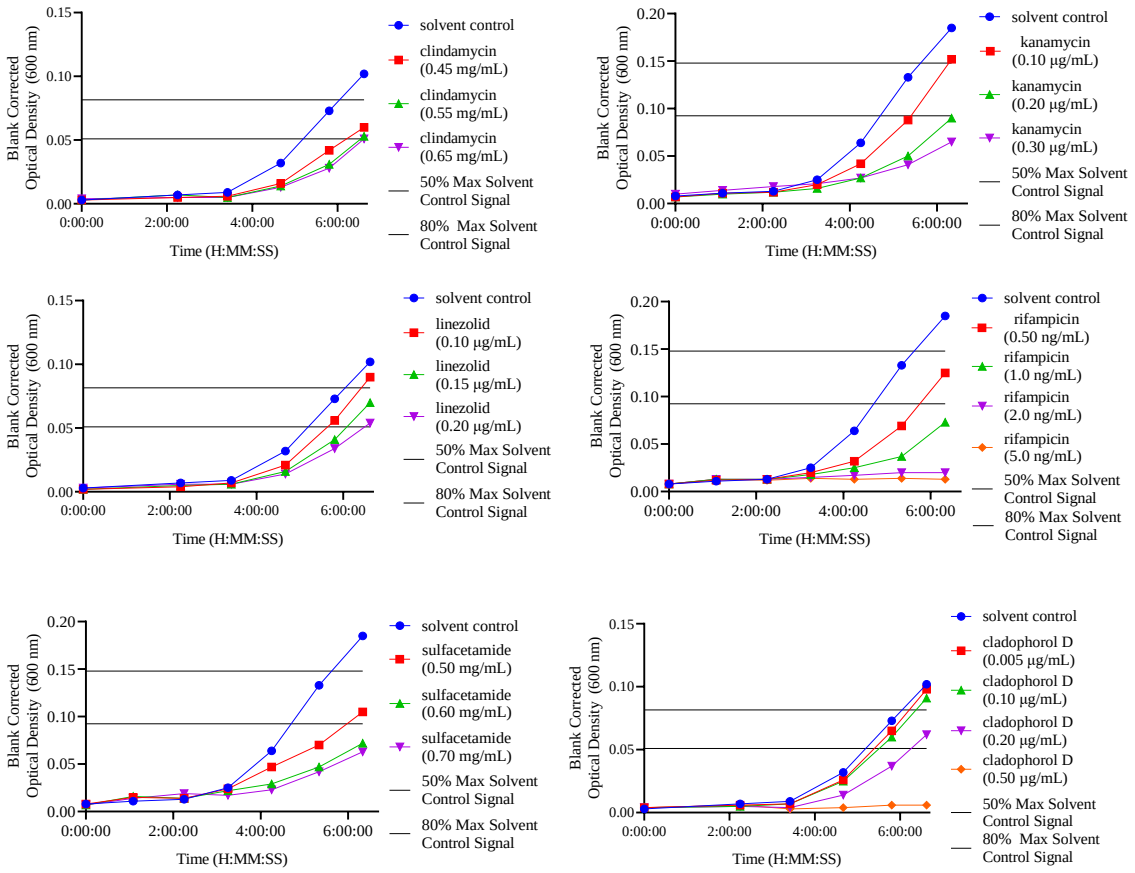

Figure 26. Follow-up evaluation of MRSA growth exposed to adjusted concentrations of the antibiotics clindamycin (**24**), kanamycin (**26**), linezolid (**27**), rifampicin (**29**), and sulfacetamide (**30**) as well as cladophorol D (**17**).

4.4.3 Preliminary Evaluation of Metabolomics Workflow with Four of the Nine Antibiotics

Before performing a full scale metabolomics experiment with cladophorol D (**17**), a pilot experiment was executed using a subset of the antibiotics to confirm that the steps shown in Figure 21 produce results that discriminate between the different treatment conditions. For each condition, a total of six replicates were included, with two replicates of each treatment generated each day for three days (i.e., in three batches). After

intracellular metabolite extraction, ^{1}H NMR spectral data were collected on an 800 MHz NMR spectrometer for both nonpolar and polar metabolites using $CDCl_3$ and phosphate buffered D_2O, respectively. The spectral data for the nonpolar metabolites contained few resonances in regions of the spectrum illustrative of important functional groups, instead revealing substantial methyl and methylene envelopes indicating the presence of fatty acids which are not distinguishable by NMR spectroscopy; these features did not vary among treatments. Thus, statistical analyses were not performed for this data set pertaining to lipid-soluble metabolites.

Spectra from the polar metabolomes exhibited a greater number of complex resonances and, by eye, appeared to vary by treatment (Figure 27). The NMR spectral data for the polar metabolites were pre-processed using Metabolab and statistically analyzed with PLS Toolbox. A principal component analysis (PCA) was employed to detect relationships between exposure to different antibiotics and features of the MRSA metabolome (Figure 28, Figure 29). Evaluation of PCA results indicated that although the treatment conditions were not distinguishable according to the first principal component (PC1), there was obvious separation between conditions in PCs 2, 3, and 4. Polar metabolomes of MRSA exposed to ciprofloxacin and monensin were statistically different from the other conditions via PC2 and were distinguishable from each other in PC3. PC4 revealed differences between the vancomycin treatment and sulfacetamide and the solvent control. Metabolomes associated with sulfacetamide exposure heavily overlapped with the solvent control which supports the previously observed minimal impact sulfacetamide had on this strain of MRSA (Figure 24, Table 8).

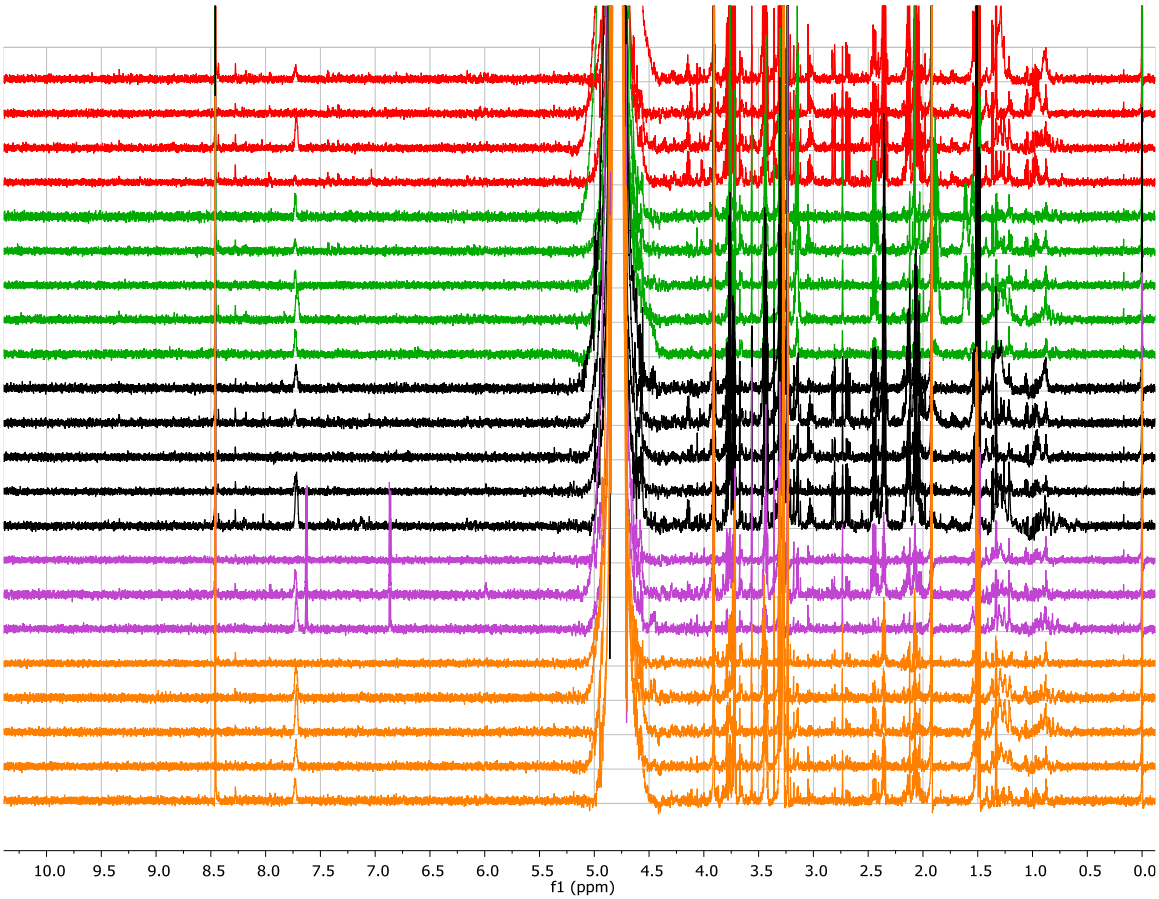

Figure 27. ^{1}H NMR spectra (phosphate buffered D_2O, 800 MHz NMR) of intracellular metabolite extracts from MRSA treated with ciprofloxacin (red), monensin (green), sulfacetamide (purple), vancomycin (orange), or a solvent control (black).

Examination of PCA loadings for PCs 2, 3, and 4 enabled preliminary consideration of MRSA metabolites whose concentrations were affected by antibiotic exposure (Figure 29). Variability in metabolite abundances among treatments arose from differences in NMR spectral signals between 1-4 ppm and 7.5-8.5 ppm. There is a wide variety of metabolites with proton spectral signals in the 1-4 ppm range, including lipids, sugars, amino acids, lactic acid, and acetate, while signals in the 7.5-8.5 ppm range might correspond to protons in purine, aromatic groups, or the amino group of an amino acid.[173,174] For PC 2, spectroscopic features with positive loadings were associated with

metabolites that have increased concentrations in MRSA treated with either ciprofloxacin or monensin. NMR spectral signals around 1.5, 1.9, 2.1, 2.4, 3.2, 3.4, 3.9, 7.7 and 8.4 ppm were all noticeably upregulated in PC 2. Positive loadings in PC 3 corresponded with increased concentrations of metabolites from treatment of MRSA with ciprofloxacin while negative loadings were associated with increased concentrations of metabolites in the other treatment conditions. Interestingly, some of the spectral signals with positive loadings in PC 2 were negative in PC 3, including 1.9, 3.2, 3.4, 3.9, 7.7, and 8.4 ppm, suggesting that their presence in the positive region of PC 2 was due to monensin. Additionally, PC 3 contained a higher concentration of the metabolite corresponding to the signal at 2.4 ppm which suggests this metabolite corresponds to treatment of MRSA with ciprofloxacin. PC 4 differentiated treatment of MRSA with vancomycin, ciprofloxacin, or monensin from treatment of MRSA with sulfacetamide or the solvent control. The loadings plot for PC 4 looked very similar to the loadings for PC 2 with only slight differences: 0.9 ppm was negative in PC 4 (absent in PC 2), 1.5 ppm had variance in both positive and negative directions (only positive in PC 2), and 3.2 ppm was absent in PC 4. Comparison of ^{1}H NMR spectral signals of extracts from MRSA treated with ciprofloxacin to the loadings plot for PC 3, which differentiated ciprofloxacin from the other treatment conditions, revealed positive peaks in the loadings plot corresponded to observable ^{1}H NMR spectral signals (Figure 30). Although NMR metabolomics produced results that showed differentiation between treatment conditions, additional analysis using mass spectrometry would aid in identification of metabolites. Thus, for the full metabolomics experiment exploring the MOA of cladophorol D (**17**), both NMR spectroscopy and LC/MS will be used to identify and quantify metabolite differences between treatment conditions.

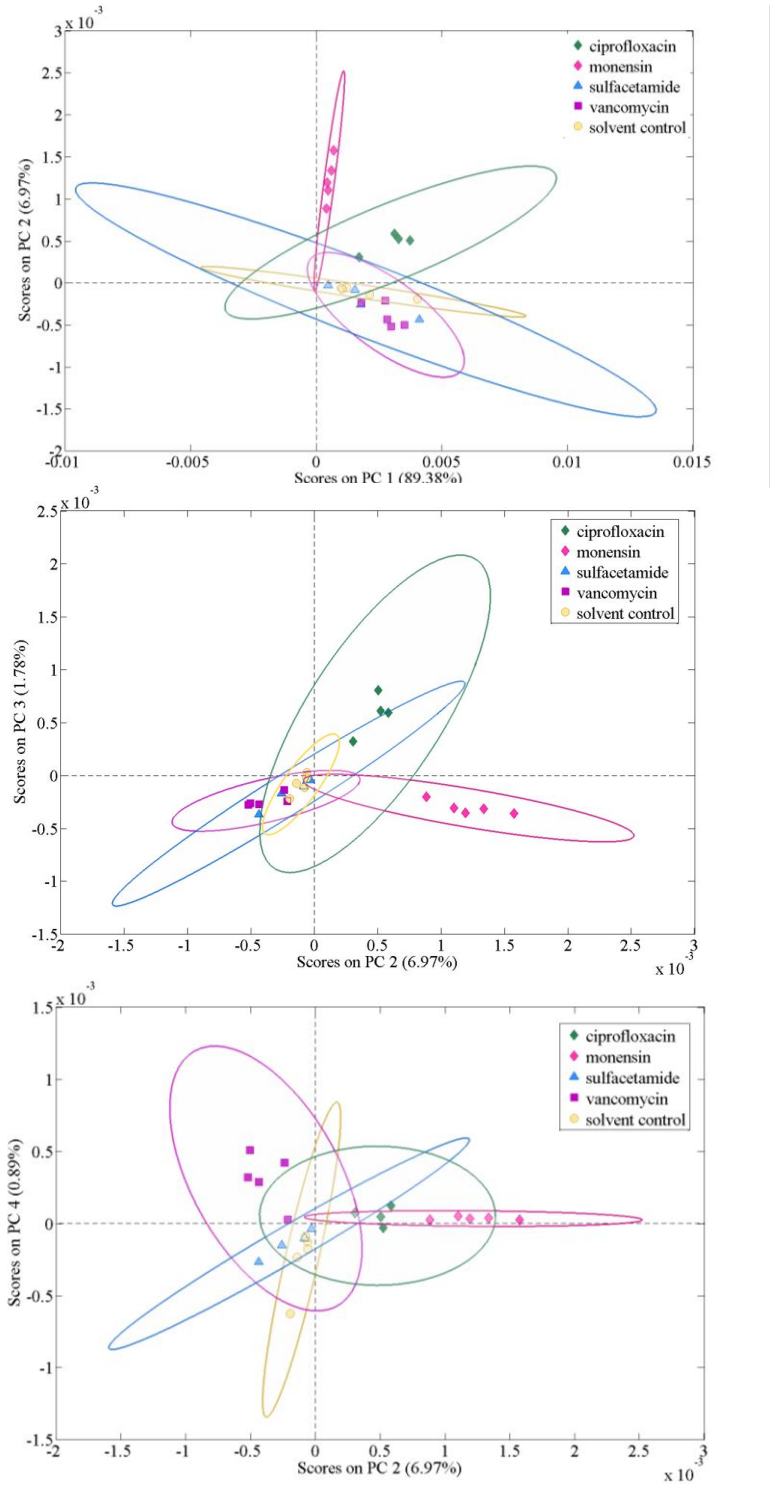

Figure 28. Principal component analysis (PCA) scores plots of metabolomics data from ^{1}H NMR spectra of polar, intracellular metabolites from MRSA (ATCC 33591) treated with either ciprofloxacin (n=4), monensin (n=5), sulfacetamide (n=4), vancomycin (n=5), or a solvent control (n=5). Colored circles correspond to the 95% confidence interval for each treatment.

A.

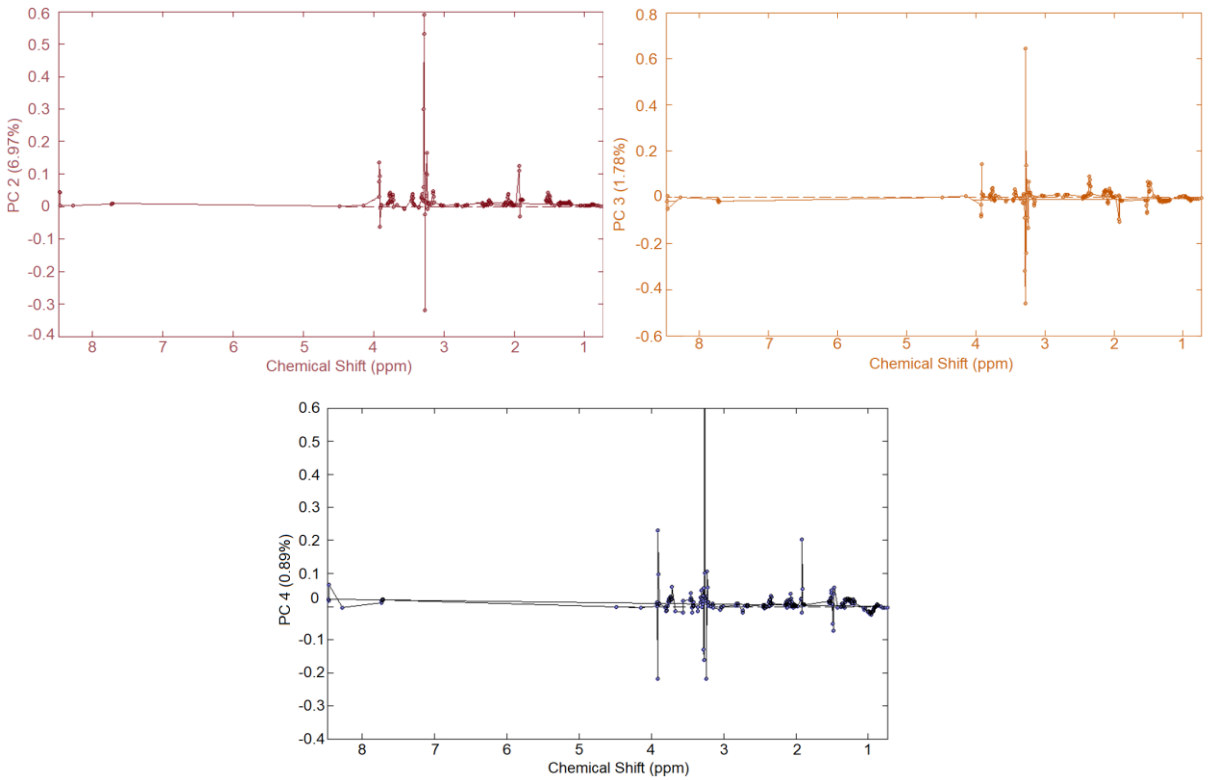

B.

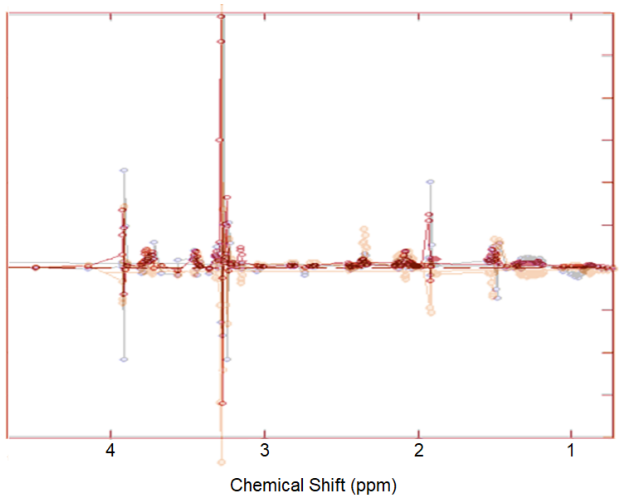

Figure 29. A. PCA loadings for ^{1}H NMR metabolomics of polar, intracellular extracts of MRSA (ATCC 33591). Spectroscopic features with positive loadings are associated with metabolites exhibiting increased concentrations in treatments that fall in the positive region of the scores plot (i.e., ciprofloxacin and monensin treatments for PC 2) whereas spectroscopic features with negative loadings indicate metabolites with increased concentrations corresponding to treatments that fall in the negative region of the scores plot (i.e., sulfacetamide, vancomycin, and solvent control treatments for PC 2). B. Overlay of loadings plots from PC 2 (red), PC 3 (orange), and PC 4 (black) in NMR spectral region with the greatest amount of variability.

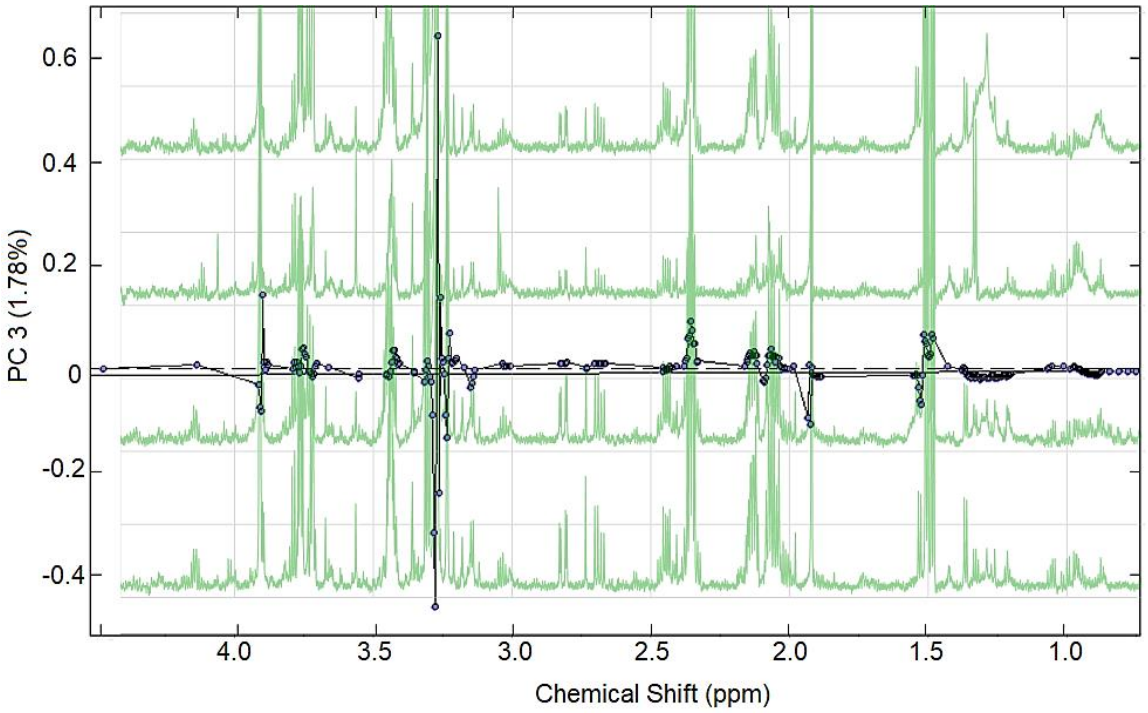

Figure 30. Overlay of loadings plot for PC 3 with NMR spectral data acquired for intracellular metabolite extracts from MRSA treated with ciprofloxacin, the treatment differentiated by PC 3. Positive loadings values correspond to NMR spectral signals that are upregulated in the ciprofloxacin treatment condition.

4.5 Discussion

Of the available techniques for evaluating mechanisms of action (MOA), a systems biology approach, such as metabolomics, is one of the most efficient and comprehensive options when the MOA of a candidate drug is completely unknown, especially when compared to approaches that assess one putative MOA at a time. The global picture provided by omics approaches allows for a fuller appreciation of perturbations to cellular pathways associated with exposure to a drug. Of the omics approaches, metabolomics measures the end products of biochemical pathways and can amplify minor changes that occur in the transcriptome, proteome, or genome.[141] Another situation where

metabolomics proves to be the best analysis option for understanding the MOA of available drugs is in cases where the target pathogen has poorly understood biology or a complex infection cycle, which makes an unbiased approach for exploring MOA more suitable than targeted methods.[175] *Mycobacterium tuberculosis* is one such pathogen that presents both of these challenges which is in part why recent MOA studies of this pathogen employ metabolomics.[148,152] Although the biology of *S. aureus* is better understood than *M. tuberculosis*, a metabolomics approach is still considered a powerful tool for elucidating MOA of novel antibiotics.

A simple approach to decipher whether a novel antibiotic acts via a known or new MOA is to compare metabolomes of the pathogen exposed to the novel antibiotic vs. antibiotics whose MOAs have previously been characterized. If the novel drug induces pathway perturbations that overlap with a known antibiotic's, this supports the hypothesis that the two antibiotics share a common MOA against the target pathogen. This approach was successfully applied in a study of *Mycobacterium smegmatis*, a non-pathogenic bacterium used as a model for *M. tuberculosis*, in which the effects of three novel chemical leads with unknown MOAs were compared to 12 antituberculosis drugs with known MOAs.[148] Through principal component analysis (PCA) and orthogonal partial least-squares discriminant analysis (OPLS-DA) of ^{1}H NMR spectral data, that study reported that the new drugs shared a common MOA with one another. Metabolomes of *M. smegmatis* exposed to these drugs also clustered with those treated with the antibiotics ampicillin, D-cycloserine, and vancomycin, all of which disrupt cell wall formation, supporting the hypothesis that the new drugs also disrupt cell wall formation. In the present study, a similar approach is planned to determine if the novel antibiotic natural product

cladophorol D (**17**) acts against MRSA via an MOA in common with one of nine antibiotics with known MOAs. The pilot experiment with the antibiotics ciprofloxacin, monensin, sulfacetamide, and vancomycin confirmed that an NMR-based metabolomics approach distinguishes metabolite differences in MRSA treated with these different antibiotics. Comparison of the ^{1}H NMR spectral signals responsible for the observed variance in antibiotic treatment conditions to NMR metabolomics studies presented in literature allowed some conclusions to be drawn. Ciprofloxacin has previously been reported to alter the pool of deoxynucleotides and peptidoglycan precursors, ultimately impacting DNA and cell wall synthesis.[150] ^{1}H NMR spectral signals for deoxyribose sugars fall within the spectral range of 1-4 ppm where differences were observed for PC 3 (principal component that differentiated ciprofloxacin from the other treatment conditions); however, downfield signals (6-8 ppm) associated with protons of the base unit of a deoxynucleotide were absent in this loadings plot, disproving the hypothesis that MRSA exposure to ciprofloxacin disrupted deoxynucleotides in the current experiment (Figure 29). A previous study reported that metabolites associated with the tricarboxylic acid cycle, including citrate, isocitrate, and 2-oxoglutarate, were upregulated during treatment of *S. aureus* with ciprofloxacin. PC 3 contains increased NMR spectral signals corresponding to these molecules.[150] Evaluation of the impact of monensin on cattle ruminal fluid, which contains a diverse array of microbes, found that metabolic pathways associated with metabolism of linoleic acid and some amino acids, including phenylalanine, are upregulated.[176] PC 2, which differentiated monensin and ciprofloxacin from the other treatment conditions, contained upregulated signals in both the upfield (1-4 ppm) and downfield (7.5-8.5 ppm) regions that might correspond to these types of metabolites. The

next step for this project will be to perform the full metabolomics experiment with all nine antibiotics and cladophorol D (**17**), combining NMR and MS-based metabolomics analysis.

If the metabolome of MRSA treated with cladophorol D (**17**) does not overlap with one of the other antibiotic treatments, another approach that can be taken to elucidate a new antibiotic's MOA is to examine which metabolites are upregulated or downregulated, without comparing to other known drugs. This information can be used to determine which biochemical pathways are impacted by any individual antibiotic. A study evaluating the effect of antibiotics against *Escherichia coli* successfully employed untargeted mass spectrometry-based metabolomics to characterize the MOAs of nine antibiotics, supporting that this is a viable approach for elucidating unknown and possibly novel MOAs.[177]

Comparing responses of related bacterial strains to an antibiotic is another possible approach for assessing MOA. By comparing metabolomes of strains from the same bacterial species with varying susceptibility to a given antibiotic treatment, it is possible to identify subtle differences indicative of how the antibiotic inhibits growth of a more sensitive strain. Additionally, this approach may lead to identification of mechanisms of resistance that have led to a susceptible strain becoming insensitive. This approach is complementary to the method presented in the current work as both methods provide information about what biochemical pathways are perturbed. This method was successfully used to evaluate *S. aureus* strains with varying degrees of susceptibility to the antibiotics methicillin, gentamicin, ciprofloxacin, erythromycin, and fusidic acid, leading to the finding that certain lipid groups are upregulated in resistant bacterial strains conferring antibiotic resistance to the bacteria.[178] The screening against *S. aureus* strains performed

by Dr. Cassandra Quave's lab pinpointed sensitive and resistant bacteria that could be used for a future study of bacterial resistance pathways relevant to cladophorol D (**17**).

4.6 Materials and Methods

4.6.1 Determination of Antibiotic Dosage for Metabolomics

MRSA (ATCC 33591) was grown at 37 °C with shaking at 120 rpm in 10 mL of Difco Nutrient Broth overnight. Optical density at 600 nm (OD600) was measured (BioTek ELx800 Absorbance Microplate Reader) and culture was diluted to obtain an OD600 of 0.030 (approximate cell density 1 x 10^8 cells/mL). MRSA culture was distributed to wells in a 96-well plate and the following antibiotics were added in serial dilution down the plate along with solvent controls based on the solubility of each antibiotic: ciprofloxacin (dissolved in 0.5% aqueous acetic acid, concentration range 0.015-33 µg/mL), clindamycin (water, 0.015-650 µg/mL), isoniazid (water, 0.015-650 µg/mL), kanamycin (water, 0.015-33 µg/mL), linezolid (dimethyl sulfoxide, 0.015-33 µg/mL), monensin (ethanol, 0.015-33 µg/mL), rifampicin (dimethyl sulfoxide, 0.00023-33 µg/mL), sulfacetamide (water, 0.015-320 µg/mL), and vancomycin (water, 0.015-33 µg/mL). Concentration ranges were selected based on reported MIC_{90} values for the antibiotics in literature. To prepare the plate, 5 µL of each treatment was added to the top row which contained 145 µL of MRSA culture. Then 50 µL of the top row was transferred, after mixing, to the next row and the same volume was transferred down the plate resulting in a final culture volume of 100 µL in all wells. The plate was incubated at 37 °C with shaking at 60 rpm for 6 hours. OD600 readings were recorded and dose response curves were plotted in GraphPad.

Based on the dose response results, antibiotic concentrations that suppressed growth by 20-50% relative to the solvent control were selected for a follow-up study performed with the MRSA culture volume intended for the metabolomics experiment (10 mL). To simplify the number of controls necessary due to the different solubilities of the antibiotics chosen for the experiment, every culture condition (treatments and control) contained a mixture of all of the solvents used to dissolve the different antibiotics (0.53% aqueous acetic acid (0.1 % of final solution); water (0.66% of final solution); ethanol (0.14% of final solution); methanol (0.08% of final solution); and dimethyl sulfoxide (0.33% of final solution)).

4.6.2 Sample Preparation, Intracellular Metabolite Extraction, and NMR Spectral Acquisition for Pilot Experiment

A total of 30 MRSA cultures (ATCC strain 33591) were grown over the course of three days (10 cultures per day for 5 treatment conditions tested in duplicate) in 7 mL of Difco Nutrient Broth dispensed in 25 mL tissue culture flasks at 37 °C with shaking at 60 rpm for 6.5 hours, the amount of time it took for MRSA to reach late exponential growth. For each test day, media was pre-treated with the different solvents and antibiotic treatments (solvent control: mix of 5 solvents described in previous section; ciprofloxacin [final concentration 0.05 µg/mL] plus ethanol, methanol, water, and DMSO to amounts defined in previous section; monensin [final concentration 0.35 µg/mL] plus dilute acetic acid, methanol, water, and DMSO; sulfacetamide [final concentration 0.6 mg/mL] plus dilute acetic acid, ethanol, water, and DMSO; and vancomycin [final concentration 0.25 µg/mL] plus dilute acetic acid, ethanol, methanol, and DMSO. The pre-treated media was then inoculated with MRSA to achieve a starting cell density of about 1 x 10^7 cells/mL.

After incubation, the cells were separated from the media using vacuum filtration with PES filters (Supor, 0.45 μm pore size, Pall Laboratory) and the cells were rinsed with chilled 0.6% aqueous NaCl solution. The filter was transferred to a sterile 50 mL polypropylene tube containing cold 70% aqueous ethanol, vortexed to transfer cells from the filter to the solvent, and the 70% aqueous ethanol was transferred to a sterile 15 mL polypropylene tube containing 0.5 mm zirconia/silica beads. The cells were lysed by vortexing the cell/methanol/bead mixture and then centrifuged to pellet the cells and beads. After the supernatant was transferred to a glass scintillation vial, the cell/aqueous ethanol/bead mixture was rinsed three times with 70% aqueous ethanol. The resulting intracellular extract was dried in a speed vacuum concentrator before being subjected to liquid/liquid partition with a 3:1.4:1.6 mixture of chloroform, water, and methanol. The resulting nonpolar and polar extracts were dried in the speed vacuum concentrator and lyophilized prior to NMR spectral analysis. The nonpolar samples were resuspended with 150 μL of $CDCl_3$ while the polar samples were dissolved in 99.8% D_2O solution containing 50 mM phosphate buffer (pH 7.2, uncorrected) and 50 μM 3-(trimethylsilyl)propionic acid-2,2,3,3-d4 (TMSP-d4) as an internal standard for chemical shift referencing before being transferred to 3 mm NMR tubes. ^{1}H NMR spectra were acquired on a 16.4 T (700 MHz for ^{1}H) Bruker Advance III HD instrument with a 5mm indirect broadband cryoprobe.

4.6.3 Metabolomic Data Analysis

^{1}H NMR spectral data were preprocessed in Metabolab. TMS was used to align spectra at 0.00 ppm and all spectra were manually phased and baseline corrected prior to removal of the spectral regions around TMS (-2.00 to 0.50), D_2O (4.50 to 5.50), and unoccupied downfield region (8.51 to 14.60). All spectra were noise filtered, binned (0.005

ppm), and probabilistic quotient normalized. PLS toolbox version 8.1 in Matlab was used to construct principal component analysis (PCA) plots.

CHAPTER 5. CONCLUSIONS AND FUTURE DIRECTIONS

Natural product drug discovery continues to provide valuable leads for new medicines despite the shift in focus of pharmaceutical companies to combinatorial chemistry and high throughput screening of synthetic chemical libraries over the last few decades.[9] The decision to deprioritize natural product discovery programs was in part due to challenges presented by the limited supply of natural products as well as difficulties encountered while pursuing synthetic routes since many natural products are comprised of complex scaffolds. Additionally, there is a high rate of re-discovery of known bioactive molecules in screening programs.[179] Taking steps to understand the mechanisms of action (MOAs) of these complex molecules, as reported in chapters 1 and 4, can help boost the likelihood that pharmaceutical companies pursue development of drugs derived from natural products, especially if the MOA is found to be novel. An additional benefit to elucidating the MOA of a natural product is that it can help identify the drug's pharmacophore which can in turn lead to a medicinal chemistry program towards development of lead molecules with reduced structural complexity.[180]

Synthetic biology provides a number of solutions to existing challenges with natural product drug development. Knowledge of the biosynthetic gene clusters encoding enzymes required for assembly of these complex molecules is the first step towards a biological solution to natural product synthesis. More specifically, genetic engineering to express biosynthetic gene clusters in a scalable microbial system such as *E. coli* can enable access to complex chemical structures (including with control of stereochemistry) with improved yields.[181] Additionally, research on cryptic biosynthetic gene clusters has

provided promising routes to promoting production of novel chemical entities.[182] In the field of chemical ecology, induction of chemical defenses produced by cryptic biosynthetic gene clusters has been reported. For example, a *Streptomyces* sp. and *Aspergillus* sp. co-isolated off Heron Island in Australia were found to be involved in chemical warfare where a metabolite produced by the fungus *Aspergillus* sp. stimulated nitric oxide production by the bacterium *Streptomyces* sp. which in turn activated a silent biosynthetic gene cluster that produced the antifungal natural product heronapyrrole B.[183] Identifying such interactions or exploring the role of a natural product in its native environment, as was done in chapter 2, can assist in promoting production of these unique, bioactive molecules from cryptic biosynthetic gene clusters.

Advancements in the field of natural products chemistry have been greatly aided by improvements in structure elucidation instrumentation, construction of small molecule databases, and the use of informatics tools to analyze complex datasets. Advances in instrumentation have made it possible to identify natural products produced in very small natural yields and to quickly identify known compounds within complex mixtures. In chapter 1, microgram quantities of new and previously identified cyanobacterial natural products were isolated; without the sensitivity and spectral dispersion of an 800 MHz NMR spectrometer, deciphering the structures would not have been feasible. Chapters 1 and 3 made use of NMR spectroscopy and LC/MS early in the isolation process to assist in dereplication efforts. Although this did lead to identification of known natural products, the novelty of the bioassays used for screening meant that even if known natural products were responsible for the observed bioactivity, their promise for treating a neglected disease with few pharmacological options provided motivation for structural characterization.

The future of natural products chemistry looks bright. Valuable resources to aid in the identification of molecules, such as the Global Natural Products Social Molecular Networking (GNPS) database,[184] MarinLit,[7] and the Natural Product Atlas,[185] continue to emerge and increase in sophistication. New approaches to data analytics, such as molecular networking, enable organization and hypothesis-driven exploration of large, complex datasets that would otherwise be overwhelming to analyze.[186] New informatics systems have also been developed to analyze NMR spectral data, for example, Small Molecule Accurate Recognition Technology (SMART).[187] This technique makes use of non-uniform sampling 2D NMR spectroscopy and deep Convolutional Neural Networks to aid in dereplication and early identification of natural products before substantial investment in purification efforts. Computer Assisted Structural Elucidation (CASE) [188,189] prevents incorrect structural assignments by computationally generating possible structures based on experimental NMR spectral features, further increasing efficiency of natural products research efforts.

This dissertation explored three distinct topics related to the field of natural products: discovery of therapeutics from marine organisms, evaluation of their MOAs against pathogens, and identification of their defensive roles in their native environment. Chapter 1 contributes valuable knowledge for possible treatment options for malaria through the discovery of nanomolar antimalarial activity in the known cyanobacterial natural product lyngbyabellin A (**3**) and through the evaluation of the MOA of the antimalarial natural product kakeromamide B (**1**). Chapter 2 provides insights about the protective role of peyssonnoside A (**7**) against a marine fungus and gives a more comprehensive understanding for why the red alga *Peyssonnelia* sp. produces this natural product in such

high abundance. Chapter 3 demonstrates the potential for identifying natural products with anthelmintic activity from marine organisms, however, further steps are still needed to identify the bioactive molecule(s). Currently, natural products from the bioactive fractions submitted to collaborators in the Aroian lab have been purified and once bioactivity results are returned, structure elucidation of the active natural product(s) will be completed with the assistance of Bhuwan Chhetri of the Kubanek lab before returning pure natural product(s) to the Aroian lab for evaluation of potency against infectious hookworms. Chapter 4 presents a viable method for exploring the MOA of a novel compound through the systems biology approach of metabolomics. To complete the work presented in this chapter, a full metabolomics experiment with cladophorol D (**17**) and nine antibiotics with known MOAs will be performed with the help of Nolan Barrett of the Kubanek lab. The resulting intracellular metabolite extracts will be evaluated using NMR spectroscopy and LC/MS analysis. Despite chapters 3 and 4 being adversely impacted by the shutdown caused by COVID-19, the work presented in this dissertation represents a substantial body of work that has positively contributed to the field of natural products. Additionally, every effort will be made to progress the research presented in chapters 3 and 4 to the point of publication.

APPENDIX A. NMR DATA TABLES AND SPECTRA

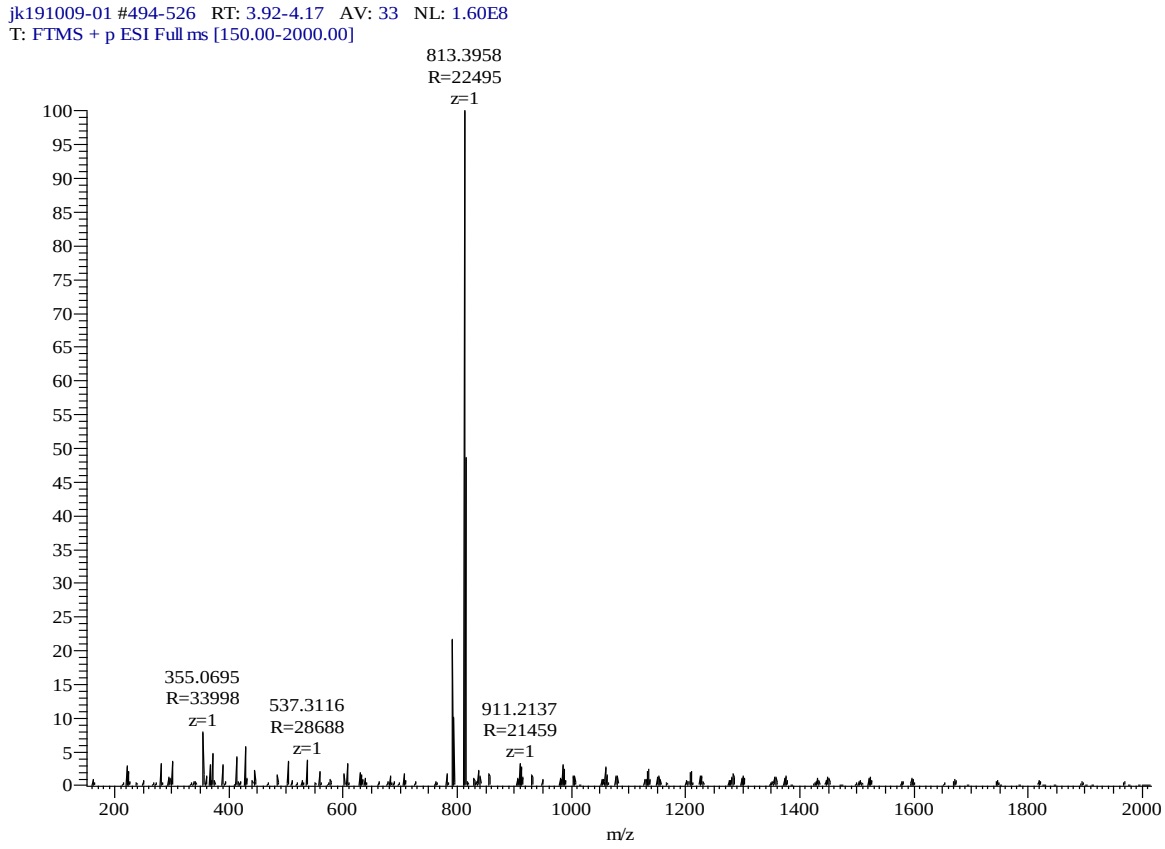

Figure A 1. HRESIMS of kakeromamide B (**1**), *m/z* $[M+H]^+$ calculated for $C_{42}H_{59}N_6O_7S$ 791.4166, found 791.4150 (Δ = 2.0 ppm); $[M+Na]^+$ calculated for $C_{42}H_{58}N_6O_7SNa$ 813.3985, found 813.3958 (Δ = 3.3 ppm).

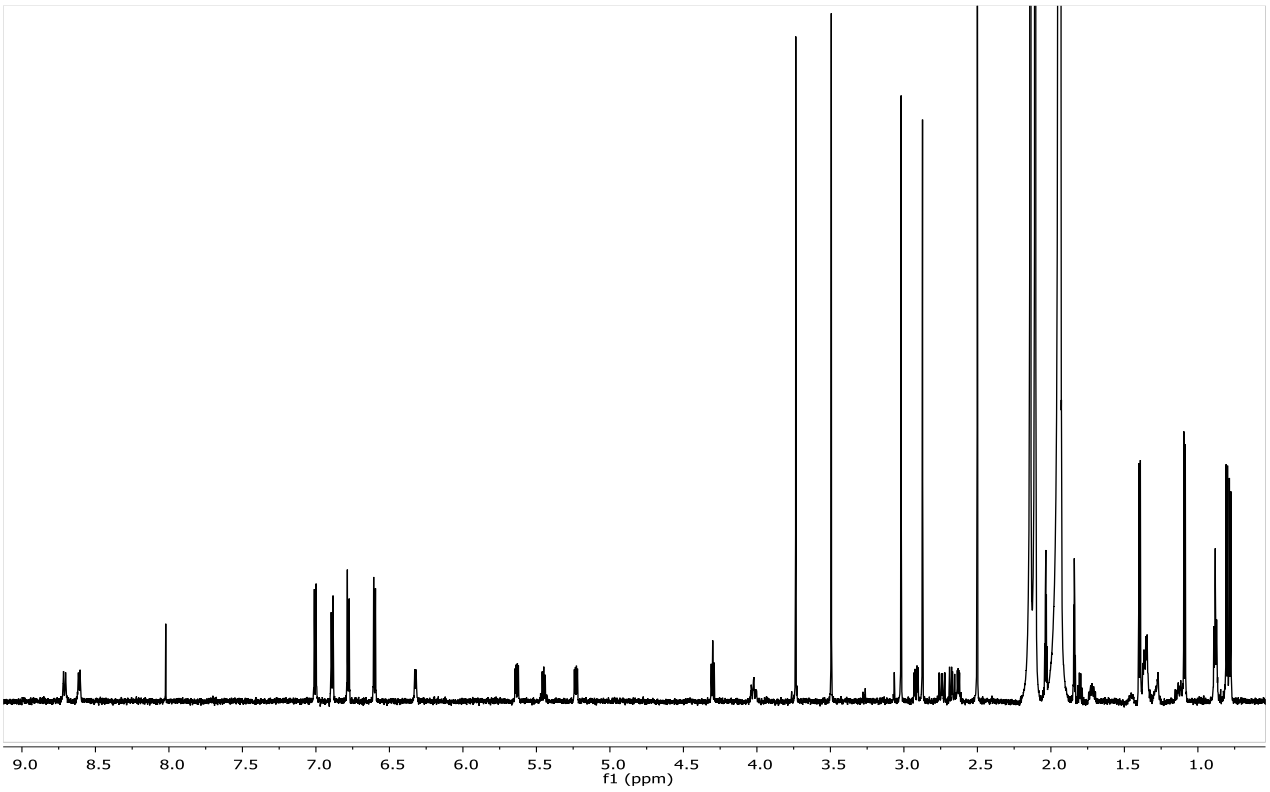

Figure A 2. ^{1}H NMR spectrum of kakeromamide B (**1**) in CD_3CN (700 MHz).

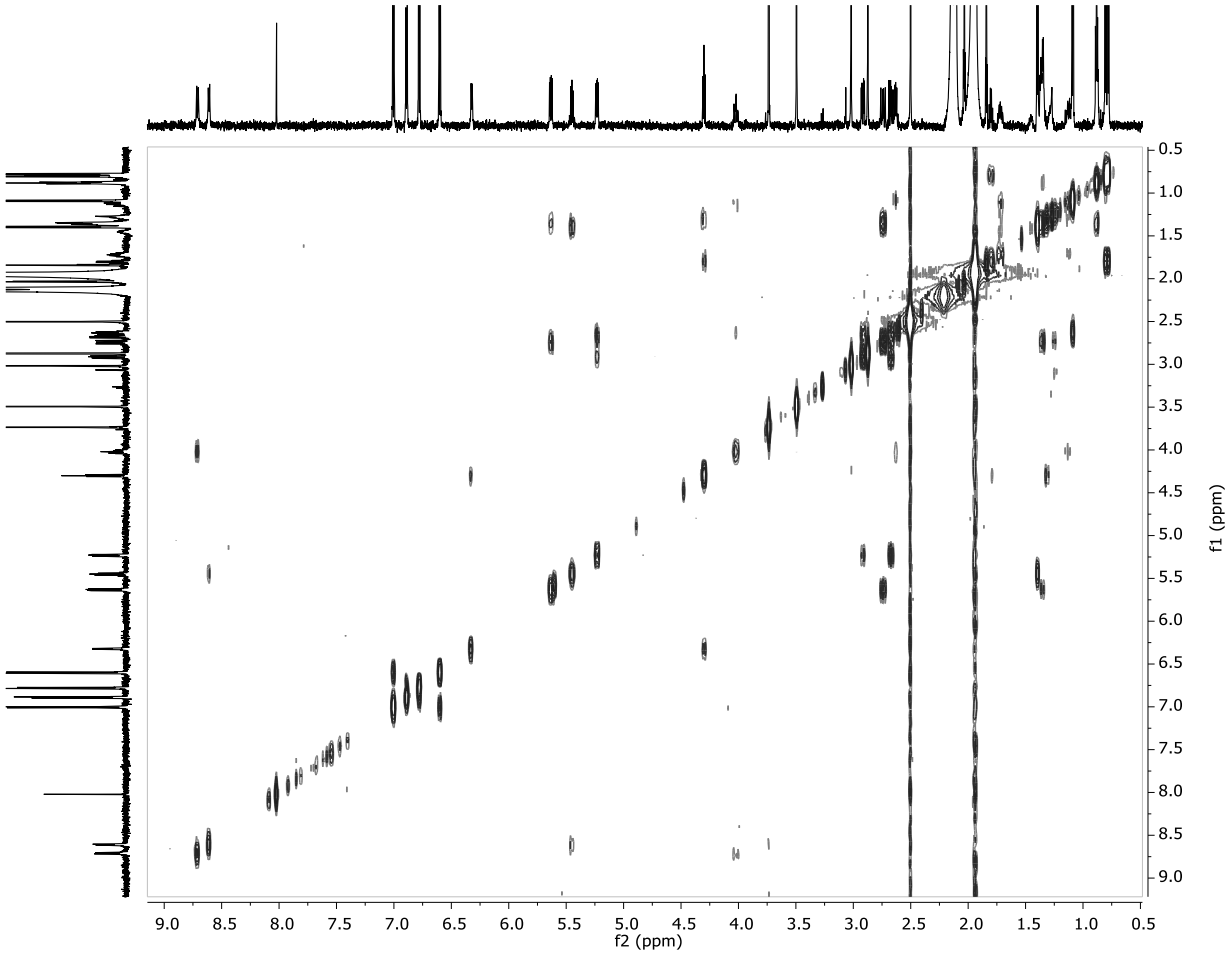

Figure A 3. COSY spectrum of kakeromamide B (**1**) in CD_3CN (700 MHz).

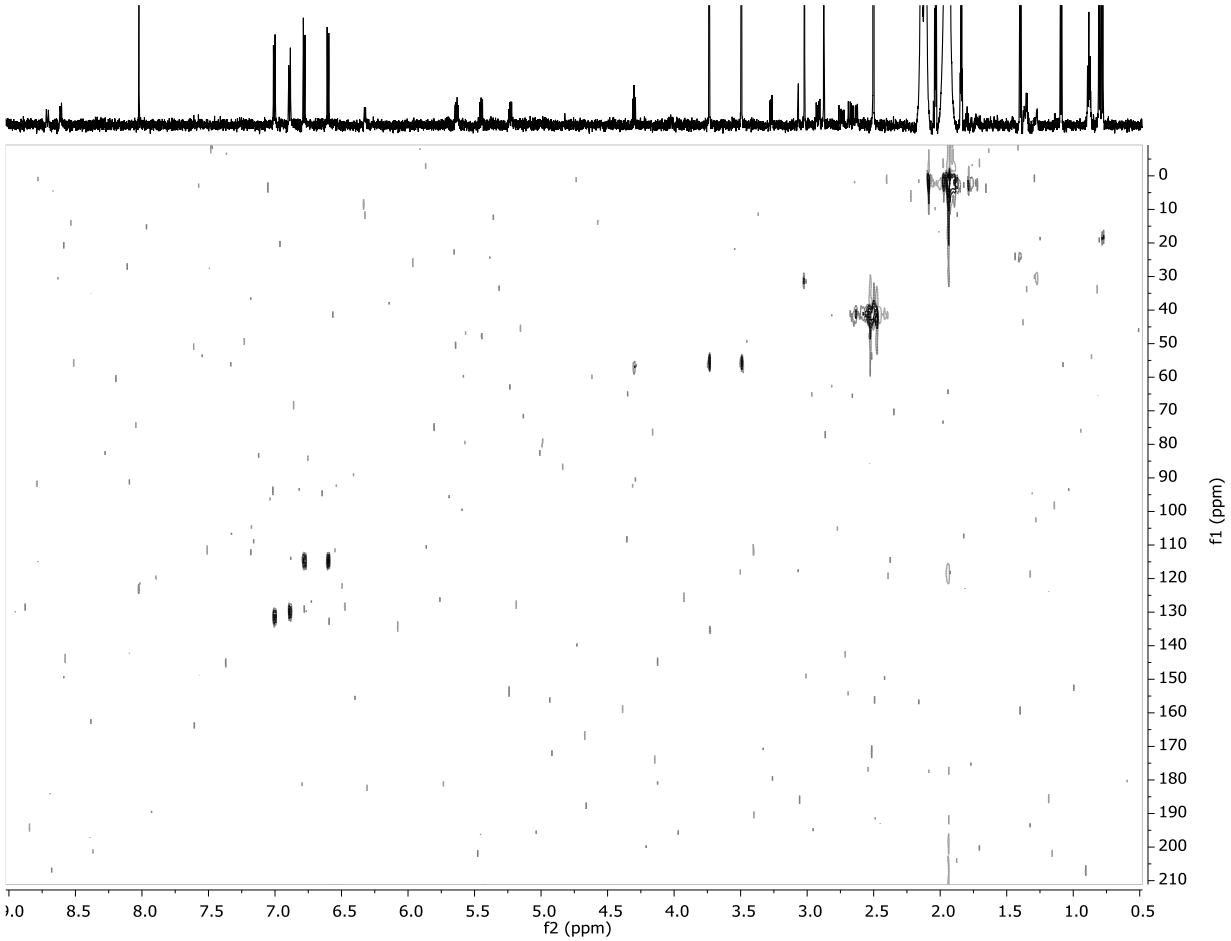

Figure A 4. HSQC NMR spectrum of kakeromamide B (**1**) in CD_3CN (700 MHz).

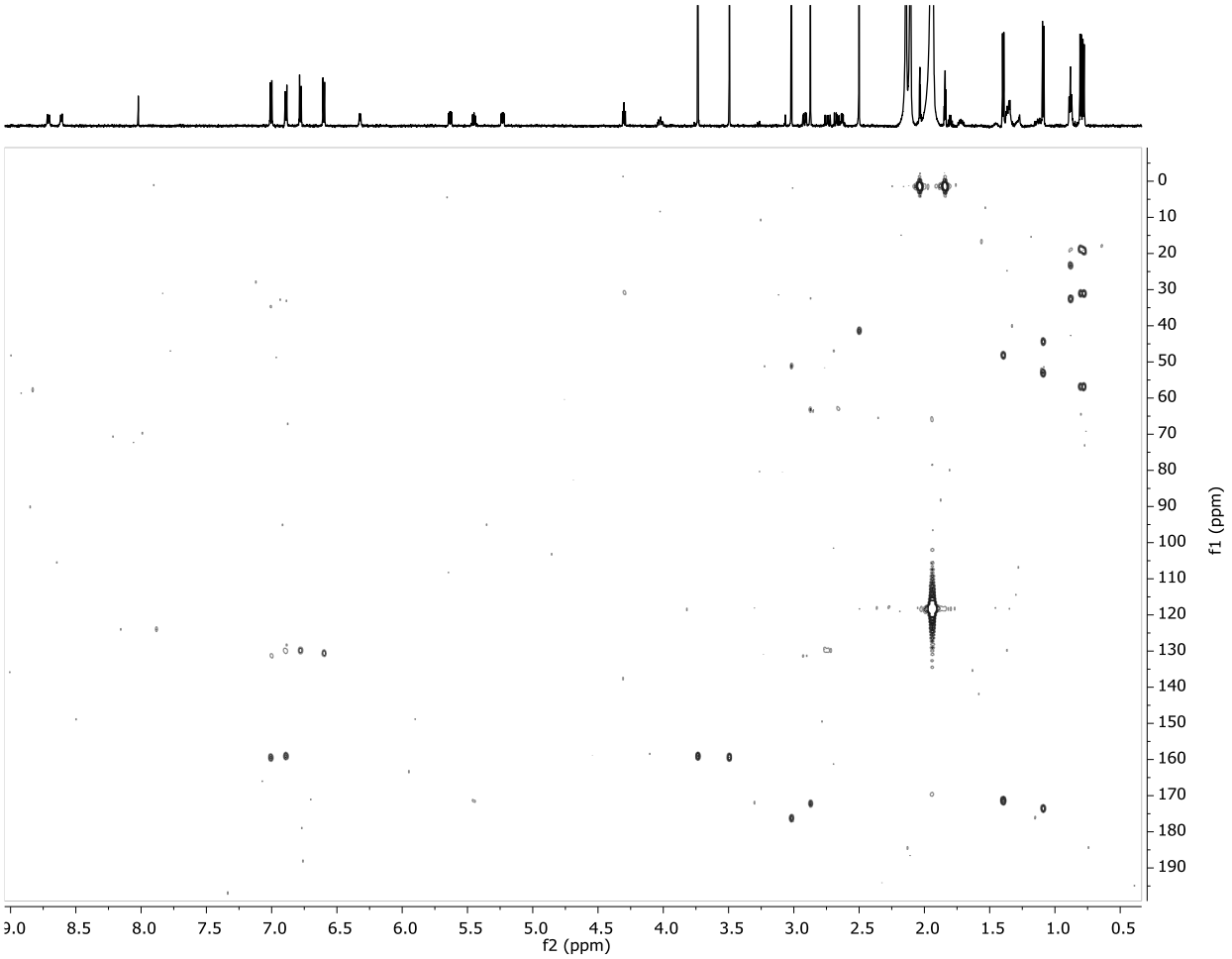

Figure A 5. HMBC NMR spectrum of kakeromamide B (**1**) in CD_3CN (700 MHz).

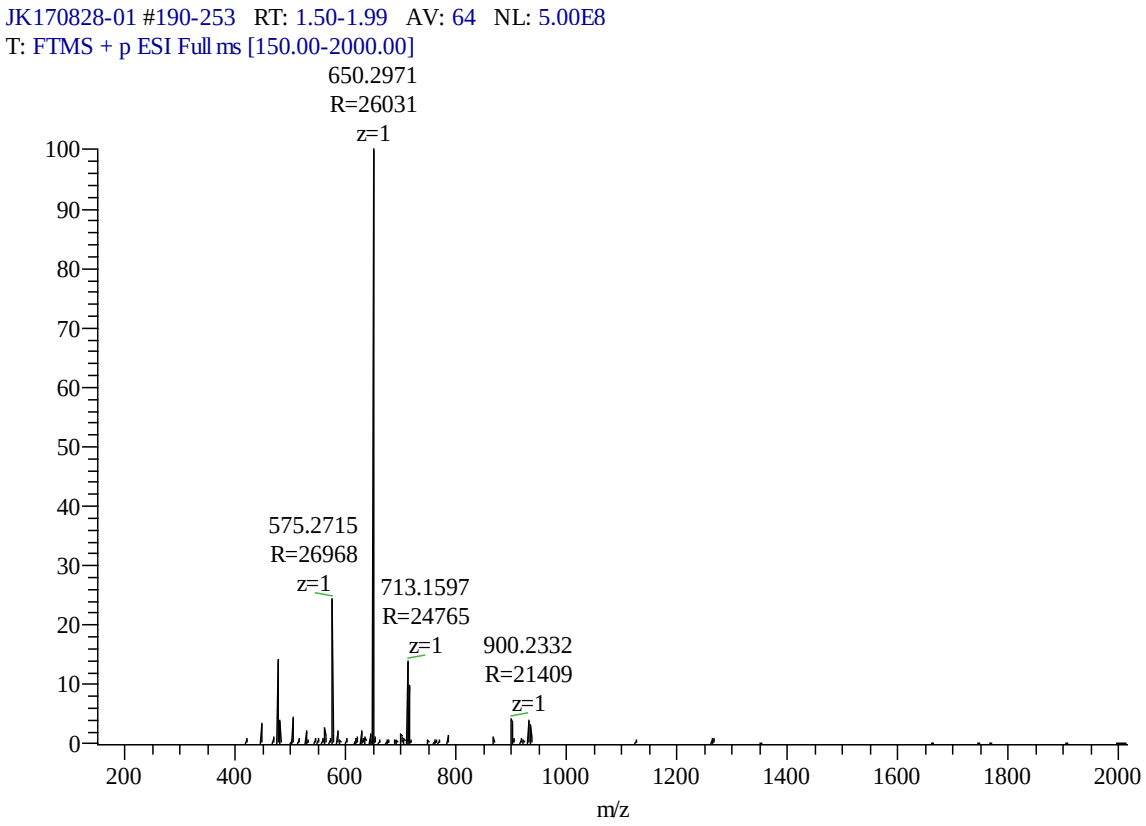

Figure A 6. HRESIMS of ulongamide A (**2**), *m/z* $[M + Na]^+$ calculated for $C_{32}H_{45}N_5O_6Sna$ 650.2983, found 650.2971 (Δ = 1.8 ppm).

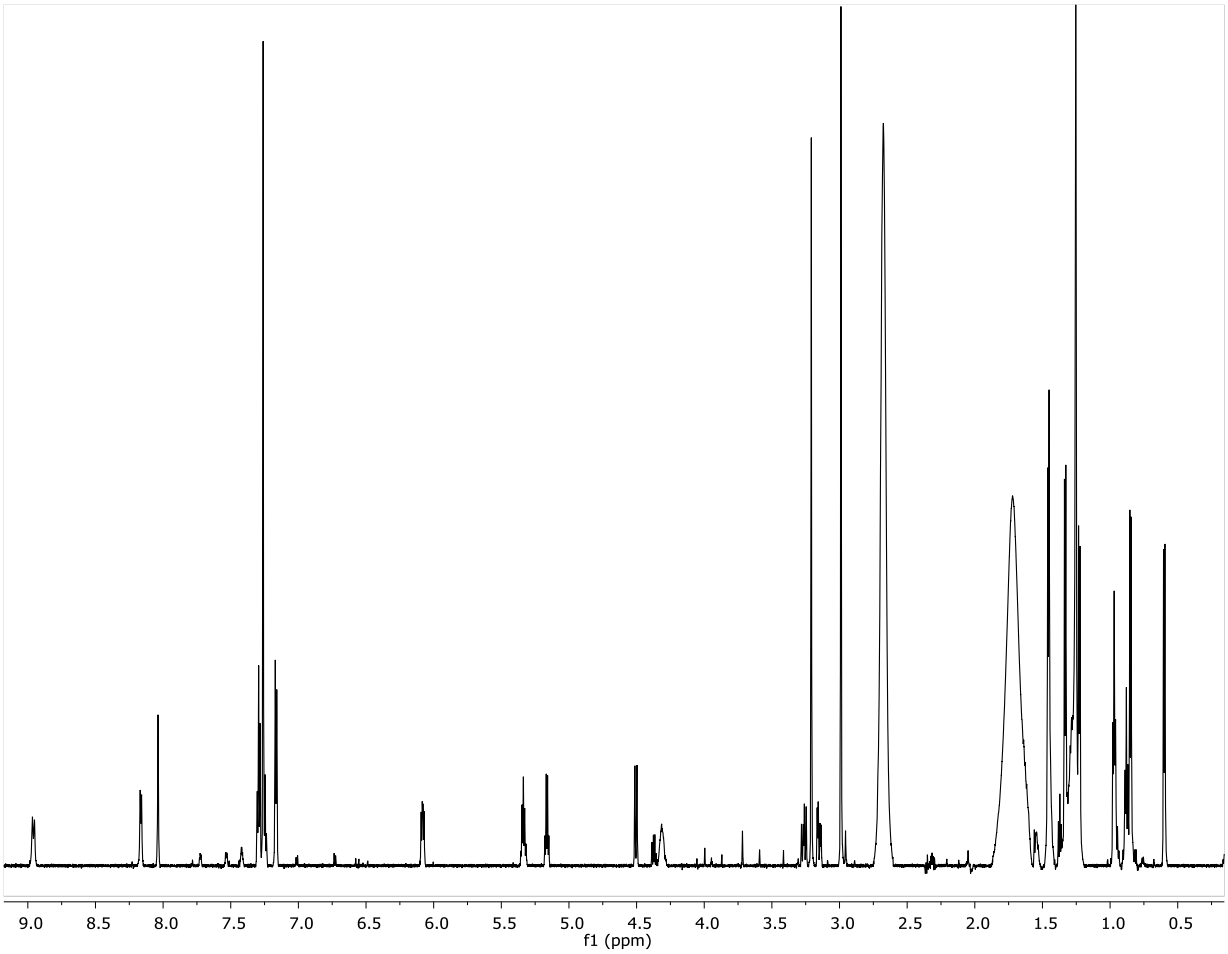

Figure A 7. ^{1}H NMR spectrum of ulongamide A (**2**) in $CDCl_3$ (700 MHz).

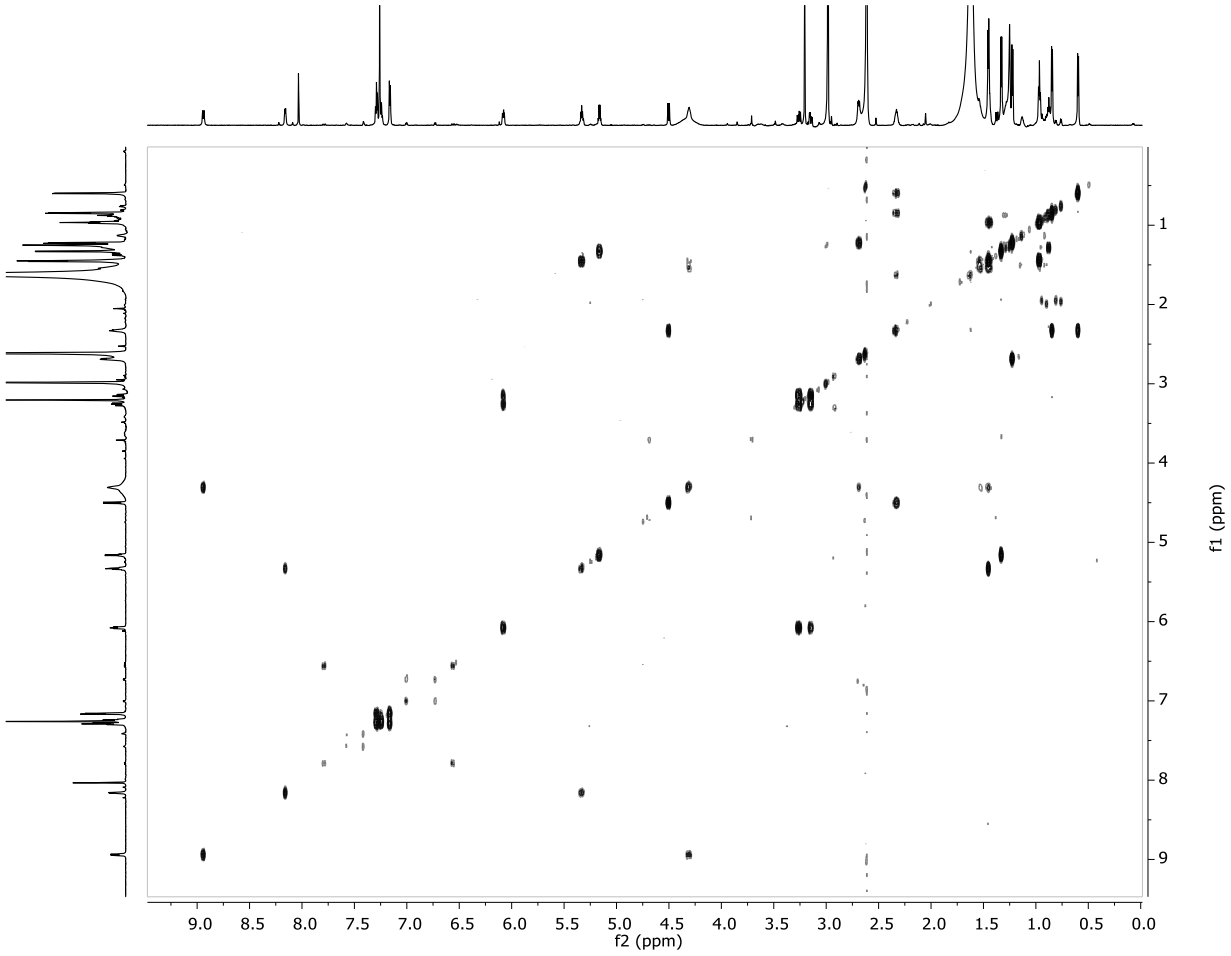

Figure A 8. COSY spectrum of ulongamide A (**2**) in $CDCl_3$ (800 MHz).

Table A 1. Comparison of ^{1}H NMR chemical shifts of ulongamide A (**2**) reported in literature [47] (500 MHz, $CDCl_3$) to experimental values of **2** (700 MHz, $CDCl_3$).

Unit	**Literature Values**		**Experimental Values (2)**	**Δ (ppm)**
	C/H no.	δ_H (*J* in Hz)	δ_H (*J* in Hz)	
Amha	1			
	2	2.68, qd (6.9, 2.8)	2.69, m	0.01
	3	4.31, m	4.31, m	0
	4a	1.43, m	1.43, m	0
	4b	1.54, m	1.55, m	0.01
	5	1.43, m	1.43, m	0
	6	0.97, t (7.0)	0.97, t (7.0)	0
	7	1.22, d (6.9)	1.22, d (6.9)	0
	NH	8.95, d (10.8)	8.94, d (10.6)	0.01
Ala-thz-ca	1			
	2			
	3	8.04, s	8.03, s	0.01
	4			
	5	5.33, quint (6.6)	5.33, quint (6.6)	0
	6	1.45, d (6.6)	1.45, d (6.7)	0
	NH	8.17, d (6.6)	8.16, d (6.7)	0.01
N-Me-Val	1			
	2	4.50, d (10.8)	4.50, d (10.8)	0
	3	2.33, m	2.33, m	0
	4	0.59, d (7.0)	0.60, d (6.8)	0.01
	5	0.84, d (6.6)	0.85, d (6.4)	0.01
	N-CH_3	2.99, s	2.99, s	0
N-Me-Phe	1			
	2	6.08, dd (9.4, 5.5)	6.08, dd (9.4, 5.6)	0
	3a	3.14, dd (−15.2, 5.5)	3.15, dd (15.2, 5.5)	0.01
	3b	3.26, dd (−15.2, 9.4)	3.26, dd (15.1, 9.4)	0

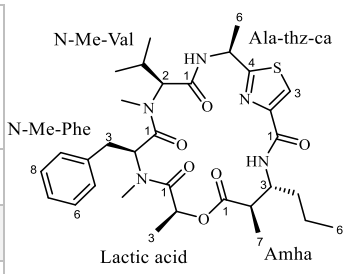

ulongamide A (**2**)

Table A 1 (continued)

N-Me-Phe	4			
	5/9	7.16, d (7.2)	7.16, d (7.5)	0
	6/8	7.29, m	7.29, t (7.5)	0
	7	7.25, m	7.24, m	0.01
	N-CH_3	3.20, s	3.20, s	0
lactic acid	1			
	2	5.15, q (6.6)	5.16, q (6.7)	0.01
	3	1.33, d (6.6)	1.33, d (6.7)	0

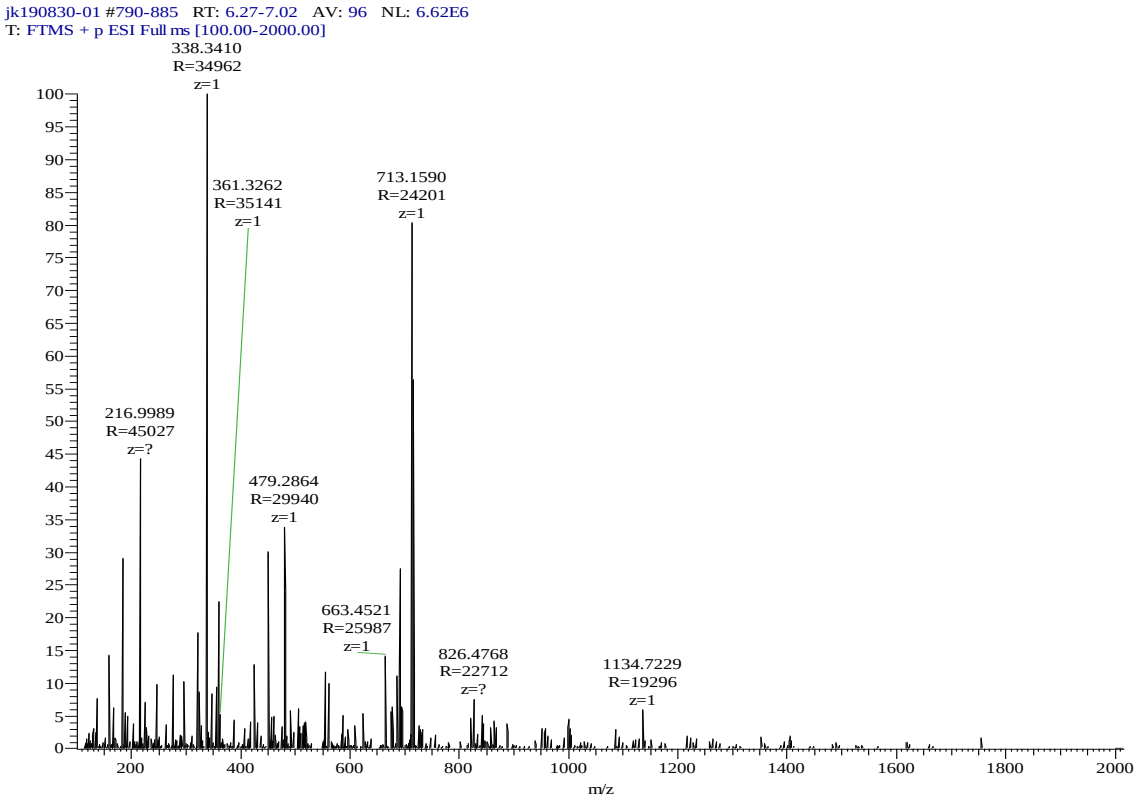

Figure A 9. HRESIMS of lyngbyabellin A (**3**), *m/z* $[M + H]^+$ calculated for $C_{29}H_{41}Cl_2N_4O_7S_2$ 691.1788, found 691.1771 (Δ = 2.5 ppm); *m/z* $[M + Na]^+$ calculated for $C_{29}H_{40}Cl_2N_4O_7S_2Na$ 713.1608, found 713.1590 (Δ = 2.5 ppm).

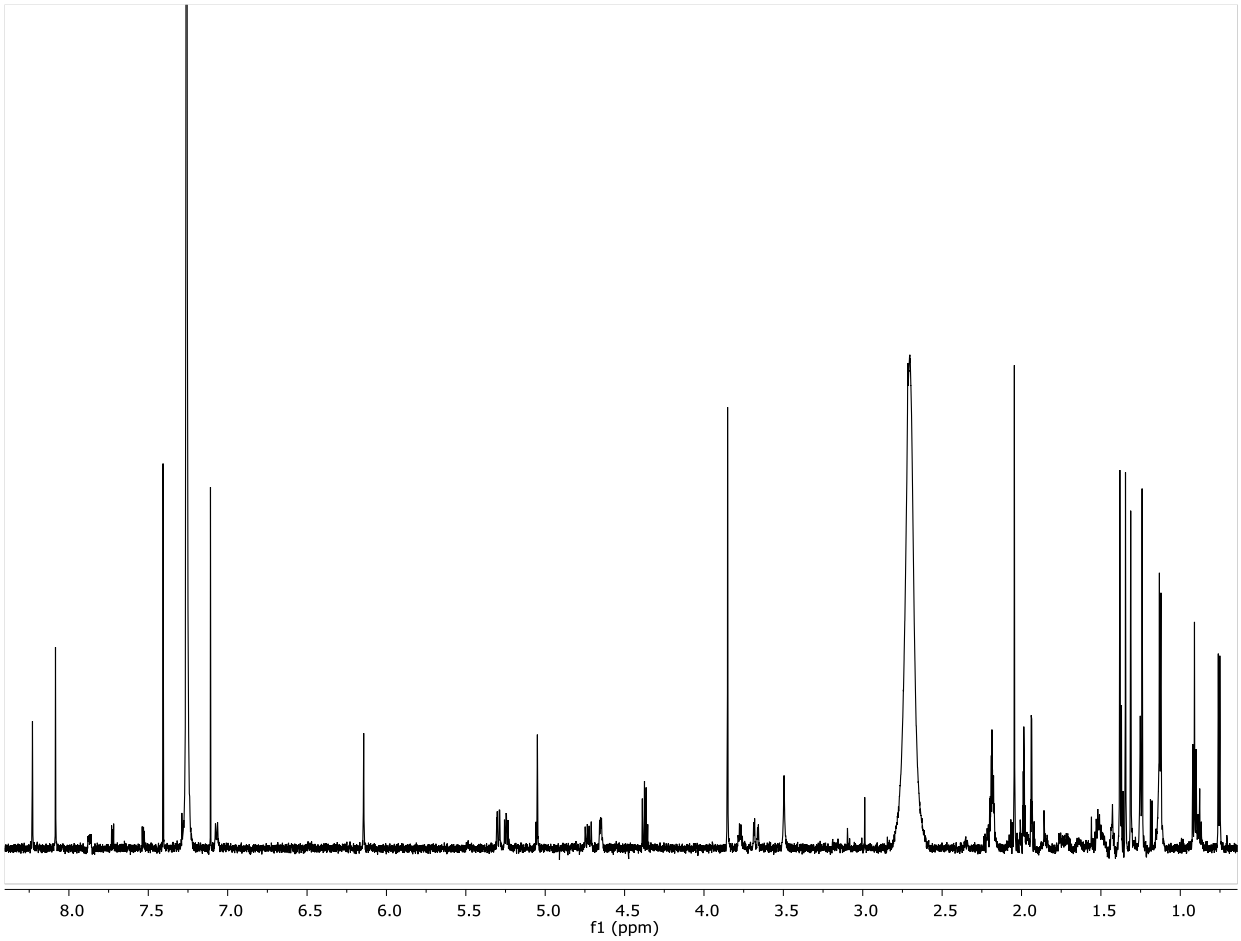

Figure A 10. ^{1}H NMR spectrum of lyngbyabellin A (**3**) in $CDCl_3$ (700 MHz).

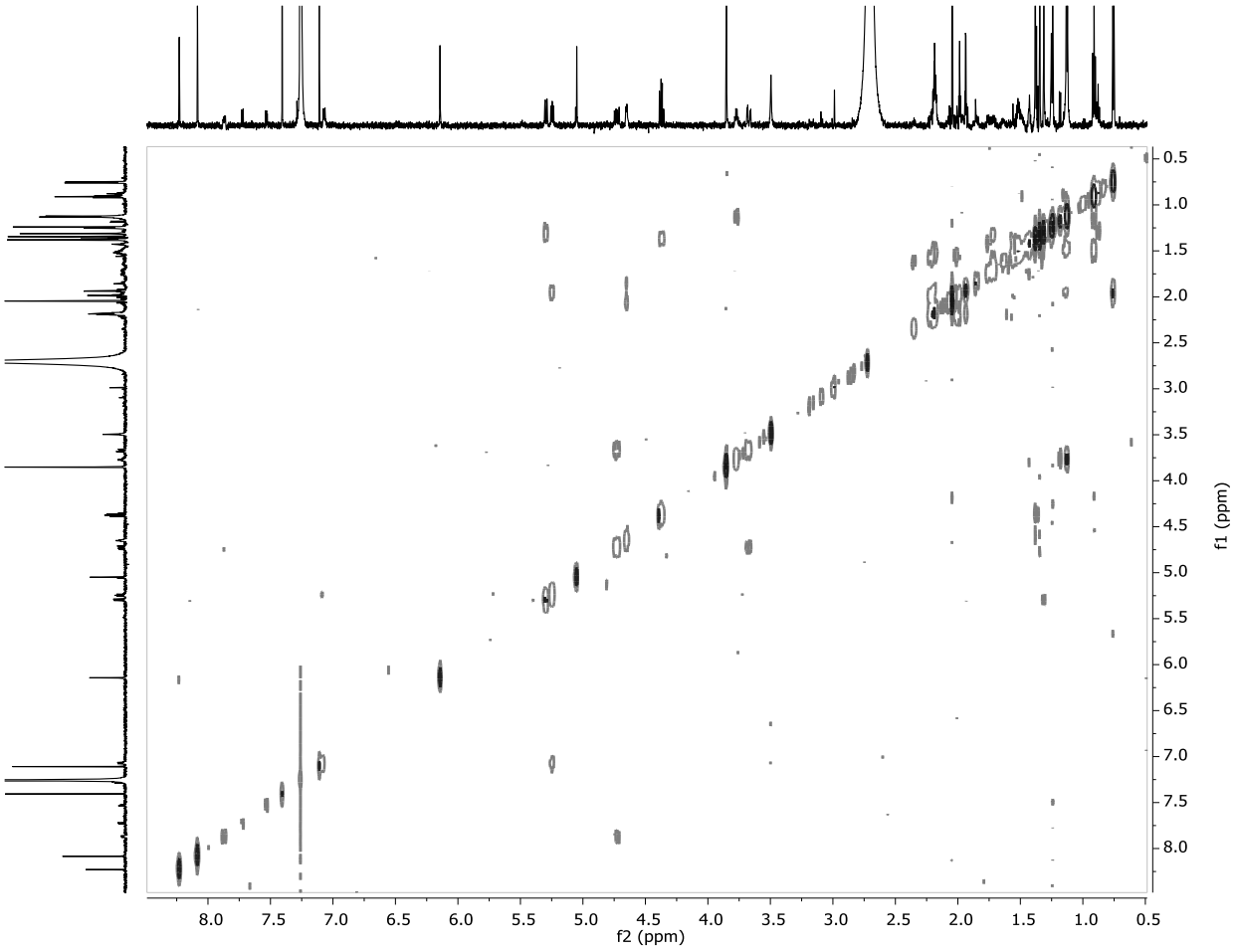

Figure A 11. COSY NMR spectrum of lyngbyabellin A (**3**) in $CDCl_3$ (700 MHz).

Table A 2. Comparison of ^{1}H NMR chemical shifts of lyngbyabellin A (**3**) reported in literature [48] (500 MHz, $CDCl_3$) to experimental values of **3** (700 MHz, $CDCl_3$).

C/H no.	Literature Values	Experimental Values (3)	Δ (ppm)
	δ_H (*J* in Hz)	**δ_H (*J* in Hz)**	
1			
2			
3	5.31, dd (10.6, 2.3)	5.30, dd (10.9, 2.3)	0.01
4a	1.33, m	1.31, m	0.02
4b	1.72, m	1.73, m	0.01
5	1.60, m	1.64, m	0.04
6a	2.00, m	1.99, p (2.4)	0.01
6b	2.22, ddd (−14.2, 10.8, 5.2)	2.22, m	0
7			
8	2.05, s	2.05, s	0
9	1.31, s	1.31, s	0
10	1.36, s	1.35, s	0.01
11			
12			
13	8.09, s	8.08, s	0.01
14			
15	5.24, dd (9.0, 6.8)	5.25, dd (8.6, 6.6)	0.01
15-NH	7.27, d (9.0)	7.07, d (9.0)	0.2
16	1.97, m	1.94, q (2.6)	0.03
17a	1.13, m	1.13, d (6.8)	0
17b	1.50, m	1.52, m	0.02
18	0.90, t (7.3)	0.91, t (7.4)	0.01
19	0.75, d (6.6)	0.76, d (6.8)	0.01
20			
21a	3.70, dd (−17.0, 4.3)	3.67, dd (17.1, 4.0)	0.03
21b	4.70, dd (−17.0, 9.2)	4.73, dd (17.1, 9.2)	0.03
21-NH	7.97, dd (9.2, 4.3)	7.87, m	0.1
22			
23			
24	8.23, d (0.8)	8.23, d (0.6)	0
25			
26	6.13, d (0.8)	6.14, d (0.6)	0.01
27			
28	1.24, s	1.24, s	0
29	1.38, s	1.38, s	0

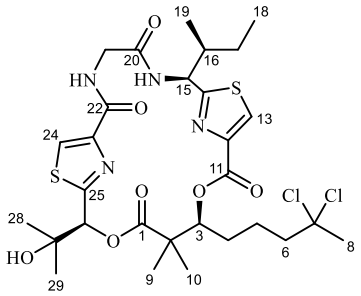

lyngbyabellin A (**3**)

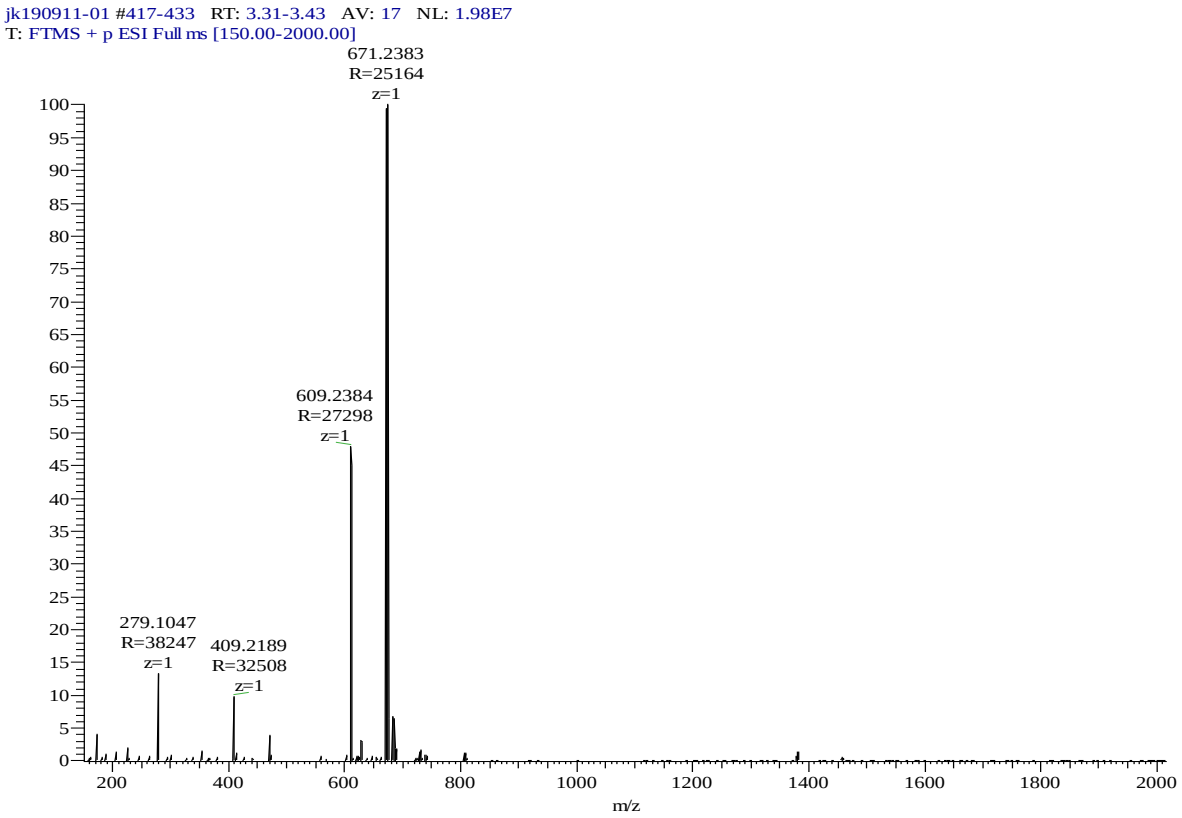

Figure A 12. HRESIMS of 18*E*-lyngbyaloside C (**4**), *m/z* $[M + Na]^+$ calculated for $C_{30}H_{49}BrO_{10}Na$ 671.2401, found 671.2383 (Δ = 2.7 ppm).

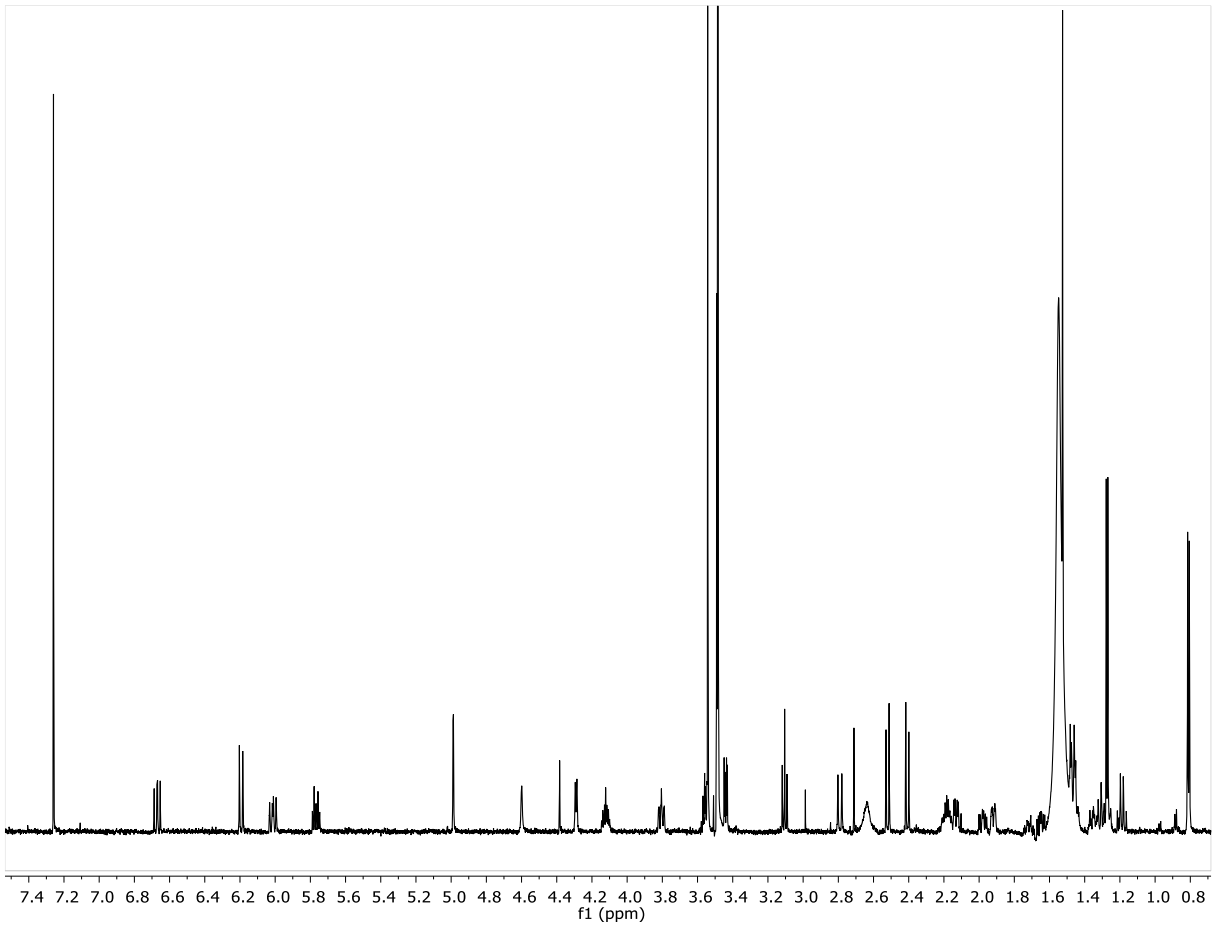

Figure A 13. ^{1}H NMR spectrum for 18*E*-lyngbyaloside C (**4**) in $CDCl_3$ (700 MHz).

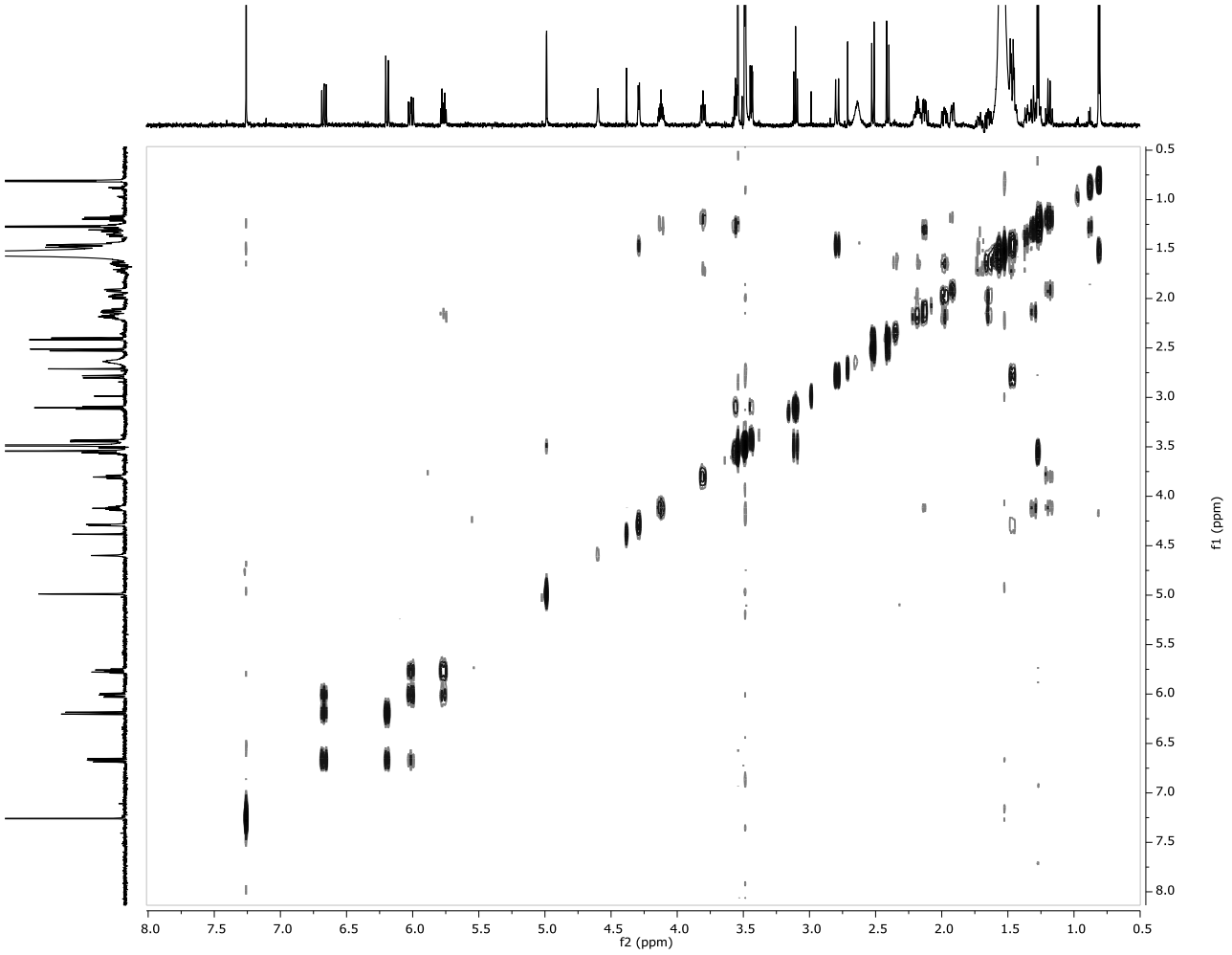

Figure A 14. COSY NMR spectrum for 18*E*-lyngbyaloside C (**4**) in $CDCl_3$ (700 MHz).

Table A 3. Comparison of ^{1}H NMR chemical shifts of *18E*-lyngbyaloside C (**4**) reported in literature [49,190] (600 MHz, $CDCl_3$) to experimental values of **4** (700 MHz, $CDCl_3$).

C/H no.	Literature Values	Experimental Values (4)	Δ (ppm)
	δ_H (*J* in Hz)	**δ_H (*J* in Hz)**	
1			
2a	2.49, d (−12.1)	2.52, d (12.2)	0.03
2b	2.38, d (−12.1)	2.41, d (12.2)	0.03
3			
3-OH	4.57, brs	4.60, s	0.03
4a	2.09, m	2.13, m	0.04
4b	1.28, m	1.26, m	0.02
5	4.10, m	4.12, m	0.02
6a	1.89, m	1.92, m	0.03
6b	1.15, m	1.19, m	0.04
7	3.79, t (10.1)	3.81, t (10.3)	0.02
8a	1.70, m	1.72, m	0.02
8b	1.45, m	1.46, m	0.01
9a	1.45, m	1.46, m	0.01
9b	1.32, m	1.30, m	0.02
10	1.48, m	1.48, m	0
11	4.26, m	4.29, m	0.03
12a	2.77, d (−15.6)	2.79, d (15.3)	0.02
12b	1.44, dd (−15.6, 5.3)	1.44, m	0
13			
14a	1.97, m	1.98, m	0.01
14b	1.63, m	1.65, m	0.02
15a	2.17, m	2.13, m	0.04
15b	2.18, m	2.18, m	0
16	5.76, dt (14.6, 5.9)	5.77, dt (14.3, 6.8)	0.01

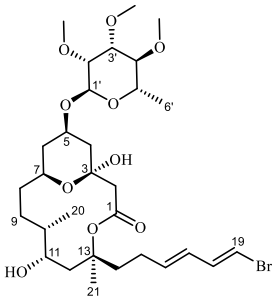

18*E*-lyngbyaloside C (**4**)

Table A 3 (continued)

17	5.99, dd (14.6, 10.6)	6.01, dd (15.2, 10.7)	0.02
18	6.63, dd (13.9, 10.6)	6.67, dd (13.5, 10.7)	0.04
19	6.17, d (13.9)	6.19, d (13.5)	0.02
20	0.80, d (7.0)	0.81, d (6.7)	0.01
21	1.50, s	1.53, s	0.03
1′	4.97, brs	4.99, d (1.9)	0.02
2′	3.46, dd (3.0, 1.0)	3.49, m	0.03
2′-O-Me	3.49, s	3.49, s	0
3′	3.42, dd (9.0, 3.0)	3.44, dd (9.4, 3.3)	0.02
3′-O-Me	3.48, s	3.48, s	0
4′	3.08, dd (10.0, 9.0)	3.11, t (9.4)	0.03
4′-O-Me	3.52, s	3.54, s	0.02
5′	3.53, dq (10.0, 6.2)	3.56, m	0.03
6′	1.25, d (6.2)	1.27, d (6.2)	0.02

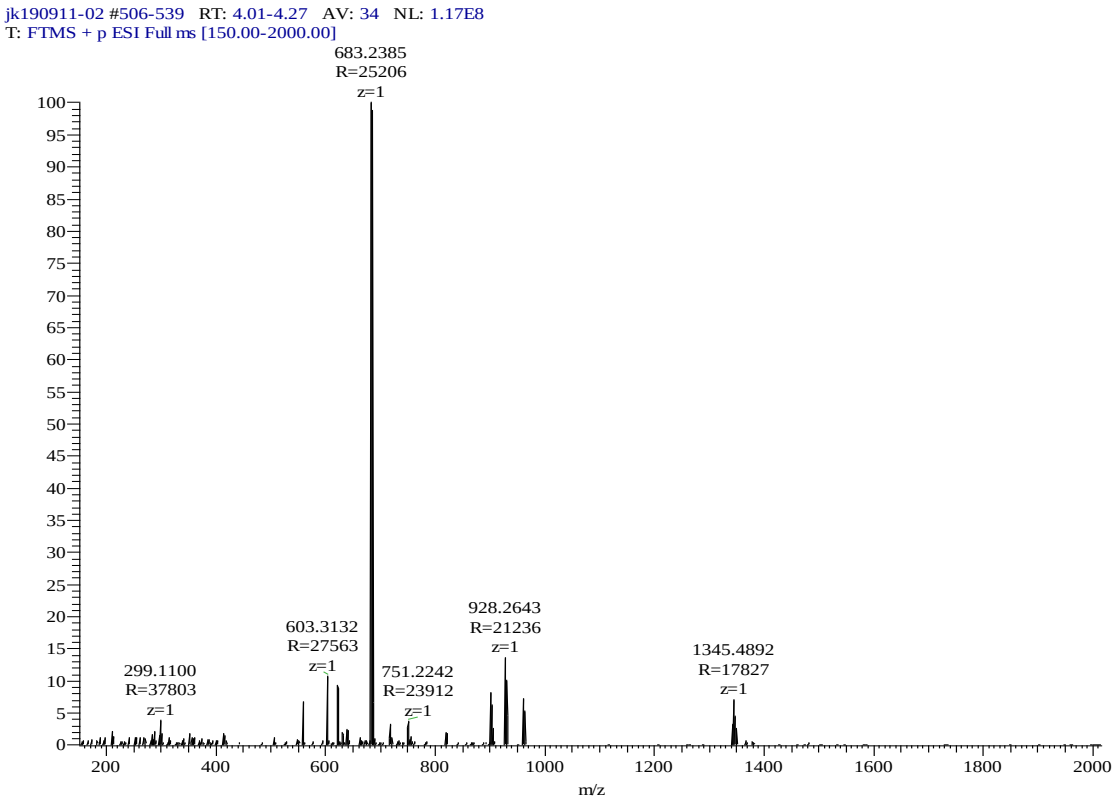

Figure A 15. HRESIMS of lyngbyaloside (**5**) *m/z* $[M + Na]^+$ calculated for $C_{31}H_{49}BrO_{10}Na$ 683.2401, found 683.2385 (Δ = 2.3 ppm).

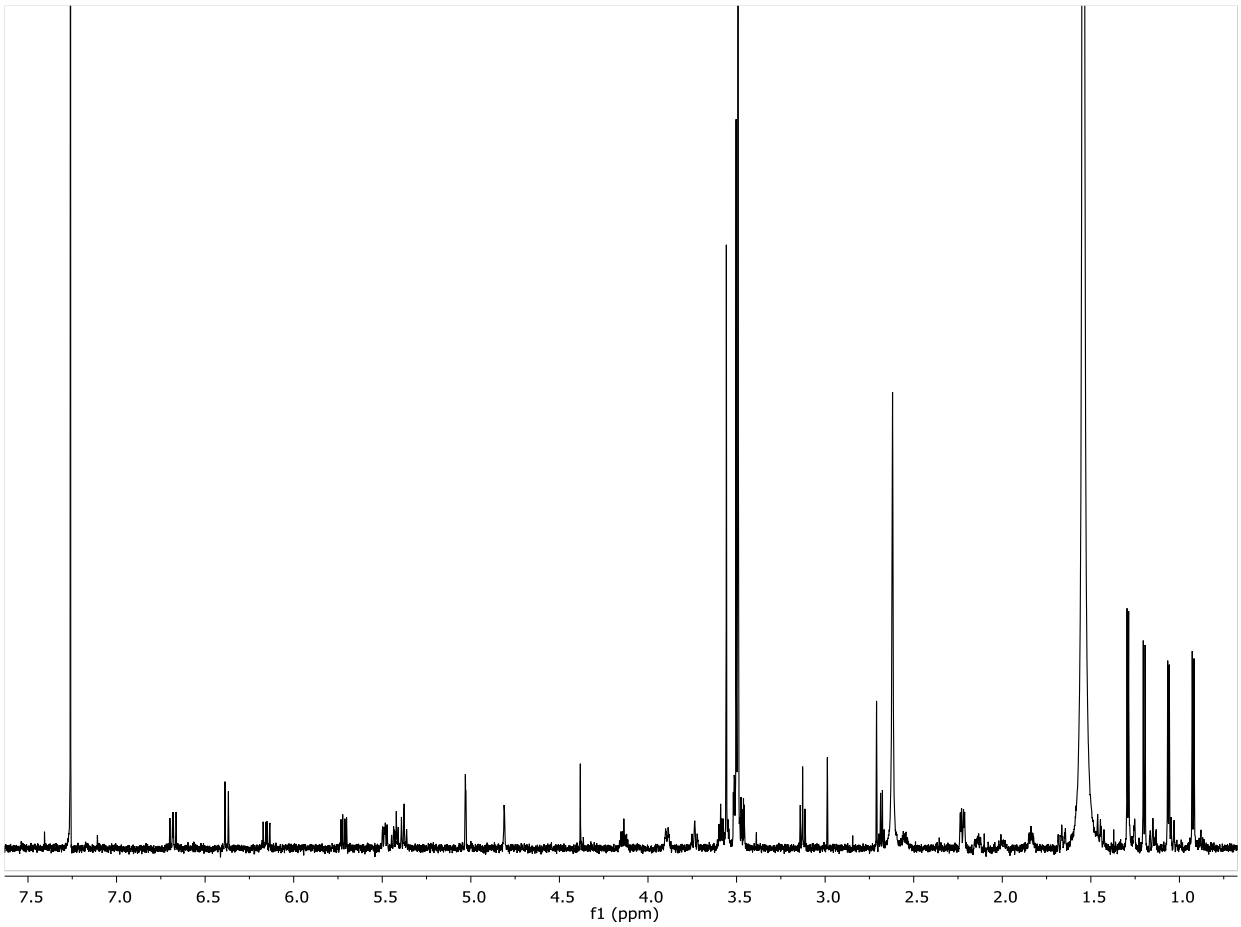

Figure A 16. ^{1}H NMR spectrum for lyngbyaloside (**5**) in $CDCl_3$ (700 MHz).

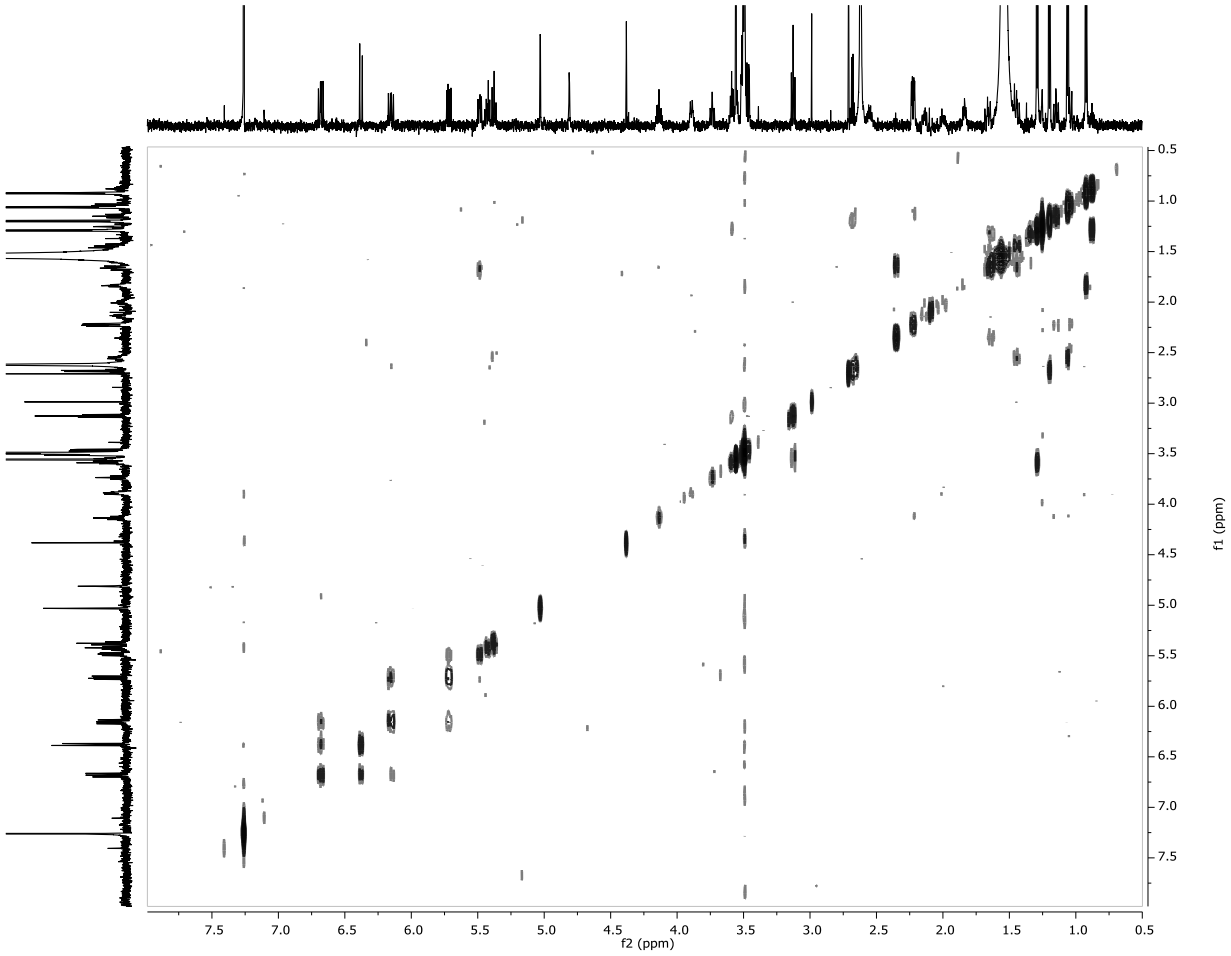

Figure A 17. COSY NMR spectrum for lyngbyaloside (**5**) in $CDCl_3$ (700 MHz).

Table A 4. Comparison of ^{1}H NMR chemical shifts of lyngbyaloside (**5**) reported in literature [50] (600 MHz, $CDCl_3$) to experimental values of **5** (700 MHz, $CDCl_3$).

C/H no.	Literature Values	Experimental Values (5)	Δ (ppm)
	δ_H (*J* in Hz)	**δ_H (*J* in Hz)**	
1			
2	2.66, q (7.0)	2.68, q (7.0)	0.02
3			
3-OH	4.79, d (2.5)	4.81, d (1.7)	0.02
4a	2.20, dd (12.0, 4.0)	2.23, dd (12.0, 4.5)	0.03
4b	1.13, t (12.0)	1.15, t (11.6)	0.02
5	4.12, m	4.14, m	0.02
6a	2.20, dd (12.0, 4.0)	2.23, dd (12.0, 4.5)	0.03
6b	1.02, q (11.5)	1.03, q (11.1)	0.01
7	3.73, bt (11.0)	3.73, bt (10.8)	0
8	1.82, m	1.84, m	0.02
9	3.87, bd (10.6)	3.89, bd (10.6)	0.02
10a	2.13, m	2.14, m	0.01
10b	1.98, m	1.99, m	0.01
11	5.40, dt (10.7, 7.5)	5.43, dt (10.7, 7.7)	0.03
12	5.37, t (10.7)	5.38, t (10.3)	0.01
13	2.54, m	2.55, m	0.01
14a	1.65, ddd (14.0, 10.0, 3.0)	1.66, m	0.01
14b	1.42, bdd (14.0, 11.0)	1.44, dd (15.0, 10.7)	0.02
15	5.48, bdd (11.0, 6.6)	5.49, dd (11.1, 6.7)	0.01
16	5.70, dd (15.3, 6.5)	5.72, dd (15.3, 6.7)	0.02
17	6.13, dd (15.3, 10.8)	6.15, dd (15.0, 11.2)	0.02
18	6.67, dd (13.6, 10.8)	6.68, dd (13.6, 10.9)	0.01
19	6.36, d (13.6)	6.38, d (13.5)	0.02
20	1.18, d (7.0)	1.20, d (7.2)	0.02
21	0.91, d (7.0)	0.92, d (7.0)	0.01
22	1.04, d (6.3)	1.06, d (6.3)	0.02
1‘	5.01, d (2.0)	5.03, d (1.7)	0.02
2‘	3.52, dd (2.7, 2.0)	3.51, dd (3.3, 1.9)	0.01
2′-*O*-Me	3.48, s	3.50, s	0.02
3‘	3.44, dd (9.3, 3.3)	3.47, dd (9.3, 3.3)	0.03
3′-*O*-Me	3.47, s	3.49, s	0.02
4‘	3.11, t (9.3)	3.13, t (9.4)	0.02

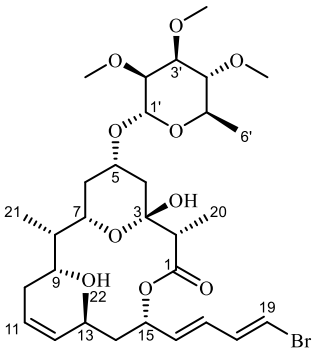

lyngbyaloside (**5**)

Table A 4 (continued)

4′-*O*-Me	3.54, s	3.56, s	0.02
5‘	3.57, m	3.58, m	0.01
6‘	1.27, d (7.0)	1.29, d (6.2)	0.02

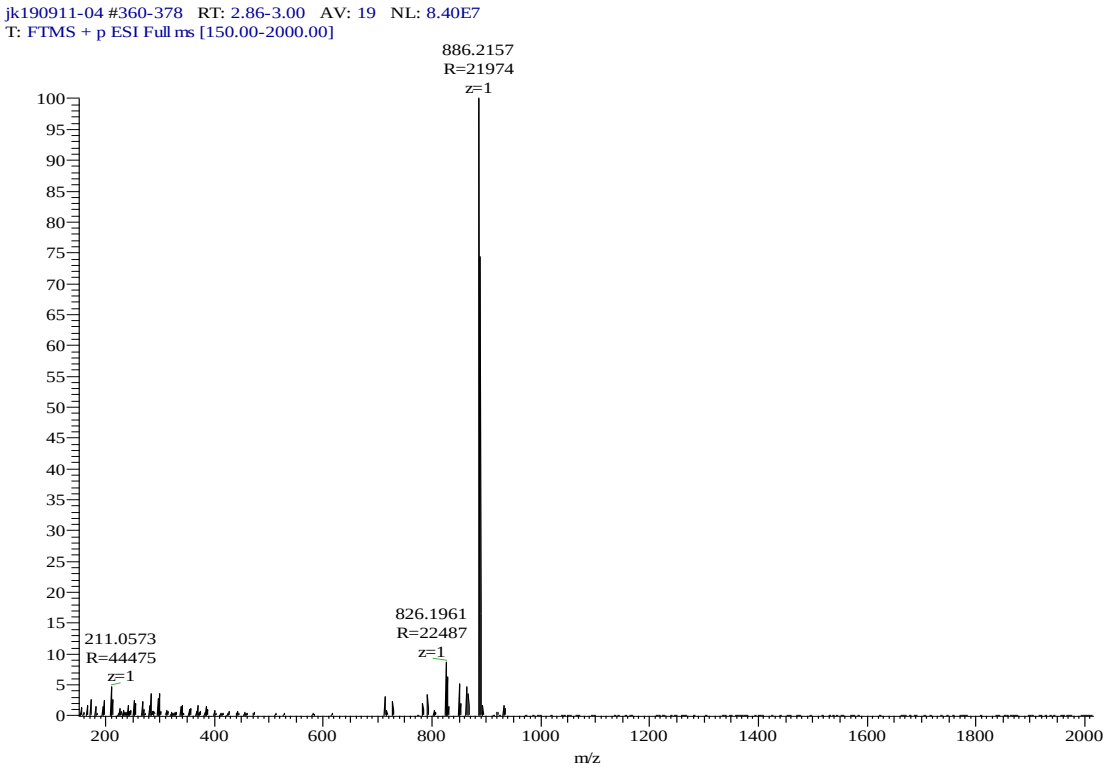

Figure A 18. HRESIMS of lyngbyabellin-like 1 (**LYN1**).

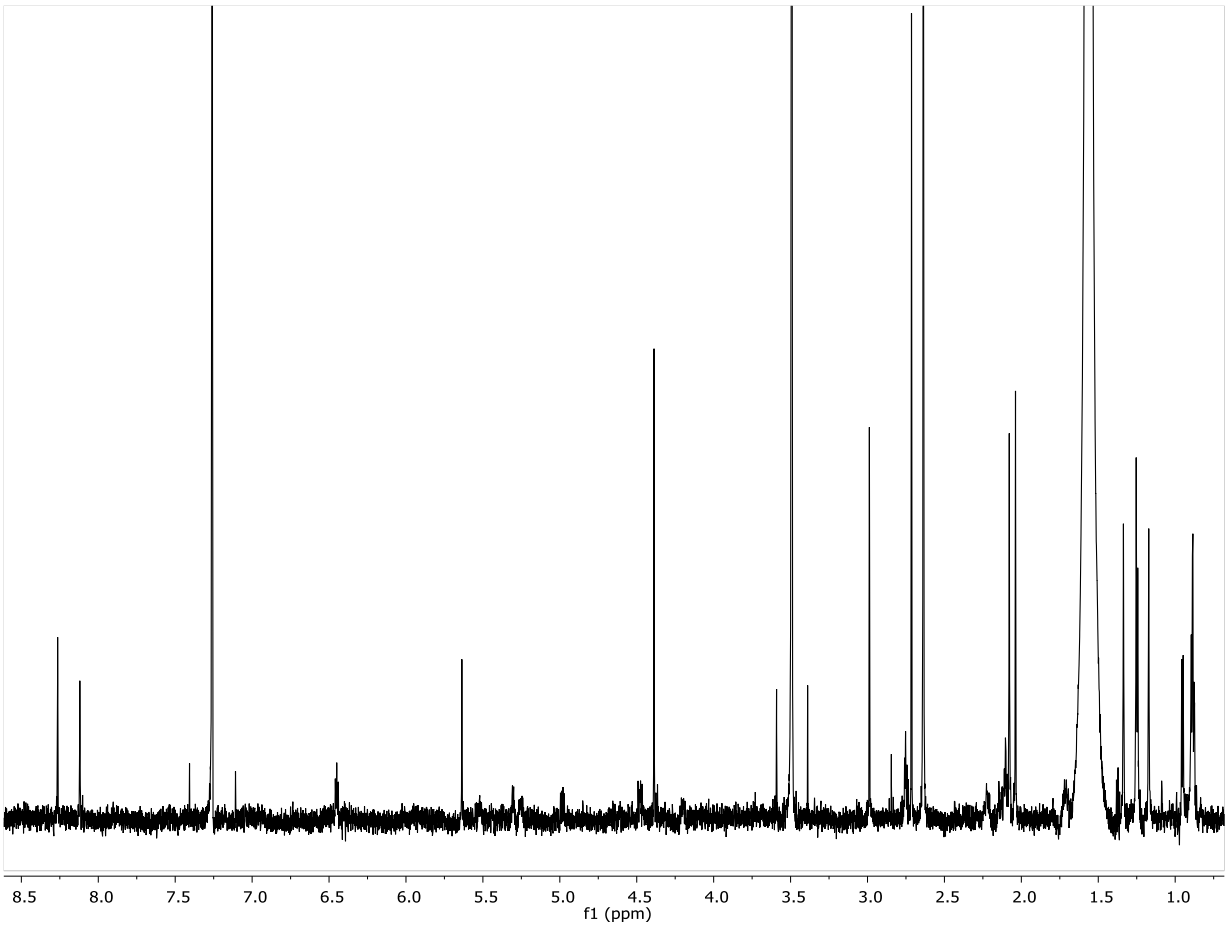

Figure A 19. ^{1}H NMR spectrum of lyngbyabellin-like 1 (**LYN1**) in $CDCl_3$ (700 MHz).

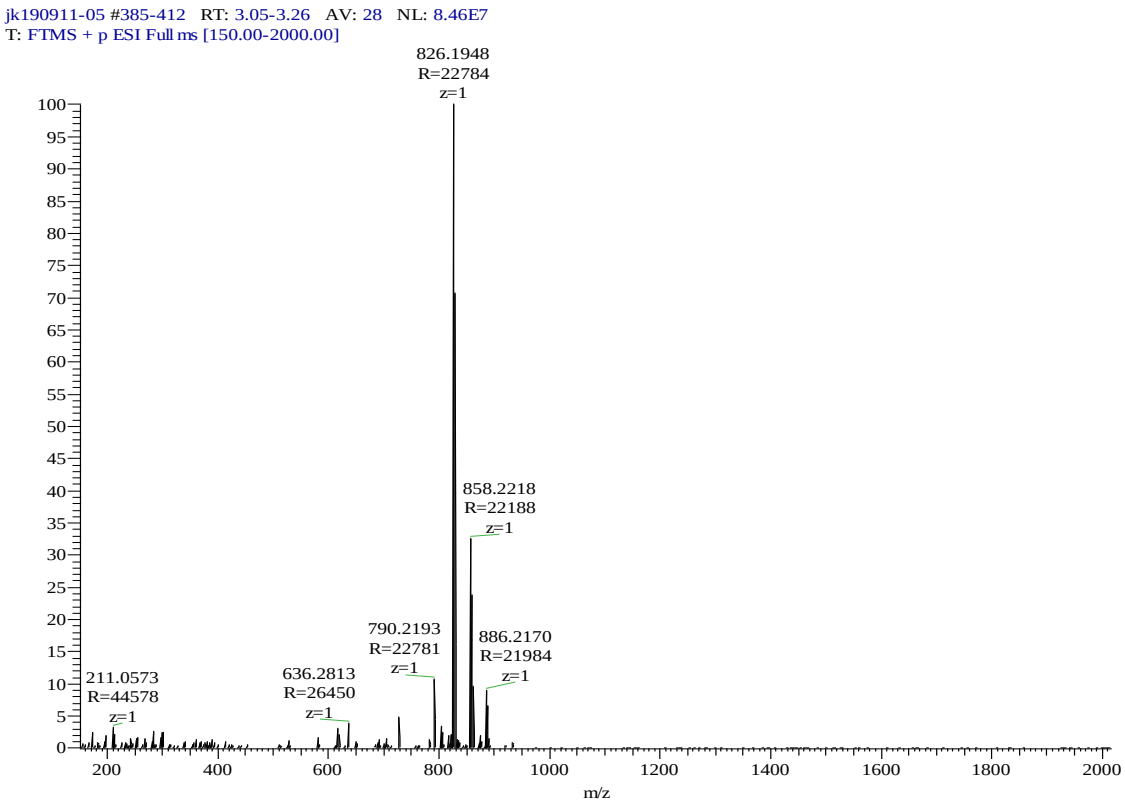

Figure A 20. HRESIMS of lyngbyabellin-like 2 (**LYN2**).

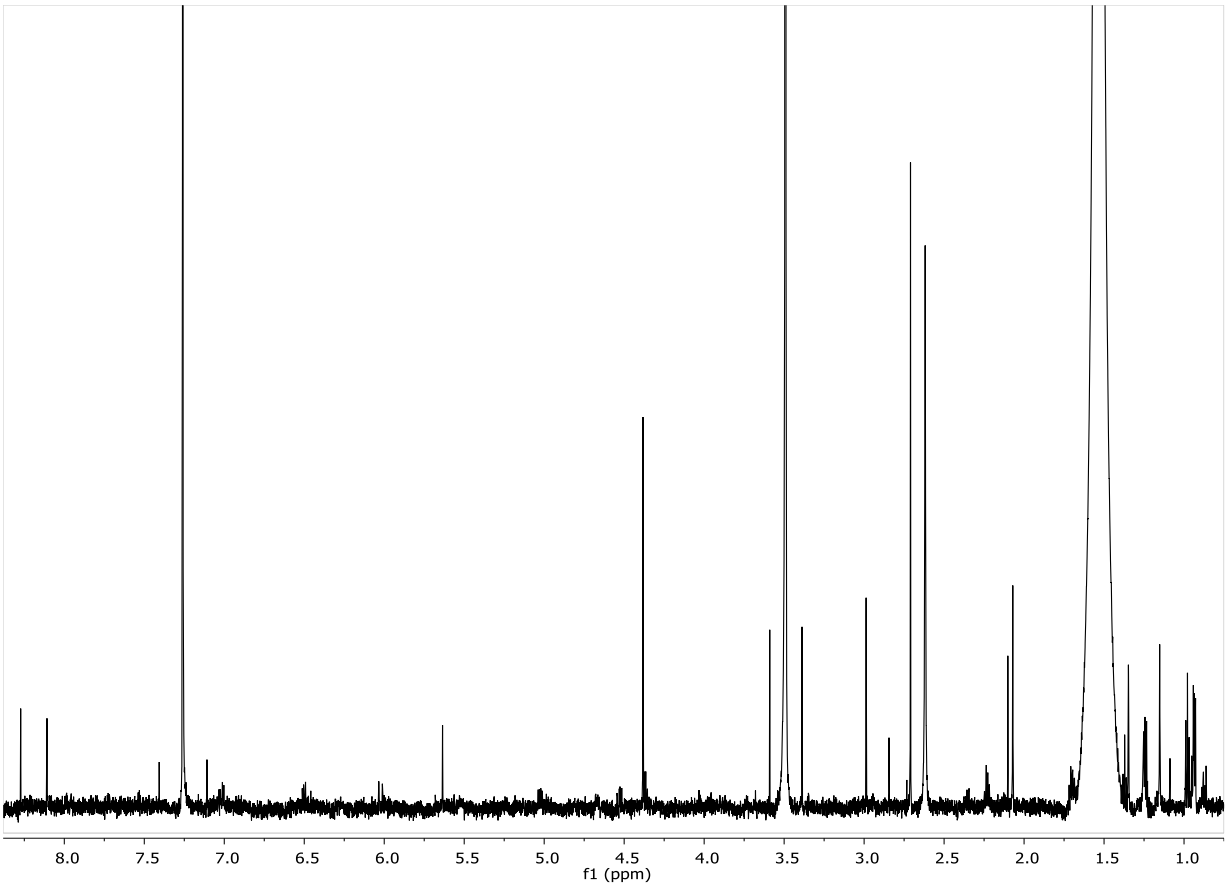

Figure A 21. ^{1}H NMR spectrum of lyngbyabellin-like 2 (**LYN2**) in $CDCl_3$ (700 MHz).

APPENDIX B. PERMISSION FOR REUSE OF COPYRIGHTED MATERIAL

Regarding Incident 3641062 Use of Content for Thesis

support@services.acs.org <support@services.acs.org>
Mon 6/29/2020 7:05 PM
To: Sweeney-Jones, Anne M <amsj3@gatech.edu>

ACS Chemistry for Life®

Dear Dr. Sweeney-jones,

Thank you for contacting ACS Publications Support.

Your permission requested is granted and there is no fee for this reuse. In your planned reuse, you must cite the ACS article as the source, add this direct link https://pubs.acs.org/doi/10.1021/acs.joc.9b00884, and include a notice to readers that further permissions related to the material excerpted should be directed to the ACS.

If you need further assistance, please let me know.

Thank you,
Ranjith Alexander
ACS Customer Services & Information

Incident Information:

Incident #: 3641062
Date Created: 2020-06-29T22:08:25
Priority: 3
Customer: Sweeney-Jones, Anne M
Title: Use of Content for Thesis
Description: Hi,

I would like to obtain permission to reuse some of the content I contributed to the article https://pubs.acs.org/doi/10.1021/acs.joc.9b00884 for my thesis. More specifically, I would like to use the information in the main text related to specimen identification and the ecological experiments (including methods), figure S4, and figure S5.

I appreciate your consideration of my request and I look forward to your response.

Anne Marie

Anne Marie Sweeney-Jones
PhD Candidate, Kubanek Lab
School of Chemistry and Biochemistry
Georgia Institute of Technology

REFERENCES

1. Koehn, F.E.; Carter, G.T. The evolving role of natural products in drug discovery. *Nature Reviews Drug Discovery* **2005**, *4*, 206-220.

2. Achan, J.; Talisuna, A.O.; Erhart, A.; Yeka, A.; Tibenderana, J.K.; Baliraine, F.N.; Rosenthal, P.J.; D'Alessandro, U. Quinine, an old anti-malarial drug in a modern world: role in the treatment of malaria. *Malaria Journal* **2011**, *10*, 144-144.

3. Kong, L.Y.; Tan, R.X. Artemisinin, a miracle of traditional Chinese medicine. *Natural Product Reports* **2015**, *32*, 1617-1621.

4. Campbell, W.C.; Fisher, M.H.; Stapley, E.O.; Albers-Schonberg, G.; Jacob, T.A. Ivermectin: a potent new antiparasitic agent. *Science* **1983**, *221*, 823-828.

5. Levine, D.P. Vancomycin: A history. *Clinical Infectious Diseases* **2006**, *42*, S5-S12.

6. Mayer, A.M.; Glaser, K.B.; Cuevas, C.; Jacobs, R.S.; Kem, W.; Little, R.D.; McIntosh, J.M.; Newman, D.J.; Potts, B.C.; Shuster, D.E. The odyssey of marine pharmaceuticals: a current pipeline perspective. *Trends in Pharmacological Sciences* **2010**, *31*, 255-265.

7. MarinLit. Availabe online: http://pubs.rsc.org/marinlit/ (accessed on 04/14/2020).

8. Lindequist, U. Marine-derived pharmaceuticals - challenges and opportunities. *Biomolecules & Therapeutics* **2016**, *24*, 561-571.

9. Dias, D.A.; Urban, S.; Roessner, U. A historical overview of natural products in drug discovery. *Metabolites* **2012**, *2*, 303-336.

10. Trindade, M.; van Zyl, L.J.; Navarro-Fernández, J.; Abd Elrazak, A. Targeted metagenomics as a tool to tap into marine natural product diversity for the discovery and production of drug candidates. *Frontiers in Microbiology* **2015**, *6*.

11. Xiong, Z.Q.; Wang, J.F.; Hao, Y.Y.; Wang, Y. Recent advances in the discovery and development of marine microbial natural products. *Marine Drugs* **2013**, *11*, 700-717.

12. Lane, A.L.; Kubanek, J. Secondary metabolite defenses against pathogens and biofoulers. In *Algal Chemical Ecology*, Amsler, C.D., Ed. Springer-Verlag: 2008; pp. 229-243.

13. Beattie, A.J.; Hay, M.; Magnusson, B.; de Nys, R.; Smeathers, J.; Vincent, J.F.V. Ecology and bioprospecting. *Austral Ecology* **2011**, *36*, 341-356.

14. Mayer, A.M.S.; Guerrero, A.J.; Rodriguez, A.D.; Taglialatela-Scafati, O.; Nakamura, F.; Fusetani, N. Marine pharmacology in 2014-2015: marine compounds with antibacterial, antidiabetic, antifungal, anti-Inflammatory, antiprotozoal, antituberculosis, antiviral, and anthelmintic activities; affecting the immune and nervous systems, and other miscellaneous mechanisms of action. *Marine Drugs* **2019**, *18*.

15. Guyant, P.; Corbel, V.; Guérin, P.J.; Lautissier, A.; Nosten, F.; Boyer, S.; Coosemans, M.; Dondorp, A.M.; Sinou, V.; Yeung, S., et al. Past and new challenges for malaria control and elimination: the role of operational research for innovation in designing interventions. *Malaria Journal* **2015**, *14*, 279.

16. Kokwaro, G. Ongoing challenges in the management of malaria. *Malaria Journal* **2009**, *8*, S2.

17. Antony, H.A.; Parija, S.C. Antimalarial drug resistance: An overview. *Tropical Parasitology* **2016**, *6*, 30-41.

18. Alonso, P.L.; Tanner, M. Public health challenges and prospects for malaria control and elimination. *Nature Medicine* **2013**, *19*, 150-155.

19. Markus, M.B. Malaria: origin of the term "hypnozoite". *Journal of the History of Biology* **2011**, *44*, 781-786.

20. Hotez, P.J.; Pecoul, B.; Rijal, S.; Boehme, C.; Aksoy, S.; Malecela, M.; Tapia-Conyer, R.; Reeder, J.C. Eliminating the neglected tropical diseases: translational science and new technologies. *PLOS Neglected Tropical Diseases* **2016**, *10*, e0003895.

21. Pedrique, B.; Strub-Wourgaft, N.; Some, C.; Olliaro, P.; Trouiller, P.; Ford, N.; Pécoul, B.; Bradol, J.-H. The drug and vaccine landscape for neglected diseases (2000–11): a systematic assessment. *The Lancet Global Health* **2013**, *1*, e371-e379.

22. Keenan, J.D.; Hotez, P.J.; Amza, A.; Stoller, N.E.; Gaynor, B.D.; Porco, T.C.; Lietman, T.M. Elimination and eradication of neglected tropical diseases with mass drug administrations: a survey of experts. *PLOS Neglected Tropical Diseases* **2013**, *7*, e2562.

23. Kubanek, J.; Jensen, P.R.; Keifer, P.A.; Sullards, M.C.; Collins, D.O.; Fenical, W. Seaweed resistance to microbial attack: A targeted chemical defense against marine fungi. *Proceedings of the National Academy of Sciences USA* **2003**, *100*, 6916-6921.

24. Thacker, R.W.; Becerro, M.A.; Lumbang, W.A.; Paul, V.J. Allelopathic interactions between sponges on a tropical reef. *Ecology* **1998**, *79*, 1740-1750.

25. Kelly, S.R.; Jensen, P.R.; Henkel, T.P.; Fenical, W.; Pawlik, J.R. Effects of Caribbean sponge extracts on bacterial attachment. *Aquatic Microbial Ecology* **2003**, *31*, 175-182.

26. Hay, M.E.; Kappel, Q.E.; Fenical, W. Synergisms in plant defenses against herbivores - interactions of chemistry, calcification, and plant quality. *Ecology* **1994**, *75*, 1714-1726.

27. Mechanism matters. *Nature Medicine* **2010**, *16*, 347-347.

28. Wagner, B.K.; Schreiber, S.L. The power of sophisticated phenotypic screening and modern mechanism-of-action methods. *Cell Chemical Biology* **2016**, *23*, 3-9.

29. Schenone, M.; Dancik, V.; Wagner, B.K.; Clemons, P.A. Target identification and mechanism of action in chemical biology and drug discovery. *Nature Chemical Biology* **2013**, *9*, 232-240.

30. Yan, M.; Xu, G. Current and future perspectives of functional metabolomics in disease studies–A review. *Analytica Chimica Acta* **2018**, *1037*, 41-54.

31. Fiehn, O. Metabolomics – the link between genotypes and phenotypes. *Plant Molecular Biology* **2002**, *48*, 155-171.

32. Patti, G.J.; Yanes, O.; Siuzdak, G. Metabolomics: the apogee of the omics trilogy. *Nature Reviews Molecular Cell Biology* **2012**, *13*, 263-269.

33. World malaria report 2019. Geneva: World Health Organization, 2019; License: CC BY-NC-SA 3.0 IGO.

34. Tse, E.G.; Korsik, M.; Todd, M.H. The past, present and future of anti-malarial medicines. *Malaria Journal* **2019**, *18*, 93.

35. Maskey, R.P.; Helmke, E.; Kayser, O.; Fiebig, H.H.; Maier, A.; Busche, A.; Laatsch, H. Anti-cancer and antibacterial trioxacarcins with high anti-malaria activity from a marine *Streptomycete* and their absolute stereochemistry. *The Journal of Antibiotics* **2004**, *57*, 771-779.

36. Shao, C.-L.; Linington, R.G.; Balunas, M.J.; Centeno, A.; Boudreau, P.; Zhang, C.; Engene, N.; Spadafora, C.; Mutka, T.S.; Kyle, D.E., et al. Bastimolide A, a potent antimalarial polyhydroxy macrolide from the marine cyanobacterium *Okeania hirsuta*. *Journal of Organic Chemistry* **2015**, *80*, 7849-7855.

37. Ang, K.K.; Holmes, M.J.; Higa, T.; Hamann, M.T.; Kara, U.A. In vivo antimalarial activity of the beta-carboline alkaloid manzamine A. *Antimicrobial Agents and Chemotherapy* **2000**, *44*, 1645-1649.

38. Wright, A.D.; Wang, H.; Gurrath, M.; König, G.M.; Kocak, G.; Neumann, G.; Loria, P.; Foley, M.; Tilley, L. Inhibition of heme detoxification processes underlies the antimalarial activity of terpene isonitrile compounds from marine sponges. *Journal of Medicinal Chemistry* **2001**, *44*, 873-885.

39. Sanchez, C.P.; McLean, J.E.; Rohrbach, P.; Fidock, D.A.; Stein, W.D.; Lanzer, M. Evidence for a *pfcrt*-associated chloroquine efflux system in the human malarial parasite *Plasmodium falciparum*. *Biochemistry* **2005**, *44*, 9862-9870.

40. Shah, S.A.A.; Akhter, N.; Auckloo, B.N.; Khan, I.; Lu, Y.; Wang, K.; Wu, B.; Guo, Y.-W. Structural diversity, biological properties and applications of natural products from cyanobacteria. A review. *Marine Drugs* **2017**, *15*, 354.

41. Demay, J.; Bernard, C.; Reinhardt, A.; Marie, B. Natural products from cyanobacteria: focus on beneficial activities. *Marine Drugs* **2019**, *17*, 320.

42. McPhail, K.L.; Correa, J.; Linington, R.G.; Gonzalez, J.; Ortega-Barria, E.; Capson, T.L.; Gerwick, W.H. Antimalarial linear lipopeptides from a Panamanian strain of the marine cyanobacterium *Lyngbya majuscula*. *Journal of Natural Products* **2007**, *70*, 984-988.

43. Linington, R.G.; Clark, B.R.; Trimble, E.E.; Almanza, A.; Urena, L.D.; Kyle, D.E.; Gerwick, W.H. Antimalarial peptides from marine cyanobacteria: isolation and structural elucidation of gallinamide A. *Journal of Natural Products* **2009**, *72*, 14-17.

44. Linington, R.G.; Gonzalez, J.; Urena, L.D.; Romero, L.I.; Ortega-Barria, E.; Gerwick, W.H. Venturamides A and B: antimalarial constituents of the Panamanian marine cyanobacterium *Oscillatoria* sp. *Journal of Natural Products* **2007**, *70*, 397-401.

45. Brylinski, M.; Skolnick, J. A threading-based method (FINDSITE) for ligand-binding site prediction and functional annotation. *Proceedings of the National Academy of Sciences USA* **2008**, *105*, 129-134.

46. Zhou, H.; Cao, H.; Skolnick, J. FINDSITE$^{comb2.0}$: a new approach for virtual ligand screening of proteins and virtual target screening of biomolecules. *Journal of Chemical Information and Modeling* **2018**, *58*, 2343-2354.

47. Luesch, H.; Williams, P.G.; Yoshida, W.Y.; Moore, R.E.; Paul, V.J. Ulongamides A−F, new β-amino acid-containing cyclodepsipeptides from Palauan collections of the marine cyanobacterium *Lyngbya* sp. *Journal of Natural Products* **2002**, *65*, 996-1000.

48. Luesch, H.; Yoshida, W.Y.; Moore, R.E.; Paul, V.J.; Mooberry, S.L. Isolation, structure determination, and biological activity of lyngbyabellin A from the marine cyanobacterium *Lyngbya majuscula*. *Journal of Natural Products* **2000**, *63*, 611-615.

49. Matthew, S.; Salvador, L.A.; Schupp, P.J.; Paul, V.J.; Luesch, H. Cytotoxic halogenated macrolides and modified peptides from the apratoxin-producing marine cyanobacterium *Lyngbya bouillonii* from Guam. *Journal of Natural Products* **2010**, *73*, 1544-1552.

50. Klein, D.; Braekman, J.C.; Daloze, D.; Hoffmann, L.; Demoulin, V. Lyngbyaloside, a novel 2,3,4-tri-O-methyl-6-deoxy-α-mannopyranoside macrolide from *Lyngbya bouillonii* (Cyanobacteria). *Journal of Natural Products* **1997**, *60*, 1057-1059.

51. Nakamura, F.; Maejima, H.; Kawamura, M.; Arai, D.; Okino, T.; Zhao, M.; Ye, T.; Lee, J.; Chang, Y.-T.; Fusetani, N., et al. Kakeromamide A, a new cyclic pentapeptide inducing astrocyte differentiation isolated from the marine cyanobacterium *Moorea bouillonii*. *Bioorganic & Medicinal Chemistry Letters* **2018**, *28*, 2206-2209.

52. Alvarado, C.; Díaz, E.; Guzmán, Á. Total synthesis of ulongamide A, a cyclic depsipeptide isolated from marine cyanobacteria *Lyngbya* sp. *Tetrahedron Letters* **2007**, *48*, 603-607.

53. Yokokawa, F.; Sameshima, H.; Shioiri, T. Total synthesis of lyngbyabellin A, a potent cytotoxic metabolite from the marine cyanobacterium *Lyngbya majuscula*. *Tetrahedron Letters* **2001**, *42*, 4171-4174.

54. Chang, C.F.; Stefan, E.; Taylor, R.E. Total synthesis and structural reassignment of lyngbyaloside C highlighted by intermolecular ketene esterification. *Chemistry – A European Journal* **2015**, *21*, 10681-10686.

55. Sone, H.; Kondo, T.; Kiryu, M.; Ishiwata, H.; Ojika, M.; Yamada, K. Dolabellin, a cytotoxic bisthiazole metabolite from the sea hare *Dolabella auricularia*: structural determination and synthesis. *Journal of Organic Chemistry* **1995**, *60*, 4774-4781.

56. Luesch, H.; Yoshida, W.Y.; Moore, R.E.; Paul, V.J. Isolation and structure of the cytotoxin lyngbyabellin B and absolute configuration of lyngbyapeptin A from the marine cyanobacterium *Lyngbya majuscula*. *Journal of Natural Products* **2000**, *63*, 1437-1439.

57. Han, B.; McPhail, K.L.; Gross, H.; Goeger, D.E.; Mooberry, S.L.; Gerwick, W.H. Isolation and structure of five lyngbyabellin derivatives from a Papua New Guinea collection of the marine cyanobacterium *Lyngbya majuscula*. *Tetrahedron* **2005**, *61*, 11723-11729.

58. Luesch, H.; Yoshida, W.Y.; Moore, R.E.; Paul, V.J. Structurally diverse new alkaloids from Palauan collections of the apratoxin-producing marine cyanobacterium *Lyngbya* sp. *Tetrahedron* **2002**, *58*, 7959-7966.

59. Williams, P.G.; Luesch, H.; Yoshida, W.Y.; Moore, R.E.; Paul, V.J. Continuing studies on the cyanobacterium *Lyngbya* sp.: isolation and structure determination of 15-norlyngbyapeptin A and lyngbyabellin D. *Journal of Natural Products* **2003**, *66*, 595-598.

60. Choi, H.; Mevers, E.; Byrum, T.; Valeriote, F.A.; Gerwick, W.H. Lyngbyabellins K–N from two Palmyra Atoll collections of the marine cyanobacterium *Moorea bouillonii*. *European Journal of Organic Chemistry* **2012**, *2012*, 5141-5150.

61. Petitbois, J.G.; Casalme, L.O.; Lopez, J.A.V.; Alarif, W.M.; Abdel-Lateff, A.; Al-Lihaibi, S.S.; Yoshimura, E.; Nogata, Y.; Umezawa, T.; Matsuda, F., et al. Serinolamides and lyngbyabellins from an *Okeania* sp. cyanobacterium collected from the Red Sea. *Journal of Natural Products* **2017**, *80*, 2708-2715.

62. Burrows, J.N.; Duparc, S.; Gutteridge, W.E.; Hooft van Huijsduijnen, R.; Kaszubska, W.; Macintyre, F.; Mazzuri, S.; Möhrle, J.J.; Wells, T.N.C. New developments in anti-malarial target candidate and product profiles. *Malaria Journal* **2017**, *16*, 26.

63. Das, S.; Lemgruber, L.; Tay, C.L.; Baum, J.; Meissner, M. Multiple essential functions of *Plasmodium falciparum* actin-1 during malaria blood-stage development. *BMC Biology* **2017**, *15*, 70-70.

64. Hallee, S.; Counihan, N.A.; Matthews, K.; de Koning-Ward, T.F.; Richard, D. The malaria parasite *Plasmodium falciparum* sortilin is essential for merozoite formation and apical complex biogenesis. *Cellular Microbiology* **2018**, *20*, e12844.

65. Mailu, B.M.; Li, L.; Arthur, J.; Nelson, T.M.; Ramasamy, G.; Fritz-Wolf, K.; Becker, K.; Gardner, M.J. *Plasmodium* apicoplast Gln-tRNA^{Gln} biosynthesis utilizes a unique GatAB amidotransferase essential for erythrocytic stage parasites. *Journal of Biological Chemistry* **2015**, *290*, 29629-29641.

66. Plaimas, K.; Wang, Y.; Rotimi, S.O.; Olasehinde, G.; Fatumo, S.; Lanzer, M.; Adebiyi, E.; König, R. Computational and experimental analysis identified 6-diazo-5-oxonorleucine as a potential agent for treating infection by *Plasmodium falciparum*. *Infection, Genetics and Evolution* **2013**, *20*, 389-395.

67. Wieland, T. Modification of actins by phallotoxins. *Naturwissenschaften* **1977**, *64*, 303-309.

68. Morton, W.M.; Ayscough, K.R.; McLaughlin, P.J. Latrunculin alters the actin-monomer subunit interface to prevent polymerization. *Nature Chemical Biology* **2000**, *2*, 376-378.

69. Cooper, J.A. Effects of cytochalasin and phalloidin on actin. *Journal of Cell Biology* **1987**, *105*, 1473-1478.

70. Bubb, M.R.; Senderowicz, A.M.; Sausville, E.A.; Duncan, K.L.; Korn, E.D. Jasplakinolide, a cytotoxic natural product, induces actin polymerization and competitively inhibits the binding of phalloidin to F-actin. *Journal of Biological Chemistry* **1994**, *269*, 14869-14871.

71. Douglas, R.G.; Nandekar, P.; Aktories, J.-E.; Kumar, H.; Weber, R.; Sattler, J.M.; Singer, M.; Lepper, S.; Sadiq, S.K.; Wade, R.C., et al. Inter-subunit interactions drive divergent dynamics in mammalian and *Plasmodium* actin filaments. *PLoS Biology* **2018**, *16*, e2005345.

72. Boddey, J.A.; Hodder, A.N.; Gunther, S.; Gilson, P.R.; Patsiouras, H.; Kapp, E.A.; Pearce, J.A.; de Koning-Ward, T.F.; Simpson, R.J.; Crabb, B.S., et al. An aspartyl protease directs malaria effector proteins to the host cell. *Nature* **2010**, *463*, 627-631.

73. Andrews, K.T.; Fairlie, D.P.; Madala, P.K.; Ray, J.; Wyatt, D.M.; Hilton, P.M.; Melville, L.A.; Beattie, L.; Gardiner, D.L.; Reid, R.C., et al. Potencies of human immunodeficiency virus protease inhibitors in vitro against *Plasmodium falciparum* and in vivo against murine malaria. *Antimicrobial Agents and Chemotherapy* **2006**, *50*, 639-648.

74. Bharti, S.K.; Roy, R. Quantitative ^{1}H NMR spectroscopy. *Trends in Analytical Chemistry* **2012**, *35*, 5-26.

75. Frank, J.A.; Reich, C.I.; Sharma, S.; Weisbaum, J.S.; Wilson, B.A.; Olsen, G.J. Critical evaluation of two primers commonly used for amplification of bacterial 16S rRNA genes. *Applied and Environmental Microbiology* **2008**, *74*, 2461-2470.

76. Huang, X.; Madan, A. CAP3: A DNA sequence assembly program. *Genome Research* **1999**, *9*, 868-877.

77. Altschul, S.F.; Gish, W.; Miller, W.; Myers, E.W.; Lipman, D.J. Basic local alignment search tool. *Journal of Molecular Biology* **1990**, *215*, 403-410.

78. Kumar, S.; Stecher, G.; Li, M.; Knyaz, C.; Tamura, K. MEGA X: molecular evolutionary genetics analysis across computing platforms. *Molecular Biology and Evolution* **2018**, *35*, 1547-1549.

79. Kimura, M. A simple method for estimating evolutionary rates of base substitutions through comparative studies of nucleotide sequences. *Journal of Molecular Evolution* **1980**, *16*, 111-120.

80. Plouffe, D.; Brinker, A.; McNamara, C.; Henson, K.; Kato, N.; Kuhen, K.; Nagle, A.; Adrian, F.; Matzen, J.T.; Anderson, P., et al. In silico activity profiling reveals the mechanism of action of antimalarials discovered in a high-throughput screen. *Proceedings of the National Academy of Sciences USA* **2008**, *105*, 9059-9064.

81. Swann, J.; Corey, V.; Scherer, C.A.; Kato, N.; Comer, E.; Maetani, M.; Antonova-Koch, Y.; Reimer, C.; Gagaring, K.; Ibanez, M., et al. High-throughput luciferase-based assay for the discovery of therapeutics that prevent malaria. *ACS Infectious Diseases* **2016**, *2*, 281-293.

82. Love, M.S.; Beasley, F.C.; Jumani, R.S.; Wright, T.M.; Chatterjee, A.K.; Huston, C.D.; Schultz, P.G.; McNamara, C.W. A high-throughput phenotypic screen identifies clofazimine as a potential treatment for cryptosporidiosis. *PLOS Neglected Tropical Diseases* **2017**, *11*, e0005373.

83. Zhang, Y.; Skolnick, J. Automated structure prediction of weakly homologous proteins on a genomic scale. *Proceedings of the National Academy of Sciences USA* **2004**, *101*, 7594-7599.

84. Bernstein, F.C.; Koetzle, T.F.; Williams, G.J.B.; Meyer Jr, E.F.; Brice, M.D.; Rodgers, J.R.; Kennard, O.; Shimanouchi, T.; Tasumi, M. The protein data bank. *European Journal of Biochemistry* **1977**, *80*, 319-324.

85. Gaulton, A.; Bellis, L.J.; Bento, A.P.; Chambers, J.; Davies, M.; Hersey, A.; Light, Y.; McGlinchey, S.; Michalovich, D.; Al-Lazikani, B., et al. ChEMBL: a large-scale bioactivity database for drug discovery. *Nucleic Acids Research* **2011**, *40*, D1100-D1107.

86. Wishart, D.S.; Knox, C.; Guo, A.C.; Shrivastava, S.; Hassanali, M.; Stothard, P.; Chang, Z.; Woolsey, J. DrugBank: a comprehensive resource for in silico drug discovery and exploration. *Nucleic Acids Research* **2006**, *34*, D668-D672.

87. Hay, M.E. Marine chemical ecology: what's known and what's next? *Journal of Experimental Marine Biology and Ecology* **1996**, *200*, 103-134.

88. Pawlik, J.R.; Amsler, C.D.; Ritson-Williams, R.; McClintock, J.B.; Baker, B.J.; Paul, V. Marine chemical ecology: A science born of scuba. *Research and Discoveries: The Revolution of Science through Scuba* **2013**, *39*, 53-69.

89. Millar, J.G.; Haynes, K.F. Methods in chemical ecology; New York, NY : Chapman & Hall: New York, NY, 1998.

90. Khatri Chhetri, B.; Lavoie, S.; Sweeney-Jones, A.M.; Mojib, N.; Raghavan, V.; Gagaring, K.; Dale, B.; McNamara, C.W.; Soapi, K.; Quave, C.L., et al. Peyssonnosides A–B, unusual diterpene glycosides with a sterically encumbered cyclopropane motif: structure elucidation using an integrated spectroscopic and computational workflow. *Journal of Organic Chemistry* **2019**, *84*, 8531-8541.

91. Efferth, T.; Kuete, V. Biodiversity, natural products and cancer treatment; World Scientific: New Jersey, 2014.

92. Paul, V.J.; Arthur, K.E.; Ritson-Williams, R.; Ross, C.; Sharp, K. Chemical defenses: from compounds to communities. *The Biological Bulletin* **2007**, *213*, 226-251.

93. de Nys, R.; Dworjanyn, S.A.; Steinberg, P.D. A new method for determining surface concentrations of marine natural products on seaweeds. *Marine Ecology Progress Series* **1998**, *162*, 79-87.

94. Rhoades, D.F. Evolution of plant chemical defense against herbivores; Rosenthal, G.A., Janzen, D.H., Eds.; Academic Press: New York, 1979.

95. Godschalx, A.L.; Stady, L.; Watzig, B.; Ballhorn, D.J. Is protection against florivory consistent with the optimal defense hypothesis? *BMC Plant Biology* **2016**, *16*, 32.

96. Henrikson, A.A.; Pawlik, J.R. A new antifouling assay method: results from field experiments using extracts of four marine organisms. *Journal of Experimental Marine Biology and Ecology* **1995**, *194*, 157-165.

97. Kohlmeyer, J.; Kohlmeyer, E. Marine mycology: the higher fungi; Academic Press: New York, San Francisco, London, 1979.

98. Engel, S.; Puglisi, M.P.; Jensen, P.R.; Fenical, W. Antimicrobial activities of extracts from tropical Atlantic marine plants against marine pathogens and saprophytes. *Marine Biology* **2006**, *149*, 991-1002.

99. Paul, V.J.; Ritson-Williams, R. Marine chemical ecology. *Natural Product Reports* **2008**, *25*, 662-695.

100. Lane, A.L.; Mular, L.; Drenkard, E.J.; Shearer, T.L.; Engel, S.; Fredericq, S.; Fairchild, C.R.; Prudhomme, J.; Le Roch, K.; Hay, M.E., et al. Ecological leads for natural product discovery: novel sesquiterpene hydroquinones from the red macroalga *Peyssonnelia* sp. *Tetrahedron* **2010**, *66*, 455-461.

101. Tsukatani, T.; Suenaga, H.; Higuchi, T.; Akao, T.; Ishiyama, M.; Ezoe, K.; Matsumoto, K. Colorimetric cell proliferation assay for microorganisms in microtiter plate using water-soluble tetrazolium salts. *Journal of Microbiological Methods* **2008**, *75*, 109-116.

102. Kumar, P.; Tarafdar, J. 2,3,5-Triphenyltetrazolium chloride (TTC) as electron acceptor of culturable soil bacteria, fungi and actinomycetes. *Biology and Fertility of Soils* **2003**, *38*, 186-189.

103. CDC. Parasites - Soil-transmitted helminths. Availabe online: https://www.cdc.gov/parasites/sth/index.html (accessed on 04/28/2020).

104. Addiss, D.G.; Berman, J. Elimination of neglected tropical diseases: catalytic investment, remarkable success, unfinished business. *Clinical Infectious Diseases* **2019**, *70*, 965-967.

105. Wainwright, E.; Evans, D.; Rotondo, L.; Pou, B.; Yevstigneyeva, V.; Zoerhoff, K.L.; Ottesen, E.A.; Reithinger, R. The elimination of neglected tropical diseases: A case study exemplifying how foreign assistance funding can be catalytic in reducing the burden of major global health conditions. *Clinical Infectious Diseases* **2020**, *70*, 958-964.

106. Crossing the billion. Lymphatic filariasis, onchocerciasis, schistosomiasis, soil-transmitted helminthiases and trachoma: preventive chemotherapy for neglected tropical diseases. World Health Organization: Geneva, 2017; Vol. Licence: CC BY-NC-SA 3.0 IGO.

107. Moser, W.; Schindler, C.; Keiser, J. Efficacy of recommended drugs against soil transmitted helminths: systematic review and network meta-analysis. *BMJ* **2017**, *358*, j4307.

108. Furtado, L.F.V.; de Paiva Bello, A.C.P.; Rabelo, É.M.L. Benzimidazole resistance in helminths: From problem to diagnosis. *Acta Tropica* **2016**, *162*, 95-102.

109. Kopp, S.R.; Kotze, A.C.; McCarthy, J.S.; Coleman, G.T. High-level pyrantel resistance in the hookworm *Ancylostoma caninum*. *Veterinary Parasitology* **2007**, *143*, 299-304.

110. Morrison, A.A.; Mitchell, S.; Mearns, R.; Richards, I.; Matthews, J.B.; Bartley, D.J. Phenotypic and genotypic analysis of benzimidazole resistance in the ovine parasite *Nematodirus battus*. *Veterinary Research* **2014**, *45*, 116.

111. Geary, T.G.; Woo, K.; McCarthy, J.S.; Mackenzie, C.D.; Horton, J.; Prichard, R.K.; de Silva, N.R.; Olliaro, P.L.; Lazdins-Helds, J.K.; Engels, D.A., et al. Unresolved issues in anthelmintic pharmacology for helminthiases of humans. *International Journal for Parasitology* **2010**, *40*, 1-13.

112. Hotez, P.J.; Bethony, J.; Bottazzi, M.E.; Brooker, S.; Buss, P. Hookworm: "the great infection of mankind". *PLoS Medicine* **2005**, *2*, e67-e67.

113. Albonico, M.; Smith, P.G.; Ercole, E.; Hall, A.; Chwaya, H.M.; Alawi, K.S.; Savioli, L. Rate of reinfection with intestinal nematodes after treatment of children with mebendazole or albendazole in a highly endemic area. *Transactions of the Royal Society of Tropical Medicine & Hygiene* **1995**, *89*, 538-541.

114. Adriko, M.; Tinkitina, B.; Arinaitwe, M.; Kabatereine, N.B.; Nanyunja, M.; E, M.T. Impact of a national deworming campaign on the prevalence of soil-transmitted helminthiasis in Uganda (2004-2016): Implications for national control programs. *PLOS Neglected Tropical Diseases* **2018**, *12*, e0006520.

115. Durmaz, E.; Hu, Y.; Aroian, R.V.; Klaenhammer, T.R. Intracellular and extracellular expression of *Bacillus thuringiensis* crystal protein Cry5B in *Lactococcus lactis* for use as an anthelminthic. *Applied and Environmental Microbiology* **2016**, *82*, 1286-1294.

116. Somvanshi, V.S.; Ellis, B.L.; Hu, Y.; Aroian, R.V. Nitazoxanide: nematicidal mode of action and drug combination studies. *Molecular and Biochemical Parasitology* **2014**, *193*, 1-8.

117. Organization, W.H. *Assessing the efficacy of anthelminthic drugs against schistosomiasis and soil-transmitted helminthiases*; World Health Organization: Geneva, 2013.

118. Elfawal, M.A.; Savinov, S.N.; Aroian, R.V. Drug screening for discovery of broad-spectrum agents for soil-transmitted nematodes. *Scientific Reports* **2019**, *9*, 12347.

119. Sepúlveda-Crespo, D.; Reguera, Rosa M.; Rojo-Vázquez, F.; Balaña-Fouce, R.; Martínez-Valladares, M. Drug discovery technologies: *Caenorhabditis elegans* as a model for anthelmintic therapeutics. *Medicinal Research Reviews n/a*.

120. Rippka, R.; Deruelles, J.; Waterbury, J.B.; Herdman, M.; Stanier, R.Y. Generic assignments, strain histories and properties of pure cultures of cyanobacteria. *Microbiology* **1979**, *111*, 1-61.

121. Tomitani, A.; Knoll, A.H.; Cavanaugh, C.M.; Ohno, T. The evolutionary diversification of cyanobacteria: Molecular–phylogenetic and paleontological perspectives. *Proceedings of the National Academy of Sciences USA* **2006**, *103*, 5442-5447.

122. Salvador, L.A.; Biggs, J.S.; Paul, V.J.; Luesch, H. Veraguamides A−G, cyclic hexadepsipeptides from a dolastatin 16-producing cyanobacterium *Symploca cf. hydnoides* from Guam. *Journal of Natural Products* **2011**, *74*, 917-927.

123. Choi, H.; Pereira, A.R.; Cao, Z.; Shuman, C.F.; Engene, N.; Byrum, T.; Matainaho, T.; Murray, T.F.; Mangoni, A.; Gerwick, W.H. The hoiamides, structurally intriguing neurotoxic lipopeptides from Papua New Guinea marine cyanobacteria. *Journal of Natural Products* **2010**, *73*, 1411-1421.

124. Simmons, T.L.; McPhail, K.L.; Ortega-Barría, E.; Mooberry, S.L.; Gerwick, W.H. Belamide A, a new antimitotic tetrapeptide from a Panamanian marine cyanobacterium. *Tetrahedron Letters* **2006**, *47*, 3387-3390.

125. Lacey, E. Mode of action of benzimidazoles. *Parasitology Today* **1990**, *6*, 112-115.

126. Abongwa, M.; Martin, R.J.; Robertson, A.P. A brief review on the mode of action of antinematodal drugs. *Acta Veterinaria* **2017**, *67*, 137-152.

127. Bai, R.; Roach, M.C.; Jayaram, S.K.; Barkoczy, J.; Pettit, G.R.; Ludueña, R.F.; Hamel, E. Differential effects of active isomers, segments, and analogs of dolastatin 10 on ligand interactions with tubulin: Correlation with cytotoxicity. *Biochemical Pharmacology* **1993**, *45*, 1503-1515.

128. Greenberg, R.M. Ion channels and drug transporters as targets for anthelmintics. *Current Clinical Microbiology Reports* **2014**, *1*, 51-60.

129. Aráoz, R.; Molgó, J.; Tandeau de Marsac, N. Neurotoxic cyanobacterial toxins. *Toxicon* **2010**, *56*, 813-828.

130. Pereira, A.; Cao, Z.; Murray, T.F.; Gerwick, W.H. Hoiamide A, a sodium channel activator of unusual architecture from a consortium of two Papua New Guinea Cyanobacteria. *Chemistry & Biology* **2009**, *16*, 893-906.

131. Tang, Y.T.; Gao, X.; Rosa, B.A.; Abubucker, S.; Hallsworth-Pepin, K.; Martin, J.; Tyagi, R.; Heizer, E.; Zhang, X.; Bhonagiri-Palsikar, V., et al. Genome of the human hookworm *Necator americanus*. *Nature Genetics* **2014**, *46*, 261-269.

132. Hu, Y.; Ellis, B.L.; Yiu, Y.Y.; Miller, M.M.; Urban, J.F.; Shi, L.Z.; Aroian, R.V. An extensive comparison of the effect of anthelmintic classes on diverse nematodes. *PLOS One* **2013**, *8*, e70702-e70702.

133. CDC. *Antibiotic resistance threats in the United States, 2019*; U.S. Department of Health and Human Services, CDC: Atlanta, GA, 2019.

134. Årdal, C.; Balasegaram, M.; Laxminarayan, R.; McAdams, D.; Outterson, K.; Rex, J.H.; Sumpradit, N. Antibiotic development — economic, regulatory and societal challenges. *Nature Reviews Microbiology* **2020**, *18*, 267-274.

135. WHO. Lack of new antibiotics threatens global efforts to contain drug-resistant infections. https://www.who.int/news-room/detail/17-01-2020-17-01-2020-lack-of-new-antibiotics-threatens-global-efforts-to-contain-drug-resistant-infections (accessed on April 30, 2020).

136. Coates, A.R.M.; Halls, G.; Hu, Y. Novel classes of antibiotics or more of the same? *British Journal of Pharmacology* **2011**, *163*, 184-194.

137. Kim, W. Tracking the global pipeline of antibiotics in development, April 2020. https://www.pewtrusts.org/en/research-and-analysis/issue-briefs/2020/04/tracking-the-global-pipeline-of-antibiotics-in-development (accessed on 6/1/2020).

138. Chellat, M.F.; Raguž, L.; Riedl, R. Targeting antibiotic resistance. *Angewandte Chemie International Edition* **2016**, *55*, 6600-6626.

139. Fontaine, B.M.; Nelson, K.; Lyles, J.T.; Jariwala, P.B.; García-Rodriguez, J.M.; Quave, C.L.; Weinert, E.E. Identification of ellagic acid rhamnoside as a bioactive component of a complex botanical extract with anti-biofilm activity. *Frontiers in Microbiology* **2017**, *8*.

140. Tyers, M.; Wright, G.D. Drug combinations: a strategy to extend the life of antibiotics in the 21st century. *Nature Reviews Microbiology* **2019**, *17*, 141-155.

141. Kell, D.B.; Oliver, S.G. The metabolome 18 years on: a concept comes of age. *Metabolomics* **2016**, *12*, 148-148.

142. Bhinderwala, F.; Wase, N.; DiRusso, C.; Powers, R. Combining mass spectrometry and NMR improves metabolite detection and annotation. *Journal of Proteome Research* **2018**, *17*, 4017-4022.

143. Dettmer, K.; Aronov, P.A.; Hammock, B.D. Mass spectrometry-based metabolomics. *Mass Spectrometry Reviews* **2007**, *26*, 51-78.

144. Dunn, W.B.; Ellis, D.I. Metabolomics: Current analytical platforms and methodologies. *TrAC Trends in Analytical Chemistry* **2005**, *24*, 285-294.

145. Boiteau, R.M.; Hoyt, D.W.; Nicora, C.D.; Kinmonth-Schultz, H.A.; Ward, J.K.; Bingol, K. Structure elucidation of unknown metabolites in metabolomics by combined NMR and MS/MS prediction. *Metabolites* **2018**, *8*.

146. Li, X.; Luo, H.; Huang, T.; Xu, L.; Shi, X.; Hu, K. Statistically correlating NMR spectra and LC-MS data to facilitate the identification of individual metabolites in metabolomics mixtures. *Analytical and Bioanalytical Chemistry* **2019**, *411*, 1301-1309.

147. Marshall, D.D.; Powers, R. Beyond the paradigm: Combining mass spectrometry and nuclear magnetic resonance for metabolomics. *Progress in Nuclear Magnetic Resonance Spectroscopy* **2017**.

148. Halouska, S.; Fenton, R.J.; Barletta, R.G.; Powers, R. Predicting the *in vivo* mechanism of action for drug leads using NMR metabolomics. *ACS Chemical Biology* **2012**, *7*, 166-171.

149. Schelli, K.; Zhong, F.; Zhu, J. Comparative metabolomics revealing *Staphylococcus aureus* metabolic response to different antibiotics. *Microbial Biotechnology* **2017**, *10*, 1764-1774.

150. Dörries, K.; Schlueter, R.; Lalk, M. Impact of antibiotics with various target sites on the metabolome of *Staphylococcus aureus*. *Antimicrobial Agents and Chemotherapy* **2014**, *58*, 7151-7163.

151. Aros-Calt, S.; Muller, B.H.; Boudah, S.; Ducruix, C.; Gervasi, G.; Junot, C.; Fenaille, F. Annotation of the *Staphylococcus aureus* metabolome using liquid chromatography coupled to high-resolution mass spectrometry and application to the study of methicillin resistance. *Journal of Proteome Research* **2015**, *14*, 4863-4875.

152. Baptista, R.; Fazakerley, D.M.; Beckmann, M.; Baillie, L.; Mur, L.A.J. Untargeted metabolomics reveals a new mode of action of pretomanid (PA-824). *Scientific Reports* **2018**, *8*, 5084.

153. Lavoie, S.; Sweeney-Jones, A.M.; Mojib, N.; Dale, B.; Gagaring, K.; McNamara, C.W.; Quave, C.L.; Soapi, K.; Kubanek, J. Antibacterial oligomeric polyphenols from the green alga *Cladophora socialis*. *Journal of Organic Chemistry* **2019**, *84*, 5035-5045.

154. Chen, J.L.; Gerwick, W.H.; Schatzman, R.; Laney, M. Isorawsonol and related IMP dehydrogenase inhibitors from the tropical green alga *Avrainvillea rawsonii*. *Journal of Natural Products* **1994**, *57*, 947-952.

155. Carte, B.K.; Troupe, N.; Chan, J.A.; Westley, J.W.; Faulkner, D.J. Rawsonol, an inhibitor of HMG-CoA reductase from the tropical green alga *Avrainvillea rawsoni*. *Phytochemistry* **1989**, *28*, 2917-2919.

156. Sun, H.H.; Paul, V.J.; Fenical, W. Avrainvilleol, a brominated diphenylmethane derivative with feeding deterrent properties from the tropical green alga avrainvillea longicaulis. *Phytochemistry* **1983**, *22*, 743-745.

157. Feng, Y.; Carroll, A.R.; Addepalli, R.; Fechner, G.A.; Avery, V.M.; Quinn, R.J. Vanillic acid derivatives from the green algae *Cladophora socialis* as potent protein tyrosine phosphatase 1B inhibitors. *Journal of Natural Products* **2007**, *70*, 1790-1792.

158. Melander, R.J.; Zurawski, D.V.; Melander, C. Narrow-spectrum antibacterial agents. *MedChemComm* **2018**, *9*, 12-21.

159. Kim, J.; Kim, K.H. Effects of minimal media vs. complex media on the metabolite profiles of *Escherichia coli* and *Saccharomyces cerevisiae*. *Process Biochemistry* **2017**, *57*, 64-71.

160. Meyer, H.; Liebeke, M.; Lalk, M. A protocol for the investigation of the intracellular *Staphylococcus aureus* metabolome. *Analytical Biochemistry* **2010**, *401*, 250-259.

161. Pinu, F.R.; Villas-Boas, S.G.; Aggio, R. Analysis of intracellular metabolites from microorganisms: quenching and extraction protocols. *Metabolites* **2017**, *7*.

162. Li, A.; Mao, D.; Yoshimura, A.; Rosen, P.C.; Martin, W.L.; Gallant, É.; Wühr, M.; Seyedsayamdost, M.R. Multi-Omic analyses provide links between low-dose antibiotic treatment and induction of secondary metabolism in *Burkholderia thailandensis*. *mBio* **2020**, *11*, e03210-03219.

163. Sanders, C.C. Ciprofloxacin: In vitro activity, mechanism of action, and resistance. *Reviews of Infectious Diseases* **1988**, *10*, 516-527.

164. Blais, J.; Tardif, C.; Chamberland, S. Effect of clindamycin on intracellular replication, protein synthesis, and infectivity of *Toxoplasma gondii*. *Antimicrobial Agents and Chemotherapy* **1993**, *37*, 2571-2577.

165. Winder, F.; Collins, P. Inhibition by isoniazid of synthesis of mycolic acids in *Mycobacterium tuberculosis*. *Microbiology* **1970**, *63*, 41-48.

166. Timmins, G.S.; Deretic, V. Mechanisms of action of isoniazid. *Molecular Microbiology* **2006**, *62*, 1220-1227.

167. Suzuki, J.; KUNIMOTO, T.; HORI, M. Effects of kanamycin on protein synthesis: inhibition of elongation of peptide chains. *The Journal of Antibiotics* **1970**, *23*, 99-101.

168. Swaney, S.M.; Aoki, H.; Ganoza, M.C.; Shinabarger, D.L. The oxazolidinone linezolid inhibits initiation of protein synthesis in bacteria. *Antimicrobial Agents and Chemotherapy* **1998**, *42*, 3251-3255.

169. Tartakoff, A.M. Perturbation of vesicular traffic with the carboxylic ionophore monensin. *Cell* **1983**, *32*, 1026-1028.

170. Campbell, E.A.; Korzheva, N.; Mustaev, A.; Murakami, K.; Nair, S.; Goldfarb, A.; Darst, S.A. Structural mechanism for rifampicin inhibition of bacterial RNA polymerase. *Cell* **2001**, *104*, 901-912.

171. Brown, G.M. Inhibition by sulfonamides of the biosynthesis of folic acid. *International Journal of Leprosy and Other Mycobacterial Diseases* **1967**, *35*, 580-589.

172. Hammes, W.P.; Neuhaus, F.C. On the mechanism of action of vancomycin: inhibition of peptidoglycan synthesis in *Gaffkya homari*. *Antimicrobial Agents and Chemotherapy* **1974**, *6*, 722-728.

173. Drazic, A.; Kutzner, E.; Winter, J.; Eisenreich, W. Metabolic response of *Escherichia coli* upon treatment with hypochlorite at sub-lethal concentrations. *PLOS One* **2015**, *10*, e0125823.

174. Yeom, J.; Shin, J.-H.; Yang, J.-Y.; Kim, J.; Hwang, G.-S. ^{1}H NMR-based metabolite profiling of planktonic and biofilm cells in *Acinetobacter baumannii* 1656-2. *PLOS One* **2013**, *8*, e57730.

175. Tuyiringire, N.; Tusubira, D.; Munyampundu, J.-P.; Tolo, C.U.; Muvunyi, C.M.; Ogwang, P.E. Application of metabolomics to drug discovery and understanding the mechanisms of action of medicinal plants with anti-tuberculosis activity. *Clinical and Translational Medicine* **2018**, *7*, 29-29.

176. Ogunade, I.; Schweickart, H.; Andries, K.; Lay, J.; Adeyemi, J. Monensin alters the functional and metabolomic profile of rumen microbiota in beef cattle. *Animals* **2018**, *8*, 211.

177. Vincent, I.M.; Ehmann, D.E.; Mills, S.D.; Perros, M.; Barrett, M.P. Untargeted metabolomics to ascertain antibiotic modes of action. *Antimicrobial Agents and Chemotherapy* **2016**, *60*, 2281-2291.

178. Hewelt-Belka, W.; Nakonieczna, J.; Belka, M.; Bączek, T.; Namieśnik, J.; Kot-Wasik, A. Untargeted lipidomics reveals differences in the lipid pattern among clinical isolates of *Staphylococcus aureus* resistant and sensitive to antibiotics. *Journal of Proteome Research* **2016**, *15*, 914-922.

179. Gerwick, W.H.; Moore, B.S. Lessons from the past and charting the future of marine natural products drug discovery and chemical biology. *Chemistry & Biology* **2012**, *19*, 85-98.

180. Wang, S.; Dong, G.; Sheng, C. Structural simplification of natural products. *Chemical Reviews* **2019**, *119*, 4180-4220.

181. Bian, X.; Huang, F.; Stewart, F.A.; Xia, L.; Zhang, Y.; Müller, R. Direct cloning, genetic engineering, and heterologous expression of the syringolin biosynthetic gene cluster in *E. coli* through Red/ET recombineering. *Chembiochem* **2012**, *13*, 1946-1952.

182. Chiang, Y.-M.; Chang, S.-L.; Oakley, B.R.; Wang, C.C.C. Recent advances in awakening silent biosynthetic gene clusters and linking orphan clusters to natural products in microorganisms. *Current Opinion in Chemical Biology* **2011**, *15*, 137-143.

183. Khalil, Z.G.; Cruz-Morales, P.; Licona-Cassani, C.; Marcellin, E.; Capon, R.J. Inter-Kingdom beach warfare: Microbial chemical communication activates natural chemical defences. *The ISME Journal* **2019**, *13*, 147-158.

184. Wang, M.; Carver, J.J.; Phelan, V.V.; Sanchez, L.M.; Garg, N.; Peng, Y.; Nguyen, D.D.; Watrous, J.; Kapono, C.A.; Luzzatto-Knaan, T., et al. Sharing and community curation of mass spectrometry data with Global Natural Products Social Molecular Networking. *Nature Biotechnology* **2016**, *34*, 828-837.

185. van Santen, J.A.; Jacob, G.; Singh, A.L.; Aniebok, V.; Balunas, M.J.; Bunsko, D.; Neto, F.C.; Castaño-Espriu, L.; Chang, C.; Clark, T.N., et al. The natural products atlas: An open access knowledge base for microbial natural products discovery. *ACS Central Science* **2019**, *5*, 1824-1833.

186. Quinn, R.A.; Nothias, L.-F.; Vining, O.; Meehan, M.; Esquenazi, E.; Dorrestein, P.C. Molecular networking as a drug discovery, drug metabolism, and precision medicine strategy. *Trends in Pharmacological Sciences* **2017**, *38*, 143-154.

187. Zhang, C.; Idelbayev, Y.; Roberts, N.; Tao, Y.; Nannapaneni, Y.; Duggan, B.M.; Min, J.; Lin, E.C.; Gerwick, E.C.; Cottrell, G.W., et al. Small molecule accurate recognition technology (SMART) to enhance natural products research. *Scientific Reports* **2017**, *7*, 14243.

188. Koichi, S.; Arisaka, M.; Koshino, H.; Aoki, A.; Iwata, S.; Uno, T.; Satoh, H. Chemical structure elucidation from 13C NMR chemical shifts: Efficient data processing using bipartite matching and maximal clique algorithms. *Journal of Chemical Information and Modeling* **2014**, *54*, 1027-1035.

189. Burns, D.C.; Mazzola, E.P.; Reynolds, W.F. The role of computer-assisted structure elucidation (CASE) programs in the structure elucidation of complex natural products. *Natural Product Reports* **2019**, *36*, 919-933.

190. Fuwa, H.; Yamagata, N.; Okuaki, Y.; Ogata, Y.; Saito, A.; Sasaki, M. Total synthesis and complete stereostructure of a marine macrolide glycoside, (−)-lyngbyaloside B. *Chemistry – A European Journal* **2016**, *22*, 6815-6829.